PATHOGEN TRANSPORT AND CAPTURE IN A POROUS MEDIA BIOFILM REACTOR

by

Kevin John Grabinski

A thesis submitted in partial fulfillment
of the requirements for the degree

of

Master of Science

in

Environmental Engineering

MONTANA STATE UNIVERSITY
Bozeman, Montana

July 2007

APPROVAL

of a thesis submitted by

Kevin John Grabinski

This thesis has been read by each member of the thesis committee and has been found to be satisfactory regarding content, English usage, format, citations, bibliographic style, and consistency, and is ready for submission to the Division of Graduate Education.

Dr. Warren Jones
Chair of Committee

Approved for the Department of Civil Engineering

Dr. Brett Gunnink
Department Head

Approved for the Division of Graduate Education

Dr. Carl A. Fox
Vice Provost

STATEMENT OF PERMISSION TO USE

In presenting this thesis in partial fulfillment of the requirements for a master's degree at Montana State University – Bozeman, I agree that the library shall make it available to borrowers under rules of the Library.

If I have indicated my intention to copyright this thesis by including a copyright notice page, copying is allowable only for scholarly purposes, consistent with "fair use" as prescribed in the U.S. Copyright Law. Requests for permission for extended quotation from or reproduction of this thesis (paper) in whole or in parts may be granted only by the copyright holder.

Kevin John Grabinski

July 2007

ACKNOWLEDGEMENTS

I was introduced to environmental engineering in 2003 by Dr. Warren Jones as an undergraduate student in Civil Engineering. His mentoring as a professor, and as a faculty advisor to Chi Epsilon, led me to pursue a Master's Degree at MSU. I have greatly appreciated his guidance as an academic advisor and graduate committee chair. I would like to thank Dr. Warren Jones and the other members of my graduate committee, Dr. Al Cunningham and Dr. Anne Camper for their willingness to assist me with my graduate research project. I would also like to thank Dr. Anne Camper for providing a truly enjoyable lab environment in which to work. Another big thanks to everyone who has helped teach an engineer how to be a microbiologist and everyone who has assisted review this document: Wes Bauman, Mark Burr, Stewart Clark, Robin Gerlach, Lu Goodrum, Ben Klayman, Lynne Leach, Andreas Nocker, and Nick Trimble.

I would also like to thank my family for their unwavering support and encouragement throughout my college "career" and the many friends I have made while here in Bozeman. Thank you all!

I would like to acknowledge the support of the Army Research Office (ARO) for providing the funding for this project and the Center for Biofilm Engineering (CBE) at Montana State University for being a fantastic research center to work at while being a graduate student.

TABLE OF CONTENTS

TABLE OF CONTENTS – CONTINUED

TABLE OF CONTENTS – CONTINUED

LIST OF TABLES

LIST OF FIGURES

Figure Page

LIST OF FIGURES - CONTINUED

Figure Page

ABSTRACT

Drinking water distribution systems pose the potential to transport biological and chemical contaminants to the consumers' tap that can be responsible for widespread waterborne disease outbreaks (WBDO). A need exists to improve the ability to monitor contaminants that can attach to the distribution system's interior surfaces and to obtain samples for diagnosing both the cause of a WBDO and the extent of contamination within the system. In this study, a porous media reactor colonized with a mixed-species drinking water biofilm was used to study the capture of *Salmonella typhimurium* as a model pathogen. Parallel reactors were operated under constant flow (CF) and constant head (CH) to compare flow-regime induced spatial variations in biofilm accumulation and the resulting pathogen capture. Parallel test reactors were operated with 0.5 mg/L supplemental carbon until the accumulation of biofilm in the CH reactor reduced the flowrate to the target sampling point (CF flowrate). Both test reactors were then inoculated with slug doses of approximately $3x10^9$ CFU *S. typhimurium*. Effluent water samples were collected for five pore-volumes, followed by the destructive sampling of the reactor. Plate counts were used to enumerate *S. typhimurium* present in effluent samples and captured within the reactor. Cell counts in effluent samples displayed an accelerated breakthrough compared with a non-reactive tracer. Compared with uncolonized control reactors (0.13%), colonized reactors (0.96%) captured significantly more cells. Despite spatial variations in biofilm accumulation, colonized CH and CF reactors captured comparable amounts of *S. typhimurium*. Increasing sampling duration to twenty pore volumes demonstrated greater retention of captured cells in the colonized reactors over the control reactors. *S. typhimurium* transport and capture was also observed in a 0.9 mm square flowcell packed with 100 μm beads using a confocal microscope. Interception and straining were responsible for capture on clean beads while biofilm accumulation narrowed pore throats sufficiently to allow for mechanical filtration to occur. This study demonstrates that using biofilm colonized porous media may be an effective tool to capture pathogens for monitoring drinking water distribution systems.

CHAPTER 1

INTRODUCTION

Background

Drinking water distribution systems are an integral part of city and community infrastructures in the United States. While necessary, these distribution systems can also pose a potential health risk to the general public because they can transport biological and chemical contaminants to the consumers' tap. These contaminants can be responsible for widespread waterborne disease outbreaks (WBDO). In addition to flowing through the system directly to the consumers tap, these contaminants can temporarily attach to the interior surfaces of the distribution system. The subsequent release of these contaminants may result in the recurrence of disease outbreaks from the initial contamination event. Interior surfaces of distribution systems are not easily accessible. Therefore, a need exists to improve the ability to monitor the contaminants attached to the distribution system's interior surfaces that influence the water quality. Furthermore, a need exists to obtain samples for diagnosing both the cause of a waterborne disease outbreak and the extent of contamination within the system.

Drinking Water Distribution Systems

The Water Science and Technology Board (WSTB) produced an updated publication in 2006 which overviews drinking water distribution systems and the possible sources for WBDOs in the United States. Public water systems in the US produce 34 billion gallons of

water daily that must be delivered from the treatment plant to the consumer. This is achieved with the use of drinking water distribution systems. They represent an essential component of every drinking water utility's infrastructure. Piping is the main component of the distribution system, but it also includes pumps, valves, storage tanks and reservoirs. The United States has almost a million miles of distribution mains with an additional five million miles of service lines and premise plumbing beyond curb stops for which utilities are not responsible. An additional 13,200 miles of new pipes are installed every year to provide water to expanding communities due to population growth [*WSTB*, 2006].

These distribution systems represent the largest portion of physical infrastructure in centralized water systems (CWS) and are a major public health concern related to potable water. The repair and replacement of failing distribution lines over the next 20 years is estimated to cost $183.6 billion [*WSTB*, 2006].

Security is an important issue with distribution systems due to the vast number of access points at storage tanks, pumps, hydrants, and consumer taps that could be used to deliberately contaminate a CWS. A distribution system could be used in a bioterrorism attack due to the ease with which a distribution system can be accessed, coupled with its ability to transport a contaminant throughout an entire municipality.

Waterborne Disease Outbreaks

Waterborne disease outbreaks occur in communities when contaminants infiltrate a water distribution system and reach the consumers' tap. Possible contaminants include microbial pathogens, native aquatic microorganisms and toxins produced by them, and chemical contaminants. Possible routes of contamination include inadequate treatment,

distribution main breaks, cross connections with sewer lines, backflow, or intentional contamination [*WSTB*, 2006]. WBDOs can result in illnesses related to infections of the ear, skin, and gastrointestinal, neurological, or respiratory systems. While chemicals and toxins occasionally are responsible for WBDOs, the vast majority of cases involve bacteria, parasites, or viruses [*CDC*, 2004].

The Center for Disease Control and Prevention (CDC) in conjunction with the Environmental Protection Agency (EPA) and state and regional epidemiologists instituted a passive voluntary surveillance system for WBDOs in 1971. There have been 764 reported drinking water outbreaks between 1971 and 2002 and this number is believed to be an underestimation due to the passive and voluntary nature of the program. It has provided valuable information useful for improving the understanding of the agents responsible for WBDOs and the risk factors involved [*WSTB,* 2006].

Some bacteria are pathogenic to humans, but the majority of bacteria found in distribution systems have been shown by the World Health Organization (WHO) not to be linked to disease outbreaks. These heterotrophic bacteria are commonly found in distribution systems and can be located in two distinct environments. Planktonic bacteria are found suspended in the bulk fluid moving through the distribution system. These planktonic bacteria can also attach and colonize the surfaces of the pipe walls and storage tanks. These attached bacteria develop into mixed-species colonies called biofilms which continue to grow and can detach from the distribution systems surfaces to re-enter the bulk fluid [*WSTB*, 2006].

Biofilms

Biofilms occur in virtually all distribution systems and are considered harmless by themselves, but they can provide safe harbor locations for opportunistic pathogens. These pathogens can integrate into the biofilm where they can persist or grow. The biofilm protects bacteria from being exposed to the disinfection residual that is used to kill or inactivate pathogens in the bulk water [*WSTB*, 2006]. The biofilm with the pathogens can detach and re-enter the bulk flow with the potential to reintegrate into biofilms downstream or cause the reoccurrence of disease outbreaks.

Pathogen Detection

This ability of pathogens to persist in a distribution system makes it difficult to determine whether their presence in drinking water poses an unacceptable risk to the public. It is difficult to monitor the interior surfaces of a distribution system as the current detection methods are difficult to perform, time-consuming, and expensive. Even when pathogens are detected in drinking water distribution systems, the methods currently used do not necessarily detect whether the isolated strain contains virulence factors that could cause a disease outbreak [*WSTB*, 2006].

Biofilm Trap

5The Army Research Office (ARO) awarded the Center for Biofilm Engineering at Montana State University (MSU) a grant in 2003 to examine the interactions between biofilms and microbial pathogens. This grant aimed to use biofilms in a beneficial role to

explore whether biofilms could be used in a monitoring device attached to a drinking water distribution system to trap pathogens.

This 'biofilm trap' would sample a portion of the flow going through the distribution main and develop a biofilm coating on the inside of the trap similar to that in the distribution main. If the drinking water passing through the main was contaminated with microbial pathogens, a portion of these pathogens would pass through the trap and attach within the device's biofilm coating. In the event of a disease outbreak, the biofilm trap would be easily accessible for sampling without disrupting the distribution mains and would provide a history of the microbial water quality. This trap could be used to reduce the time required to identify the causative agent of the outbreak, locate the source of the contamination, and predict the ultimate fate of the pathogen in distribution system.

Prior Research

Prior research on this topic has been performed at MSU with the same model reactors to look at the capture in porous media biofilms of microspheres as surrogate pathogens [*Goodrum,* pers. comm.] and a pathogenic strain of *Escherichia coli* 0157:H7 [*Bauman,* 2007]. All of the previous research with these reactors used peristaltic pumps to introduce the flow of water through the porous media to deliver nutrients necessary for biofilm growth and for the inoculation of microspheres or bacteria.

Prior research with flat-plate reactors [*Sharp et al.,* 2005] containing a network of micron-sized pore channels, showed flow-regime induced spatial variations in the growth of biofilm that altered the fluid flow through the reactor. The two flow regimes examined were termed constant flow (CF), which used a peristaltic pump to force water through the reactor

at a constant flow rate, and constant head (CH), which used a constant pressure gradient across the reactor to allow fluid to freely flow through the reactor at a variable flow rate.

As biofilm development occurred in the flat plate reactors, it grew from the reactor surface into the pore channels reducing the effective size of the available pore space. In the constant flow reactors this reduction in pore space resulted in a corresponding increase in fluid velocity. However in the CH reactors, this reduction in available pore space results in a reduction in fluid flow rate and velocities. This difference in flow-regime leads to spatial variations in biofilm growth within the reactors as shown in Figure 1.

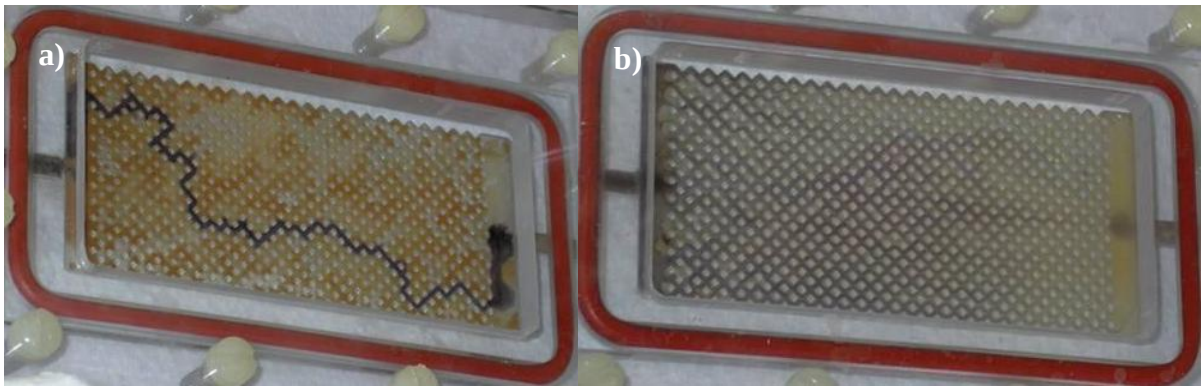

Figure 1. Flat plate reactors operated under Constant Flow (a) and Constant Head (b) flow regimes showing respective flow pattern spatial variations due to biofilm growth *(Images courtesy of Levinson, Sharp, Gerlach, and Cunningham).*

In the CF reactors, the observed biofilm growth in some pores was sufficient enough to prevent fluid from flowing freely through the pore. This causes other pores to carry an increased fluid flow and preferential channeling occurred in the reactor. These preferential channels carried the majority of the flow through the CF reactors resulting in higher fluid velocities and increased shear forces. Higher growth rates occur in the preferential channel

due to nutrient availability in the bulk fluid while the remainder of the pore spaces has lower growth rates due to limited nutrient availability. The biofilm growth continues to occur in the preferential channel until the growth closes/clogs the channel. The constant flowrate from the peristaltic pump requires the development of a new preferential channel which occurs where the biofilm/porous media matrix is the weakest. The CH reactors exhibited a more uniform biofilm growth into the pore channels resulting in a more uniform fluid flow through the reactor [*Sharp et al.*, 2005]. As a result of these observed spatial variations in biofilm growth in flat plate reactors, constant head and constant flow model reactors for this research were operated in parallel to examine the effect of flow-regime on pathogen capture.

Thesis Objective

This thesis examines two aspects of the biofilm trap project. The first examines whether a difference in operating flow regimes, and the resulting biofilm growth in the trap, will affect the pathogen capture ability of the device. Lab scale reactors are easily operated by pumping water under constant flow conditions using a peristaltic pump. An actual device attached to a water distribution main will allow water to flow through the trap because of the induced pressure gradient across the device. This difference in flow regimes results in different spatial arrangements of biofilm within the porous media trap that could affect the device's capture ability. The second aspect this thesis addresses is an attempt to determine the capture mechanism(s) of pathogens in biofilm grown on a porous media and the mechanisms of detachment that would reintroduce the pathogen back into the bulk fluid.

CHAPTER 2

LITERATURE REVIEW

Porous media refers to a fixed bed of granular material that contains pores through which a fluid may flow [*McDowell-Boyer et al.*, 1986]. Fluids in porous media often contain small suspended particles known as colloids that interact with the surfaces of the porous media. These interactions can result in the fixation of the colloid to the porous media. Temporary interactions can also occur which do not result in permanent fixation to the porous media surface but slow down, or retard, the transport of the colloid in comparison to the bulk fluid.

Many factors exist that influence the transport and retention of colloids in porous media. The following section is a literature review discussing the methods of retention and transport of colloids in the experiments performed in this study. These factors include the size ratio of the colloids to a single porous media collector, the surface properties of the porous media, the water chemistry and velocity of the bulk fluid, the concentration of colloids in suspension and their interactions with each other, and characteristics unique to bacteria that are termed biocolloids.

Porous Media

Porous media is a structure or arrangement of solids that contain interconnected void spaces, or pores, within the material. Imagine a jar filled with glass marbles of equal size as shown in Figure 2. The jar itself defines the total space the porous media occupies, the

marbles form the solid matrix, and the space between the marbles is the void space. In this case the voids are filled with air but could also be filled with water. While the all of the marbles as a whole are referred to as porous media, a single marble within the matrix would be referred to as a grain or a collector.

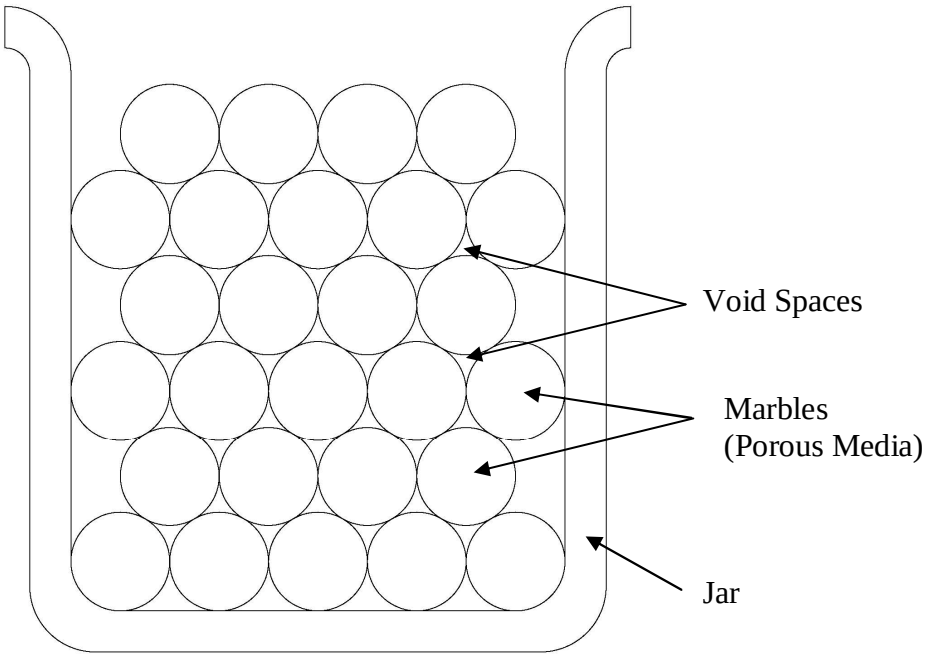

Figure 2. Simplified porous media example.

Figure 2 is a simplified example. In nature, the grains are often small enough that it becomes difficult to distinguish between the matrix and the pores with the naked eye, as in the case of soil, which is a porous media of frequent environmental interest.

While the solid matrix of a porous media remains fixed in location, a fluid can flow past the matrix through the pores. A series of connected pore spaces are referred to as a pore channel. A porous media comprised of uniformly-sized solids that are packed in a repeatable geometric arrangement would have pore channels that exhibit a uniform size and spacing.

This, however, does not commonly occur in nature as the grains comprising the solid matrix are not normally uniform in size and exhibit a random packing arrangement. The corresponding pore channels have a range of sizes, spacing, and lengths with the largest pore channels referred to as macropores and the smallest micropores.

The porous media itself is considered a relatively stable and unchanging structure. Changes that do occur to the porous media generally happen over long periods of time compared to the flow of fluid through the media. These changes include physical and chemical alterations of the media or media surface. Soils are one type of porous media and can compact over time from self-weight or from outside forces that can shift or compact the media and alter the available flow paths. The water movement itself can physically erode the surface of the porous media and redeposit this eroded material down-gradient. Interactions with the bulk fluid passing through the porous media can chemically alter the properties of the exposed porous media surface over time.

The deposition of colloids onto the media surface and the possible re-entrainment of those colloids have environmental implications that have been studied extensively. These processes have large implications for microbial contamination of drinking water supplies including the rate and extent to which that contamination will spread. The nature of the colloids and the porous media determines the transport rates and retention amounts of colloids.

Colloids

Colloids are small particles with effective diameters in the range of 1 nm to 10 μm [*Sirivithayapakorn and Keller*, 2003; *Bradford et al.*, 2002] that are carried in suspension by a moving fluid. Organic, inorganic, and microbiological colloids exist in natural groundwater systems including humic materials, mineral precipitates, iron and aluminum oxides, silicate clays, viruses, and bacteria. Naturally occurring colloids in groundwater vary in concentration from 10^8 to 10^{17} particles L^{-1} [*Bradford et al.*, 2002]. A better understanding of the mechanisms responsible for colloid transport and capture is needed to estimate the spread of groundwater contaminants, to engineer bioremediation solutions, and to protect drinking water supplies and surface water environments.

Mechanisms of Colloid Capture

As colloids pass through a porous media, some of the colloids may be retained (captured) in the media. Colloid retention in a saturated porous media is governed by three main mechanisms of deposition. These mechanisms are mechanical (surface) filtration, straining filtration, and attachment (physical-chemical filtration) [*McDowell-Boyer et al.*, 1986].

Mechanical Filtration

Mechanical filtration occurs when suspended particles in solution are too large to enter the pore channels of the filter media as shown in Figure 3 and results in the formation of a surface cake on the inlet side of the pore throat. As the surface cake thickens from the

addition of more colloids, the headloss across this cake layer increases and the permeability is reduced resulting in a decrease in flowrate.

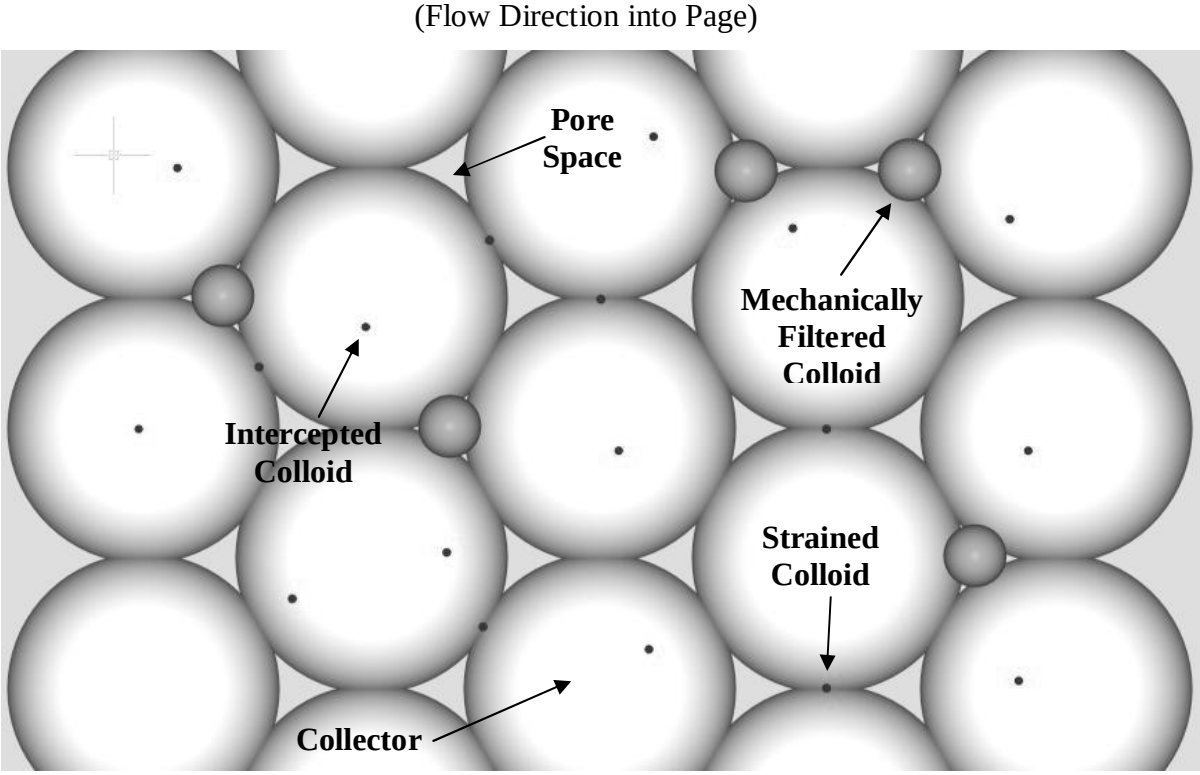

Figure 3. Porous media collectors showing mechanically filtered, strained, and intercepted colloids.

Straining

Straining filtration occurs when colloids (particles) are small enough to enter the main pore channels of a filter media yet become captured in down-gradient pore throats that are too small to allow particle passage or by crevices in the pore throat formed by grain-to-grain contacts of the filter media [*Bradford et al.,* 2002], as shown in Figure 3 and Figure 4. The extent to which straining occurs is dependent upon the ratio of the diameter of the colloid to

the diameter of the collector, or media. This ratio is defined as d_p/d_m for homogenous filter media or as d_p/d_{50} for heterogeneous filter media with d_{50} referring to the median grain size.

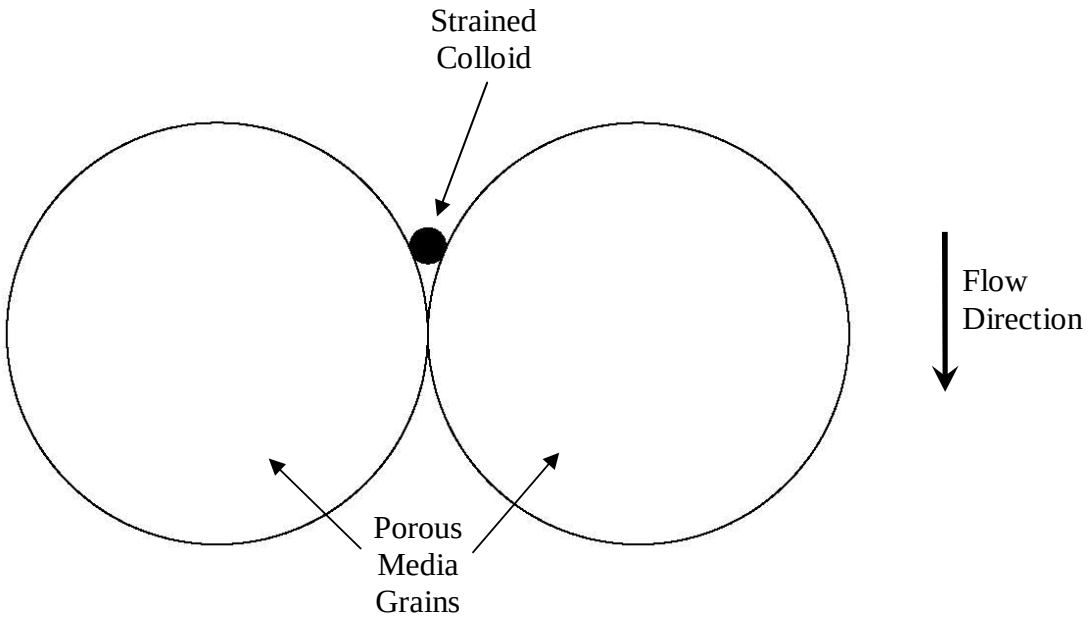

Figure 4. Straining filtration of colloid in grain-to-grain crevice of porous media collectors.

Herzig et al. [1970] considered straining from a purely geometric standpoint and determined that little straining was expected for $d_p/d_m < 0.083$. This analysis predicted that for a $d_p/d_m = 0.05$ that 0.53% of the bed volume was available for particles to be captured in crevices and this was reduced to 0.053% for $d_p/d_{50} = 0.02$. The effects of straining were originally ignored based upon these types of predictions [*Bradford et al.*, 2006]. However, recent work suggests that straining may play a more important role in colloid capture than previously thought. *Bradford et al.* [2002] suggests straining should be considered when $d_p/d_m > 0.0017$ and that it can become significant when $d_p/d_{50} > 0.005$ [*Bradford et al,.* 2005]. Straining is also a depth-dependent phenomenon with the greatest straining observed

at the inlet to the porous media or at textural interfaces within a porous media where the median grain size decreases [*Bradford et al*., 2005].

Straining can be enhanced by increasing the size of the particles or decreasing the size of the porous media collectors, both of which would increase the value of d_p/d_m. This has been shown at the pore scale with scanning electron micrograph (SEM) images by *Auset and Keller* [2006] who created flat micromodels 15 μm deep and used negatively-charged spherical polystyrene latex particles as model colloids (Figure 5). The micromodel had collectors 35 μm across and pore throats 7 to 9 μm wide that remained constant through their experiments while the size of the colloids varied from 3 to 7 μm.

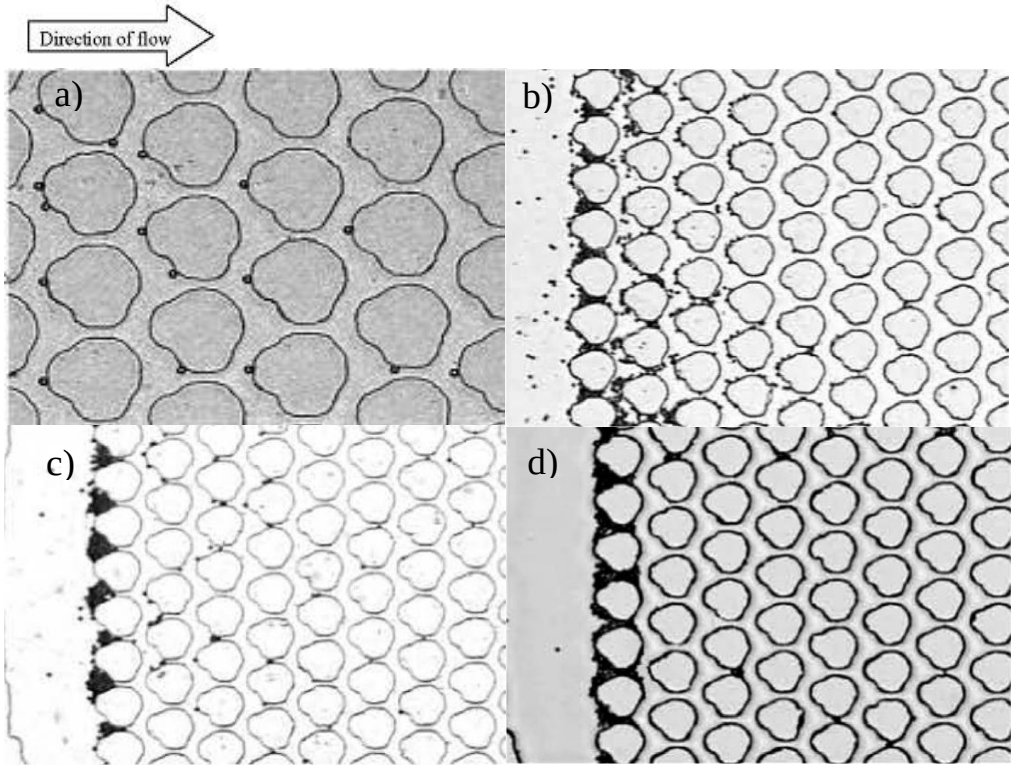

Figure 5. *Auset and Keller* [2006] images of flat micromodels showing a) interception and attachment of 3 μm colloids b) straining and attachment of 4 μm colloids c) straining of 5 μm colloids, and d) straining of 7 μm colloids.

The 3 μm colloids showed no straining behavior and particle capture occurred due to interception and attachment (discussed in the next section) with 6% capture after 120 pore-volumes. The 4 μm colloids showed an increase in capture to 51% after only 50 pore-volumes, attributed to both straining and attachment. These processes occurred simultaneously, but with notable differences in spatial orientation. Attachment occurred from the inlet to the 6^{th} row of grains while straining occurred only within the first 2 rows. The colloids captured initially by attachment at the inlet facilitated straining by decreasing the effective pore throat size, thus increased the effective value of d_p/d_m.

Straining occurred for the 5 and 7 μm colloids at the inlet of the micromodel and accounted for 95% and 99% capture, respectively, after 50 pore-volumes. With these larger colloids, straining occurred at a great enough extent to block the pore throats. With the pore throats blocked, the capture mechanism for subsequent colloids switched to mechanical filtration and a filter cake formed at the model inlet. This behavior is more predominant in the micromodel as it mainly has two-dimensional flow as compared to the three-dimensional flow that would occur in a natural system. Nonetheless, it demonstrates the transition from attachment to straining to mechanical filtration that occurs with an increasing d_p/d_m ratio.

Attachment

Attachment is a well-documented mechanism of particle capture that requires two distinct steps as described by *Yao et al.* [1971]. The suspended particle must first be transported to the solid-liquid interface of the filter media and after collision, must adhere to the media surface. Transport can occur due to interception, sedimentation, or diffusion.

Figure 3 demonstrates the difference in capture mechanisms between mechanical filtration, straining, and attachment.

Colloid Transport. The physical properties of a colloid determine how it is transported from the bulk fluid to the surface of the porous media. Fluids in a steady-state system flow in defined courses known as streamlines. However, forces from gravity, buoyancy, and drag alter the course that suspended colloids follow. The altered course that the colloid actually follows is called the pathline.

Interception occurs when a suspended colloid comes into contact with the filter media by virtue of the colloid's size. This occurs when the pathline the colloid follows carries it within at least a colloid radius away from the media surface. Sedimentation occurs when a colloid has a density much greater than that of water and the force of gravity causes the colloid to settle out of suspension and deposit on the surface of the porous media. Diffusion is the process by which a particle is randomly struck in different directions by molecules of the suspending fluid and results in random deviations from the pathline. Examples of these transport mechanisms are shown in Figure 6.

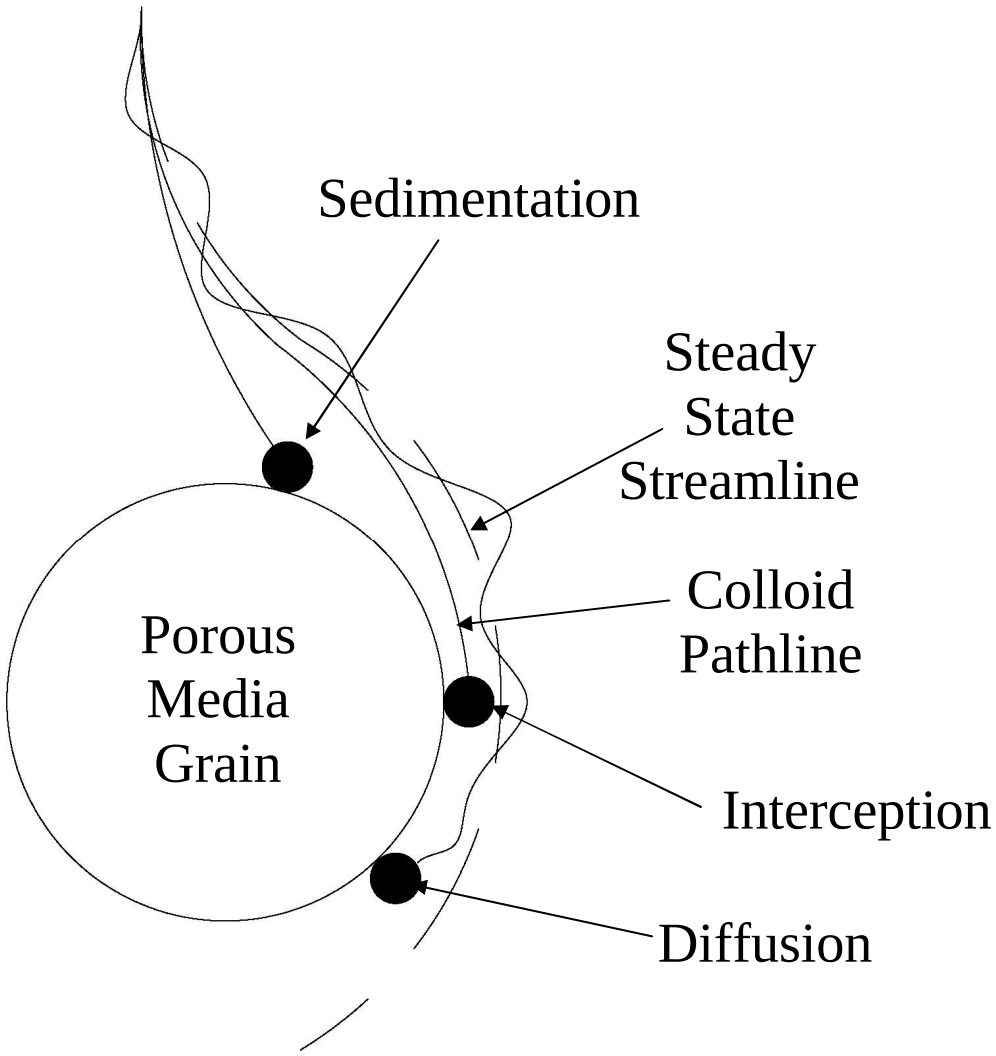

Figure 6. Colloid transport mechanisms to porous media surface.

Effect of Colloid Size. A colloid can be simultaneously affected by interception, sedimentation, and diffusion; from a transport modeling perspective these three transport mechanisms are considered to be additive [McDowell-Boyer et al., 1986], although individual mechanisms can dominate depending on the colloid size. Colloid filtration theory suggests that there is a particle size for which transport efficiency is at a minimum. This

occurs where there is a balance between transport to the collector surface by diffusion and transport by interception and sedimentation (Figure 7). This minimum transport efficiency colloid size is typically assumed to be around 1 μm [Yao et al., 1971] although McDowell-Boyer et al. [1986] propose a range of 1-5 μm. Colloids smaller than this critical size are influenced more by diffusion and the transport efficiency increases with decreasing colloid size. Larger particles are influenced more by interception and/or sedimentation and transport efficiency increases rapidly with particle size [Yao et al., 1971].

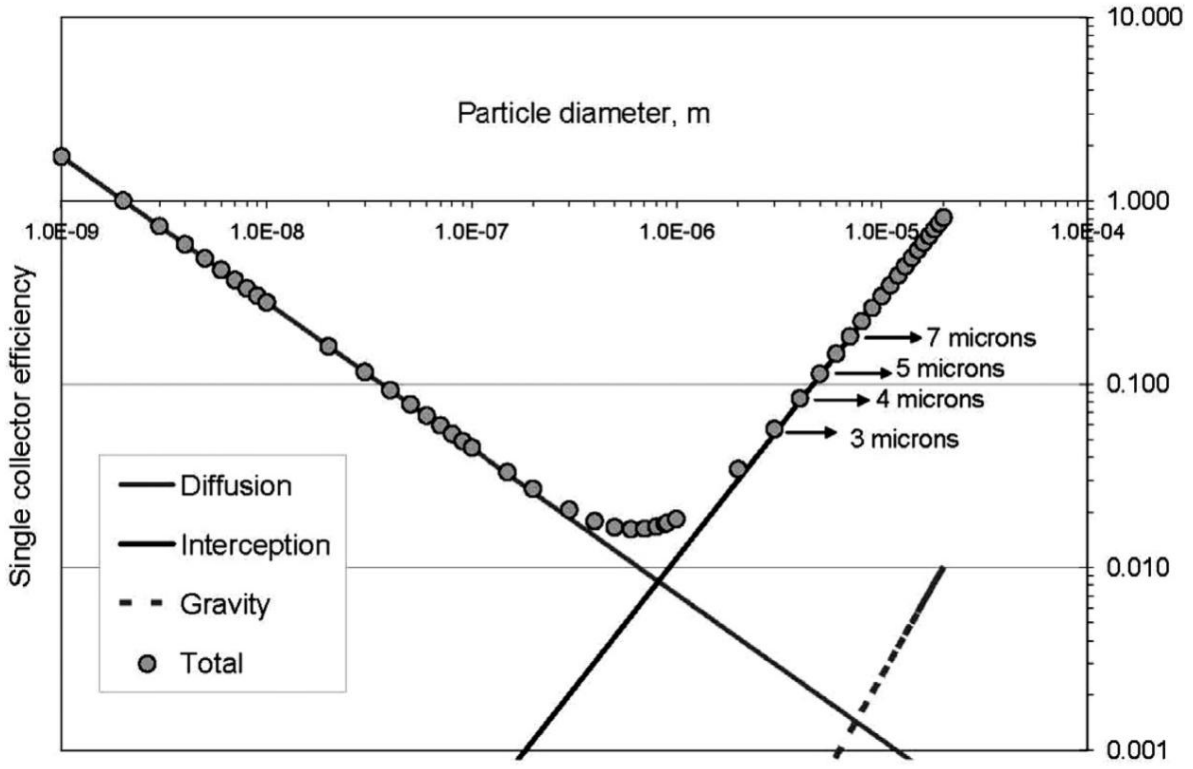

Figure 7. Single collector efficiency size graph from *Auset and Keller* [2006] showing the combined effects of diffusion, interception, and sedimentation (gravity) based on particle size (particle density (ρ_p) = 1,050 kg/m^3).

Colloid Attachment Force Balance. After a colloid is transported to the solid-water interface of the collector, a force and torque balance acting on the colloid must be evaluated to determine whether attachment occurs. The forces considered are gravity and buoyant forces, fluid drag, electrostatic interactions, and London-van der Waals interactions. While particle inertia is important in aerosol filtration, it is assumed to be negligible in water.

As the colloid approaches the collector surface from the center of a pore it enters a zone where fluid flow decreases from maximum velocity in the pore space to zero velocity (no slip condition) at the collector surface. This gradient in velocities across the colloid creates an imbalance in shear forces on the colloid resulting in an applied torque [*Cushing and Lawler*, 1998]. For attachment to occur, the forces from electrostatic and London-van der Waals interactions have to be stronger than the shear forces and torques applied to the colloid by the bulk fluid flow.

Gravity and buoyant forces are increasingly important as the density of the colloid deviates from that of water. For colloids with densities close to that of water (such as bacteria), the effects of gravity and buoyant forces are small and often times neglected from a modeling perspective.

Electrostatic interactions occur between a charged particle and a charged media surface are the main force that controls attachment [*McDowell-Boyer et al.*, 1986] and can be attractive or repulsive dependent upon the charges of the particle and media surface. London-van der Waals forces are the result of attractive forces from dipole-dipole attractions that occur at the atomic level [*McDowell-Boyer et al.*, 1986] and are not as strong as electrostatic interactions.

Double Layer & Ionic Strength. Electrostatic charges on the surface of media and particles are neutralized in an aqueous environment by the accumulation of oppositely charged ions in solution. The electrostatic attraction of these counter ions forms a diffuse electric double layer close to the surface where the concentration of ions is greater than that in the bulk fluid [Stevik et al., 2004]. This concentration of ions can mask the particle or media surface charge at sufficient separation distances [McDowell-Boyer et al., 1986].

Derjaguin, Landau, Verway, and Overbeek modeled the attractive and repulsive forces between particles and media surface and developed the double layer theory (DLVO). This theory assumed that particle attraction would occur over a short distance (< 1 nm) called the primary minimum and a long distance (5-10 nm) called the secondary minimum. Located between these two minima is a zone of maximum electrostatic repulsion [*Stevik et al.,* 2004]. The thickness of the double layer is inversely proportional to the ionic strength of the bulk fluid. Increasing the ionic strength decreases the thickness of the double layer and forces the secondary minimum closer to the media surface and the particle surface. This allows colloids to approach closer to the media surface.

Adsorption, Desorption, and Adhesion. A thick double layer could prevent a colloid from attaching to the porous media surface. However, compressing the double layer may allow a particle to come close enough to the media surface that the London-van der Waals attraction can overcome the repulsion barrier [Stevik et al., 2004] and attach the particle to the media surface in the secondary minimum. This attachment is the result of a weak interaction that could be reversible and in some literature is referred to as unfavorable attachment or adsorption. Theoretical analysis predicts that a particle may be retained in this

secondary minimum only under very low fluid velocities [McDowell-Boyer et al., 1986]. Particles placed into the primary minimum involve a larger amount of energy and create a stronger bond referred to as adhesion or favorable attachment. This commonly occurs when a negatively charged colloid comes into contact with a positively charged media surface and the attraction energy is large enough to place the colloid in the primary energy minimum [Stevik et al., 2004]. Nevertheless, if the shear force on the particle is large enough, it can detach a particle from the media surface and return it to the bulk fluid. This process is known as desorption or detachment.

Factors Affecting Colloid Capture

There are many factors that influence whether a colloid is transported to the surface of a collector and captured. These factors include the velocity and water chemistry of the bulk fluid, the shape, surface roughness, and surface charge of the porous media, interactions with previously attached colloids, the concentration of the colloids in the bulk fluid, and unique characteristics of bacteria, or biocolloids.

Bulk Fluid Velocity. The capture of colloids in porous media is inversely related to the flowrate of the bulk fluid. An increase in flowrate results in an increase in flow velocity of the fluid through the porous media. However, this is not a proportional increase in flow velocity in all of the pore networks as the increased flowrate is preferentially carried in macropores. This can also be viewed as a relative decrease in the proportion of flow carried by the remainder of the pore channels. An increase in flowrate also results in a shorter contact time for a colloid on a collector and increases the shear forces on the colloid. Pore

exclusion reduces the amount of porous media surface area utilized and increases the distance between a colloid and a collector. Thus an increased flowrate reduces colloid capture as a result of these effects.

Porous Media. The nature of the porous media can have a significant effect on the capture of colloids. The size, shape, and surface roughness of the collectors all influence colloid capture. As collector size decreases and/or surface roughness increases, the surface area per unit volume (L^2/L^3) available for colloid capture increases. A rough surface also provides capture locations that can shelter the colloid from the bulk fluid shear that would normally detach the colloid from a smooth collector.

This increased capture by rough media surface has been shown by *Auset and Keller* [2006] using micromodels and small colloids. Attachment was the dominant capture mechanism rather than straining or mechanical filtration. Both smooth and rough versions of their micromodels were created to investigate the affect of surface roughness on capture. The smooth micromodels' collectors were 35 μm across with surfaces nearly perpendicular to the micromodel base resulting in uniform pore throats 7 to 9 μm wide. The rough micromodels' collectors contained protrusions and rippled walls resulting in pore throats that were 6 to 8 μm wide at the base and 15 to 20 μm wide at the top (Figure 8).

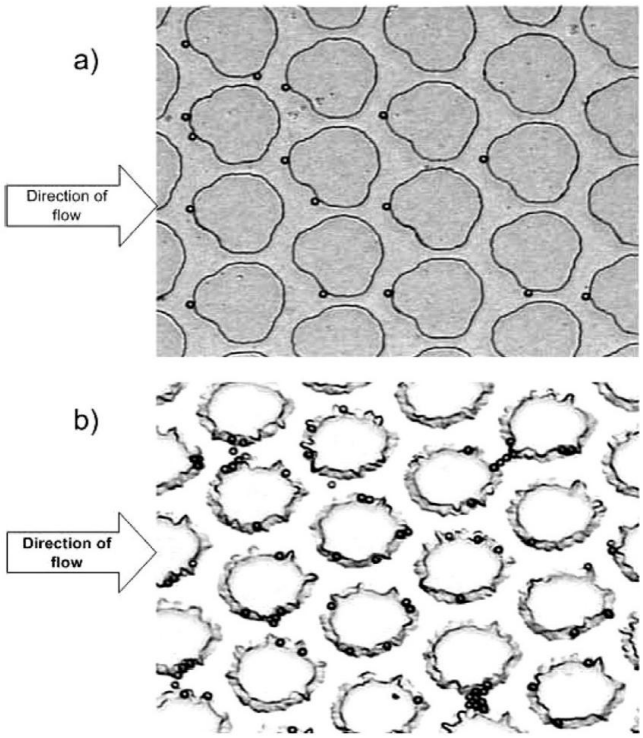

Figure 8. Images by *Auset and Keller* [2006] of 3 μm colloid attachment in a) smooth micromodels and b) rough micromodels.

In the smooth micromodel, all of the capture occurred at upstream locations with the majority of it occurring at stagnation points due to flow bifurcation. Anytime a colloid was observed being transported to the downstream side of a collector it was sheared off before attachment could occur. The rough micromodel showed capture occurring all around the collector in recessed alcoves provided by the protrusions and rippled walls that sheltered the colloid from shear forces. The rough micromodel also had collision efficiencies 3 times higher than the smooth micromodel for the 3 μm colloids and 2 times higher for the 4 μm colloids. This is attributed to the effect that surface roughness has on fluid hydrodynamics.

Surface Charge. Solid surfaces that comprise porous media collectors in natural systems often have a net negative surface charge. The presence of clays, organic matter, and charged molecules in the porous media affects colloid capture as it can alter the surface charge of the porous media. Clay particles can influence the adhesion of other colloids due to their small size, platy shape, large surface area per unit volume, and positively charged groups on the edge of the clay crystal lattice that facilitate electrostatic adhesion. Oxide coatings, such as iron oxide, can make the surface charge of the porous media more positive which lends itself to more favorable attachment with negatively charged colloids.

Blocking and Ripening. When attachment theories were originally developed, the assumption made was that a colloid in the bulk fluid was attaching to a clean collector. In reality, this is rarely the case as colloids in the bulk fluid interact with both the porous media collectors as well as any colloids that are already attached to the collector surface. Attachment will be enhanced when previously attached colloids are favorable sites for subsequent colloid attachment. This behavior is known as ripening. Conversely, if colloids that are attached already occupy the favorable sites and are not suitable for subsequent attachment themselves, this is known as blocking and diminished attachment will be observed. As a result of blocking and ripening, time dependent attachment rates arise due to different behaviors between clean media and media that already contain attached colloids [Bradford et al., 2005].

Colloid Concentration. The concentration of colloids in suspension can affect the amount of capture observed in porous media. Bradford et al. [2005] investigated this by

examining the transport and capture of negatively charged 1.0 and 3.2 □m carboxyl latex colloids when passing through porous media comprised of 150, 240, or 360 □m quartz sands. The input concentration of colloids was varied at 2.0, 1.0, 0.5, and 0.25 times a reference concentration. The pulse duration for each concentration was altered such that the total mass of colloids introduced into the porous media remained constant. These experiments showed that the lower input concentration resulted in a greater colloid mass retention in the porous media.

This behavior is the opposite of that observed when the colloid used is a bacterial cell where the rate of attachment has been suggested to increase linearly with the cell concentration. It has been observed that the number of attached cells has increased with bacterial concentration up to the point where the collector surfaces become saturated. An increased concentration of bacteria has been shown to increase the number of collisions that occur with the media surface which results in more opportunities for bacteria to attach [*Stevik et al.*, 2004]. The capture differences observed between inert colloids and bacteria may be due to differences in blocking and ripening behavior that occur, as well as some advantages for surface attachment that living organisms possess that inert colloids do not.

Biocolloids

When the colloid in consideration for capture is a bacterial cell, it is referred to as a biocolloid. Bacteria vary in size, shape, and surface charge. Biocolloids have many characteristics that can facilitate or hinder capture that an inert colloid does not possess.

Bacteria also vary in motility, number and type of appendages, and hydrophobicity. Bacteria can secrete polymers outside their cell walls which aid in the attachment to a collector.

Size and Shape

Size and shape varies widely among different species of bacteria. *Abedon* [1998] provides a review of the extreme variability found among bacteria. Some of the smallest are 100 to 200 nm in diameter, which is around the size of the largest viruses. Some of the largest are big enough for a single cell to be visible by the naked eye. The cyanobacterium *Oscillatoria* is roughly 7 μm in diameter which is the same as a red blood cell. Spirochetes have been found to reach lengths of 500 μm. However, an average size is around 1.1 to 1.5 μm wide by 2.0 to 6.0 μm long. It is important to note that this size for an average bacterium places it in the minimum transport efficiency range as discussed previously.

The size of a bacterial cell is important to capture, but so is the general shape of the cell. *Salerno et al.* [2006] demonstrated a shape effect with latex microspheres that had different aspect ratios (length:width). Microspheres were used in their experiment as the surface properties of this model colloid are more easily controlled. The 1.0 mm spherical polystyrene latex microspheres were heated, stretched to a desired aspect ratio, and then cooled quickly. The surface characteristics of these stretched microspheres were checked and found to be unchanged. An increase in aspect ratio from 1:1 to 2:1 resulted in an increased collision efficiency by a magnitude of 8.6 times. The 3:1 microspheres showed an increased collision efficiency by a magnitude of 24 times over the 1:1 microspheres. From this it can be concluded that rod-like colloids will be captured at a greater rate than spherical colloids with the same volume and surface properties.

Bacteria display as much diversity in their shapes as they do in their range of sizes. The three major shape classes are cocci (spherical), spiral, and bacilli (rod) and the most common bacterial shape is the rod. In addition to the basic rod shape, sub-variations of the rod exist such as the tapered rod, staff, cigar, oval, or curved rod. In addition to the individual cell shape, the behavior of bacteria after they undergo cell division plays a role in the shape of groups of bacteria found in nature. Some bacteria separate into individual cells after they divide, others can be found in pairs, chains, groups of four forming squares, or groups of eight forming cubes and some remain in unstructured sheets or clumps [*Abedon,* 1998].

Some bacteria display the same general shape all the time, but others do not. Monomorphic bacteria tend to display the same shape regardless of environmental or physiological conditions. Polymorphic bacteria can display different shapes depending on their environmental or physiological conditions and some even display differences within the same culture [*Abedon,* 1998].

Cell Surface Charges

Bacterial cells have surface charges that can affect their ability to attach to a porous media surface. The dissociation of carboxyl and amino groups on the outer surface of the bacteria cause these electrostatic charges. Most bacteria found in a natural environment with a pH around neutral possess a net negative surface charge. This negative charge in combination with the negative charge found on most porous media surfaces create a repulsive force between the two resulting in unfavorable attachment conditions. While the

net charge on most bacteria is negative, many of them possess appendages which are positively charged [*Stevik et al.* 2004] and can increase capture.

Cell Structure Appendages

Many bacterial cells possess filamentous appendages that extend outward from the cell surface such as flagella, fimbriae, and pili. These structures increase the effective diameter of the bacteria cell and can facilitate the attachment of bacteria to the porous media surface. An increased effective cell diameter alters the repulsive effects experienced between the cell and the zone of maximum repulsion on the collector located between the primary and secondary minimum of the double layer. From the DLVO theory, the double layer is on the order of nanometers thick while many cell appendages are on the order of micrometers long. This order of magnitude difference allows the electrostatic barrier to be penetrated by the cell appendages more effectively [*Stevik et al.,* 2004] without the cell itself being close enough to the porous media surface to experience repulsive forces.

Fimbriae and pili are around 10 nm in width and generally between 0.2 and 1.5 μm in length [*Duguid et al.*, 1966]. They are structurally similar to each other and the names are used interchangeably in some literature, however there are some differences. Generally only a few pili are found on the surface of bacteria [*Brock*, 2003] and are often used for the transfer of DNA between mating bacterial cells. Fimbriae are commonly found on Gram-negative, but can also be found on some Gram-positive bacteria. They are shorter than pili and more numerous with bacteria frequently containing several hundred fimbriae distributed uniformly around the cell. Fimbriae are also believed to play an active role in the attachment of the bacterial cell to a surface [*Todar*, 2004]. *Duguid et al.* [1966] examined 1,453

different strains of *Salmonella* and discovered that the presence of fimbriae was dependent upon factors such as the growth stage and rate. Fimbriae typically were not present during the log stage of growth but appeared after 24 to 48 hours when the bacteria were in the stationary growth phase.

A bacterial flagellum is about the same diameter as a pilus or fimbria but significantly longer and is usually associated with motility. Flagella are only 10 to 20 nm wide but can be upwards of 15 to 20 μm long [*Stevik et al.,* 2004], which would be rather significant on an average bacterial cell that is 2.0 to 6.0 μm in length. Flagella are helically shaped and rotated like a propeller by a motor that is anchored in the cell wall.

Bacteria may have none, one, or many flagella and the arrangement of flagella around the cell varies. In polar flagellation, a cell has flagella that are attached at one or both ends of the cell. When a group of flagella are all attached at one end of the cell this is called lophotrichous flagellation. Bacteria can also display peritrichous flagellation when the flagella are attached all around the cell surface [*Brock,* 2003]. The type of flagellation a bacteria cell has will result in different types of motility and affect capture.

Motility

Bacteria that can move are called motile, while those that cannot are called non-motile. While the presence of fimbriae on some bacteria can be responsible for an observed twitching motion [*Todar,* 2004] the main source of motility for bacteria is the presence of a flagellum [*Stevik et al.,* 2004]. Flagellar rotation can result in bacteria moving at speeds upwards of 60 cell lengths per second (~ 48 μm/sec) through a liquid media. Peritrichously flagellated bacteria usually move slower in a straight line, while polarly and lophotrichously

flaggelated bacteria are more rapid and random in direction, appearing to dart from one location to the next [*Brock*, 2003]. Motile bacteria have a better chance of penetrating electrostatic repulsive forces and contacting a possible attachment surface [*Stevik et al.*, 2004].

Some bacteria that are filamentous or rod-shaped lack flagella but are still motile. These bacteria cannot swim in the bulk fluid but are capable of "gliding" along a solid surface at speeds upwards of 10 μm/sec. A specific gliding mechanism has not been identified but it is suspected to occur through the secretion of a polysaccharide slime or the ratcheting of proteins located in the cell wall [*Brock*, 2003]. Movement mechanisms such as these clearly do not play a role in the initial capture of a bacterial cell from the bulk fluid, but could occur afterwards and have implications in the location that a cell is observed on a collector if sufficient time has lapsed since the capture occurred.

Korber et al. [1994] evaluated the effect that flagellum-induced motility had with respect to the ability for two strains of *Pseudomonas fluorescens* to attach to the surfaces of glass flow cells. One strain of this organism was motile (Mot^+) while the other strain was nonmotile (Fla^-). Both of these strains had identical growth rates ($\mu = 0.49$) when grown planktonically or attached. They found that the Mot^+ strain attached approximately 2.8 times more rapidly than the Fla^- strain during a two hour competitive attachment assay. The saturated attached cell density was also compared for these two strains. It was determined that the Mot^+ strain had a saturated cell density approximately 3.6 times greater than that of the Fla^- strain. The authors concluded that the possession of a functional flagellum allowed the motile strain to colonize locations that were inaccessible to nonmotile cells. It has been

shown that particles attached on a surface inhibit subsequent deposition of further particles in their immediate vicinity and the authors conclude that this blocking behavior may be responsible for creating the inaccessible sites that nonmotile cells could not colonize.

Korber et al. [1994] also used a heat treatment to impart the Mot^+ strain with a nonfunctional flagellum and subjected the Fla^- strain to the same treatment for use as a control. The attachment of the treated Mot^+ strain was identical to that of the treated and untreated Fla^- strains. From this the authors concluded that active flagellar motility, and not the flagellum itself, was responsible for the increased attachment of the motile strain. Another interesting observation by *Korber et al.* [1994] was that the Mot^+ strain was frequently observed undergoing rotational movements after initial surface contact and frequently exhibited reversible attachment. On the contrary, the Fla^- strain showed very little observable movement after the initial surface contact and quickly became irreversibly attached. These observations would suggest that while the possession of a functional flagellum increases the likelihood of a cell reaching a surface and attaching, that the possession of this same flagellum is also responsible for cell movements leading to detachment events.

Hydrophobicity

Stevik et al, [2004] covered hydrophobicity in his review and reported that the capture of bacteria is also influenced by the nature in which the cell interacts with water. Non-polar molecules are repelled by water and called hydrophobic, while polar molecules are attracted to water and called hydrophilic. The degree of hydrophobicity a cell exhibits is influenced by its growth phase and growth rate. Increased hydrophobicity has been observed during

exponential growth. While electrostatic interactions are the main mode of attachment of hydrophilic bacteria, hydrophobicity is the dominating force in hydrophobic bacteria, regardless of the cell's surface charge. It is also important to note that pili are hydrophobic, which may be why they aid in the attachment of a cell.

Biofilm

When a bacterium first contacts a collector surface it is typically considered to be adsorbed or reversibly attached. Adhesion then occurs if the bacteria remains adsorbed for enough time and the cell can excrete polymers to form a bridge to connect the cell to the surface [*Stevik et al.,* 2004]. This cell is then irreversibly attached. Biofilms begin to form when bacteria attached to a surface form these polymer bridges connecting the bacteria to the surface and to each other. The biofilm then grows and develops into a complex, three-dimensional, attached community. The polymers secreted by the cells are molecular strands known as extracellular polymeric substances (EPS) [*Cunningham & Ross*, 2007].

According to *Omoike and Chorover* [2004], EPS is a complex mixture of macromolecular polyelectrolytes including polysaccharides, proteins, and nucleic acids with a composition that depends on growth phase and solution chemistry. This mixture mediates cell adhesion through interfacial processes including covalent or ionic bonding, dipole interactions, steric interactions, and hydrophobic associations. It is also believed that free EPS, which is transported in the bulk fluid but no longer attached to a bacterium, may adsorb to porous media surfaces creating a "conditioning film" before cell attachment occurs. This

conditioning film would alter the surface characteristics of the collector and make attachment more favorable.

The presence of a biofilm on a collector has the ability to improve capture of subsequent bacteria or colloids. The biofilm will enhance attachment due to the adhesive nature of the EPS. The growth of biofilm from the collector surface into the pore channel also decreases the effective size of the pore throat which will facilitate straining of colloids and biocolloids.

Literature Review Conclusions

Colloid transport and capture in porous media has been studied extensively in the past. This previous research has greatly enhanced the general knowledge of how colloids interact with the porous media and what factors effects this interaction in respect to transport and capture. Much of this research has been performed to model and understand the interactions between colloids transported through soil. In an effort to study the effect of one parameter, the model systems have been simplified and often consist of well-defined porous media. However, little research has been conducted to understand how naturally occurring biofilms on the surface of the porous media affect the transport and capture of colloids. Further research is needed to understand how colloids interact with biofilms in this setting.

CHAPTER 3

MATERIALS AND METHODS

This chapter details the experimental design for the operation of the model reactor used in the experiments, and the analytical methods used to evaluate the experimental data. The experimental design gives an overview of the research performed. The reactor design provides details of the construction of the reactor, its assembly, and preparation for use. The reactor operation and sampling details the plumbing used for the two flow regimes studied and the preparation of the reactor feed water. It also contains the methodology used to monitor the reactor during biofilm growth, conduct a non-reactive tracer study, inoculate a reactor with a model pathogen, sample the reactor, and enumerate the breakthrough and capture of the pathogen.

Experimental Design

The central focus of the research performed was to determine the extent of capture that occurs when a spike dose of a pathogenic bacteria is introduced to the water flowing through a saturated porous media. The porous media consisted of glass beads packed within a cylindrical reactor as shown in Figure 9. The capture and bacteria was examined in clean reactors that were uncolonized as well as colonized reactors, which had been allowed to operate for sufficient time that a mixed species biofilm developed on the surface of the porous media.

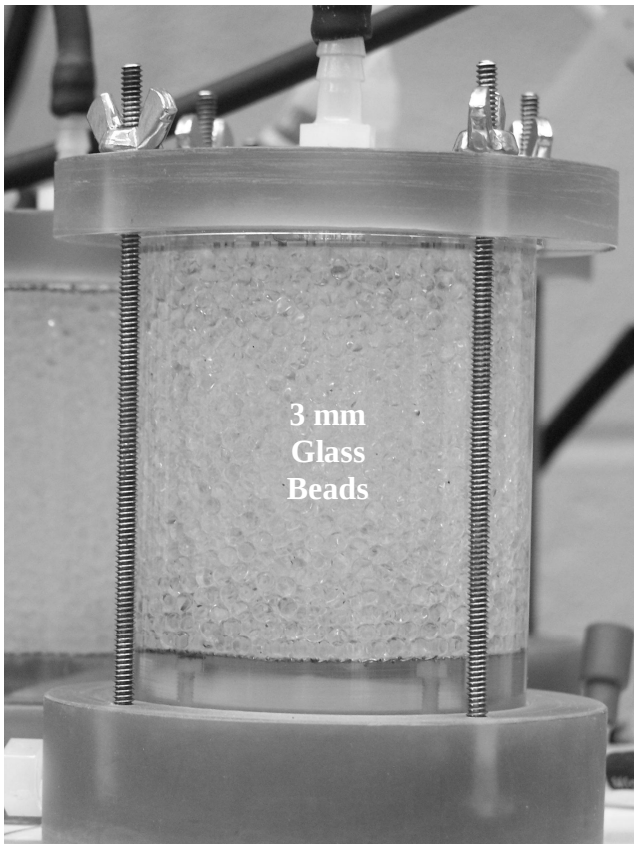

Figure 9. Porous media model reactor.

The results and methodology developed in previous experiments at MSU [*Goodrum*, pers. comm.; *Bauman*, 2007] served as the initial framework for the research conducted and were modified as needed to fit the experiments performed. All of the previous research with these cylindrical reactors water was pumped through the porous media to deliver nutrients necessary for biofilm growth and for the inoculation of bacteria. The preferential channeling that was observed in flat-plate reactors [*Gerlach*, pers. comm.] was likely occurring in these cylindrical reactors used for pathogen capture. This phenomenon would reduce the surface area available for capture in the constant flow reactors.

It was hypothesized that using a constant head flow-regime would better utilize the porous media surface area and result in increased pathogen capture. To test this hypothesis, separate reactors were operated under constant flow (CF) and constant head (CH). The CH reactors would start at a flow rate greater than the CF reactors. As biofilm growth occurred in the CH reactor, the flowrate through the reactor would diminish.

The reactors were allowed to continue to run until the CH flowrate was approximately the same as the CF flowrate (Figure 10). At this point in time, the CH reactor would be inoculated with a spike dose of the pathogen. The effluent water would be collected to evaluate the breakthrough of the pathogen, and the reactor would be sampled to determine the amount of capture that occurred in the porous media. This process was run in parallel for the CF reactor.

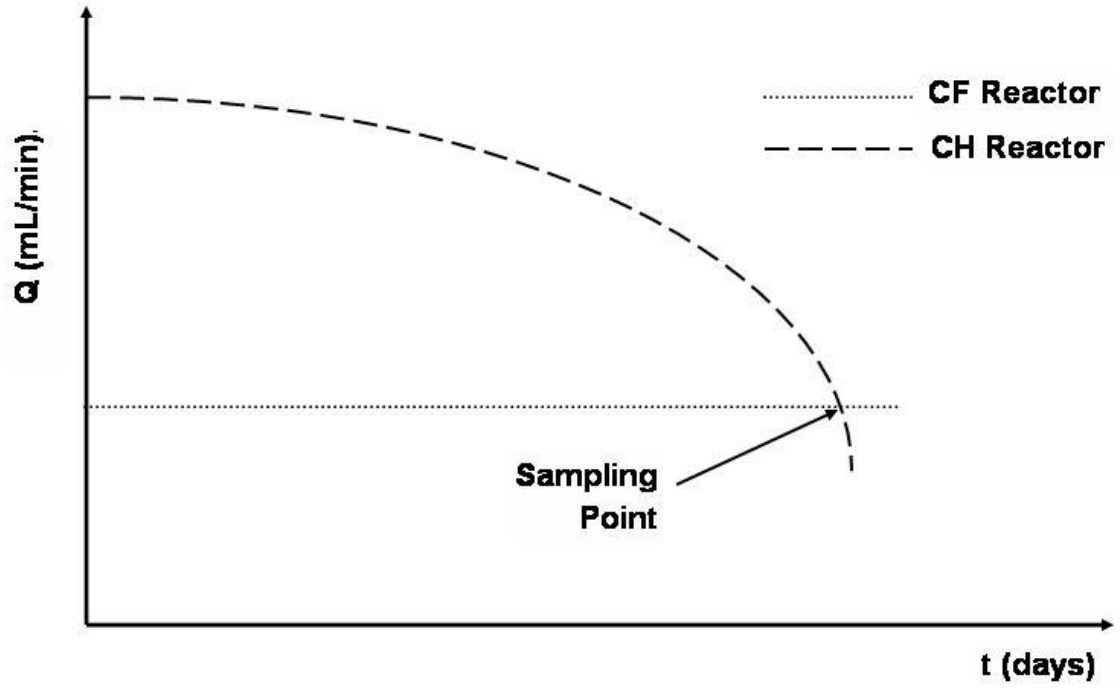

Figure 10. Constant flow and constant head flowrates and sampling point.

Reactor Design

The model reactor used for these experiments was a cylindrical polycarbonate reactor (7 cm in height and 5.7 cm in diameter) designed by researchers at MSU and manufactured by the University's Technical Services Engineering Department. The reactor is filled with 3 mm borosilicate glass beads (Chem Glass, Inc. CAT # CG-1101-02) with a random packing arrangement to comprise the porous media. The glass beads were autoclaved for 30 minutes and then baked at 550° C for 5 hours prior to packing. The number of beads placed into each reactor was determined by mass with 218 ± 0.02 grams of beads being poured into the reactor. While the packing arrangement of the beads was random, the reactors consistently had a porosity of around 0.43. The calculated porosity was the ratio of the fluid volume above the lower screen in a packed reactor and an empty reactor. The reactors influent and effluent ports were wrapped in aluminum foil and the assembled reactors were autoclaved for 30 minutes. This ensured that all reactors contained sterile interior surfaces prior to use.

A schematic of the reactor is shown in Figure 11. The reactor base contained a conical mixing chamber with a magnetic stir bar spinning at 200 rpm in the direction opposite of the influent water which facilitated even mixing of the influent water. A stainless steel screen was placed above the stir bar to support the glass beads, and a second stainless steel screen was placed above the packed beads to prevent fluidized beads from clogging the effluent port. The reactor lid rested directly on top of the second screen. Both the reactor base and lid had a recessed groove for a gasket to create a water-tight seal with the cylindrical reactor. Four threaded tension posts were anchored in the reactor base and

extended through the lid such that wing nuts could provide confining pressure to ensure the reactor was water-tight and to prevent the 3 mm glass beads from shifting during operation.

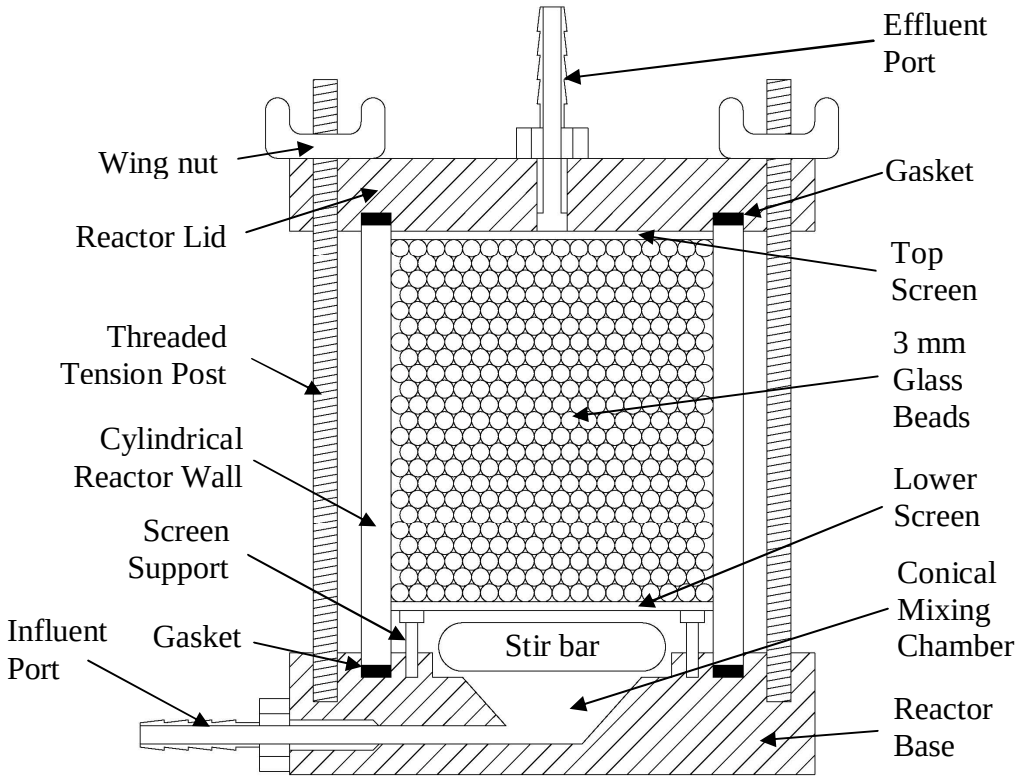

Figure 11. Model reactor schematic.

The fluid volume of the assembled reactor base below the bottom screen was 20 mL. The pore-volume of the actual porous media between the bottom and top screens was 68 mL. The reactors were operated in an upflow mode with a horizontal influent port placed into the bottom of the mixing chamber and a vertical effluent port centered in the reactor lid. Running the reactors in an upflow mode allowed any air bubbles that formed from off-gassing to work their way out of the reactor instead of becoming trapped which would result in partially unsaturated flow conditions.

Reactor Operation Conditions and Sampling Procedures

This section details the construction and operation of an elevated reservoir for the constant head reactors, the operating parameters for the constant flow reactors, the monitoring performed on the reactors during their operation, the criteria used to determine sampling dates, the preparation of reactor feed water to promote biofilm growth, the preparation of a planktonic bacterial culture for reactor inoculation, the pathogen capture sampling protocol, and the non-reactive tracer sampling protocol.

Reactor Plumbing and Flow Regimes

As the goal of this research was to investigate differences in capture that occur due to spatial variations in biofilm growth between constant flow (CF) and constant head (CH) flow regimes, an elevated reservoir was required for the CH reactor. This reservoir consisted of a capped 4-inch PVC pipe necked down to a 3-inch PVC pipe. A schematic of the reservoir is shown in Figure 12. The 4-inch cap contained a centered influent port with 8 effluent ports arranged radially around it. An overflow port was installed in the side of the 3-inch PVC pipe approximately 5 inches below the top of the reservoir. A peristaltic pump delivered effluent water from a biologically activated carbon (BAC) filter column to the influent of the reservoir at a constant rate of 250 mL/min. A second peristaltic pump delivered concentrated carbon stock from the sterile 20 L carboy to a T-fitting in the influent BAC line approximately 4 inches before the reservoir influent at a constant rate of 0.85 mL/min. Sufficient feed water was pumped into the reservoir such that the water remained constant at

the level of the overflow port. This constant water level created a constant pressure head in the reservoir and the attached CH reactors.

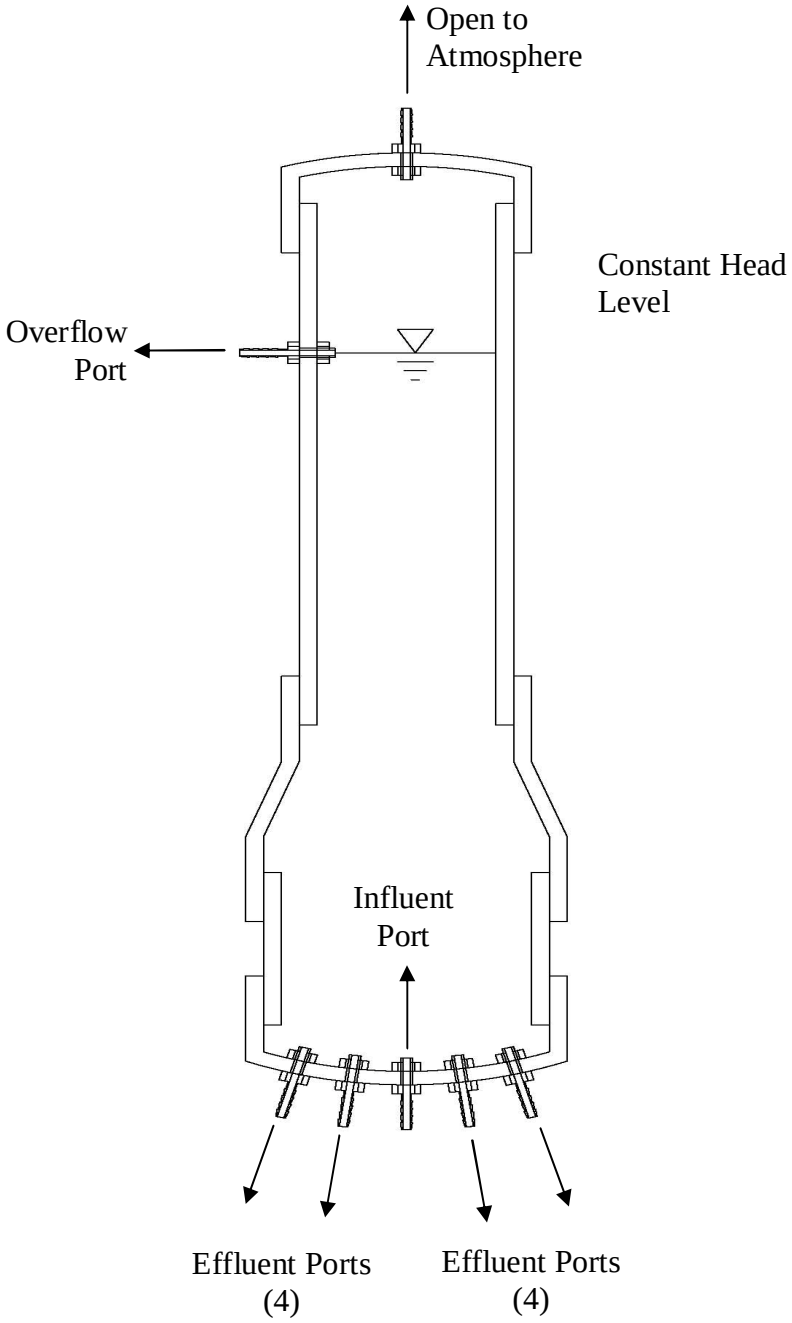

Figure 12. Constant head reservoir schematic.

A full experimental flow schematic is shown in Figure 13. An assembled reactor was placed on a magnetic stir plate and Norprene® tubing (Masterflex CAT # 06404-16) connected the influent port on the reactor to the effluent port of the elevated reservoir. The effluent port on the reactor was connected to the bottom of an elevated T-fitting. Tubing (Masterflex CAT # 06402-17) was connected to the side of the T-fitting that extended back down to a common effluent collection basin. The top of the T-fitting and was open to the atmosphere to prevent a siphon-effect from pulling water from the reactor. The elevation of the effluent T-fitting could be varied and set the pressure head on the effluent end of the reactor. The elevation difference between the reservoir overflow port and the effluent line T-fitting set the constant pressure gradient driving the flow of carbon-enriched BAC water through the CH reactor.

In order to use the same water in the CF reactor as in the CH reactor, a third peristaltic pump was attached to one of the reservoir effluent ports with Norprene® tubing. This peristaltic pump delivered reservoir water to the CF reactor at a constant flow of 25 mL/min. CH reactors were run under two operating pressure heads, 0.5 feet (0.22 psi, 1.49 kPa) and 1.0 feet (0.43 psi, 2.99 kPa). These selected pressure heads resulted in initial flowrates in excess of the 25 mL/min in the CF reactors. As time progressed, the mixed-species heterotrophic bacteria from the BAC column colonized the reactors and developed into a biofilm. The formation of the biofilm in the porous media constricted the size of the pore channels, increasing the headloss across the reactor, and decreasing the flowrate through the reactor.

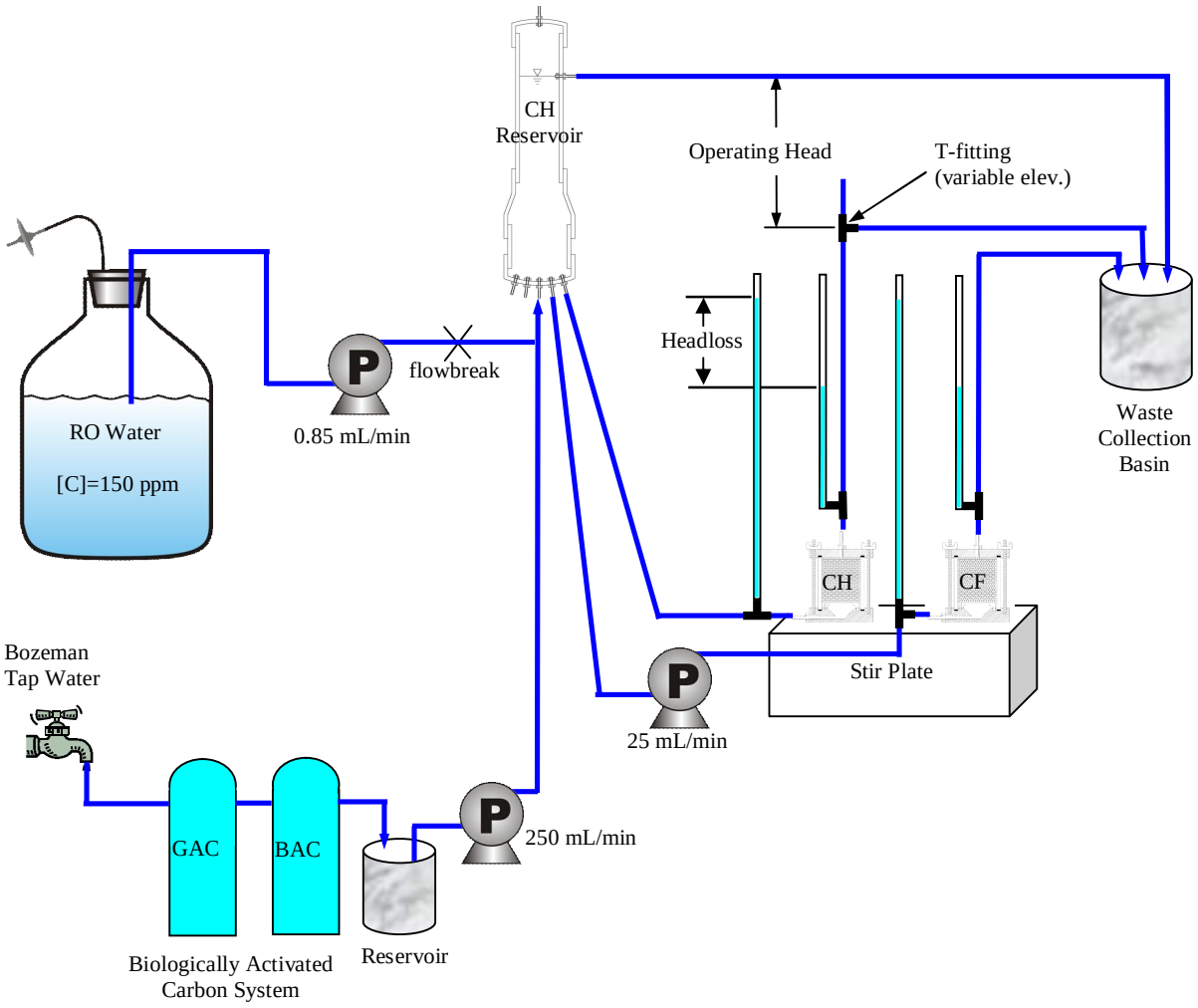

Figure 13. Overall experimental flow schematic of constant head (CH) and constant flow (CF) reactors operating in parallel.

Clear tubing (Masterflex CAT # 96400-15) was connected directly before the reactor influent port and after the effluent port and extended vertically to serve as manometers. This was used to monitor the pressure on the influent and effluent sides of the reactor as water would rise up into the clear tubing to a level equivalent to the pressure. The difference in elevation between the influent and effluent lines was used to monitor the headloss across the reactor. Headloss and flowrate measurements were collected on a daily basis.

For these experiments the CF reactors operated at 25 mL/min. To limit the effect that variations in flowrate would have upon capture, this flowrate was also the target sampling flowrate for the CH reactors. When the flowrate in the CH reactor dropped to approximately 25 mL/min, it was then inoculated with a spike dose of pathogens. The number of days the CH reactor was allowed to operate and develop biofilm on the porous media before inoculation varied depending on how quickly the reactor fouled thus reducing the flowrate to the target rate.

Due to the amount of time required to inoculate and sample a reactor, the CH and CF reactors could not be sampled on the same day. Given the fouling rate of the CH reactor setting the duration of the experiment, this reactor had to be sampled first and the CF reactor would be sampled the subsequent day. To be able to compare the pathogen capture between the CH and CF reactors the same time period of operation was chosen. As the CF reactor was sampled one day after the CH reactor, the CF reactor was started one day after the CH reactor. In addition to the colonized test reactors, clean control reactors were inoculated and sampled to quantify the increase in capture by the biofilm over clean porous media. Table 1 outlines the experiments performed during this research and their operating parameters.

Table 1: Reactor Operating Parameters

Number	Type	Colonized?	Flow Regime	Operating Level	Sample Point
(1)	Control	No	CH	variable*	after ~ 20 PV
(2)	Control	No	CF	25 mL/min	after ~ 20 PV
(3)	Test	Yes	CH	0.5 ft head	until Q -> 25 mL/min @ t_1
(4)	Test	Yes	CF	25 mL/min	t_1
(5)	Test	Yes	CH	1.0 ft head	until Q -> 25 mL/min @ t_2
(6)	Test	Yes	CF	25 mL/min	t_2

*Effluent "T" elevation adjusted to achieve flowrate of 25 mL/min under CH condition

Reactor Feed Water

During operation, the reactors were supplied with tap water from the city of Bozeman, Montana that was filtered through laboratory-scale granular activated carbon (GAC) and biologically activated carbon (BAC) filter columns. The GAC column removed any chlorine residual from the tap water. The BAC column removed any readily degradable organic carbon from the tap water and served as a source of mixed-species heterotrophic bacteria to the reactors that were acclimated to drinking water conditions. Effluent water from the BAC columns was mixed with a sterile organic carbon substrate in proportions to raise the final organic carbon concentration by 0.5 ppm carbon.

The organic carbon substrate carboys were prepared by autoclaving reverse osmosis (RO) water and adding filter-sterilized carbon stock to the cooled bottles in a laminar flow hood. The carbon stock was a nutrient solution with seven compounds (Table 2) that were selected to represent major classes of organics typically found in drinking water [*Ellis et al.*, 1999]. These compounds were added to a liter of RO water, placed on a magnetic stirplate

overnight until the compounds dissolved into solution. The pH was adjusted to 7 with NaOH and the solution was filter-sterilized through a 0.22 μm filter into a sterilized media bottle. The media bottle was stored at 4° C.

Table 2: Carbon Stock Formula (Sigma Chemical Co.)

Compound	Formula	Mass (g)
Glucose	($C_6H_{12}O_6$)	4.7
Glutamic Acid	($C_5H_9NO_4$)	5.3
Aspartic Acid	($C_4H_7NO_4$)	5.5
Serine	($C_3H_7NO_3$)	4.7
Alanine	($C_3H_7NO_2$)	4.8
Galactose	($C_6H_{12}O_6$)	4.8
Arabinose	($C_5H_{10}O_5$)	4.8

Planktonic Culture Preparation.

Salmonella typhimurium (Gideon, Missouri; waterborne outbreak strain, provided by Eugene Rice of US Environmental Protection Agency, Cincinnati) was used as the model pathogen to study pathogen capture in the lab scale reactors. This organism was modified to contain a plasmid [*Clark,* pers. comm.] which was encoded for both carbenicillin resistance and green fluorescent protein (GFP). An overnight culture was grown in LB broth (EMD CAT # 1.10285.0500) supplemented with 250 μg/mL carbenicillin (Mediatech Inc. CAT # 46-100-RG). A single colony was scraped from a refrigerated LB-carbenicillin plate with a flame-sterilized inoculation loop and the colony was transferred to the Falcon tube. The culture was placed in a shaking incubator (New Brunswick Scientific -Innova 4000) at 30° C and 200 rpm and allowed to grow for 16 hours.

The culture was then starved to acclimate it to the low nutrient environment found in a drinking water distribution system. To separate the suspended cells from the nutrients, the culture was placed in a centrifuge (Sorvall Instruments RC5C with a Piramoon Technologies, Inc. F15S-8x50c rotor) and spun at 2,900xg for ten minutes to obtain a cell pellet. The supernatant (LB broth) was decanted and the cell pellet was resuspended in 10 mL of filter-sterilized BAC effluent. To ensure the removal of any readily degradable carbon and efficient starvation the washing step was repeated and the cell pellet was resuspended in 10 mL of filter-sterilized BAC effluent. The culture was then placed on a shaking table (New Brunswick Scientific – Innova 2300 platform shaker) at 200 rpm and room temperature for 24 hours prior to inoculating a reactor.

Reactor Inoculation and Sampling

After starving the culture for 24 hours, the reactor was inoculated with *S. typhimurium.* An effluent sample was collected from the reactor to determine effluent heterotrophic plate counts (HPCs) and placed on ice prior to reactor inoculation. A sterile 1 mL syringe and subQ needle (size $26G^{5}/_{8}$) was used to inoculate the reactor with 1 mL of the *S. typhimurium* culture after the 24 hour starvation period. Effluent samples from the reactor were collected in 50 mL Falcon tubes for five clean bed pore-volumes (total 68 mL) in half pore-volume (34 mL) increments for a total of ten samples. These samples were immediately placed on ice after collection to prevent bacterial growth.

After collecting the effluent samples, the influent line was clamped with a hemostat. The reactor was then disconnected from the influent and effluent tubing and transferred to a laminar flow hood. The fluid remaining in the reactor mixing chamber and pore space was

allowed to freely drain into a 100 mL graduated cylinder and the volume was recorded. A 34 mL aliquot of this pore-fluid was transferred to a 50 mL Falcon tube and placed on ice with the other samples. Any fluid still remaining in the reactor was assumed to be associated with the attached biofilm.

The reactor was then disassembled for destructive sampling of the porous media to enumerate captured *S. typhimurium*. A metal spatula was used to transfer the top and bottom halves (as determined by mass) of the porous media into separate 250 mL flasks. 50 mL of filter-sterilized BAC water was added to the first flask. The flask was then subjected to a succession of vortex (IKA lab dancer), sonication (Fisher Scientific FS15), vortex, sonication on a 30 second cycle to dislodge attached biofilm from the surface of the collector beads. The fluid was then decanted through a sterile screen into a separate 250 mL beaker. An additional 50 mL of filter-sterilized BAC water was added to the flask and the process was repeated for a final volume of approximately 100 mL of BAC water, which contained the detached biofilm and any captured *S. typhimurium*. A small portion of the fluid remained attached to the beads due to capillary action and was not recovered. Therefore, the mass of the decanted fluid was measured and recorded to determine the volume recovered. A 34 mL aliquot of the recovered fluid was transferred to a 50 mL Falcon tube and placed on ice. This procedure was then repeated for the second half of the porous media.

Following this, the reactor surfaces were sampled to determine the amount of *S. typhimurium* that attached to the reactor itself. The surfaces were rewet, scraped with a rubber policeman, and rinsed into a 250 mL beaker. A total of 100 mL was used for this step, distributed among surfaces as outlined in Table 3. The mass of the recovered fluid was

measured, recorded and a 34 mL aliquot was transferred to a 50 mL Falcon tube and placed on ice.

Table 3: Reactor Surfaces Rinse Volumes

Surface	Volume (mL)
Lid	15
Sides	30
Screens	10 each
Stir bar	10
Base	25
Σ =	100

Non-Reactive Tracer Study.

A sterile 1 mL syringe and subQ needle was used to inoculate the reactor with 1 mL of red food dye as a conservative tracer. The food dye (manufactured by McCormick) was diluted to ten percent of its original concentration with sterile nanopure water. An effluent sample was collected prior to inoculating the reactor to serve as a baseline measurement. The tubing was pierced with the needle immediately upstream of the influent port and a timer was started simultaneously with the inoculation. Effluent samples from the reactor were collected in 50 mL Falcon tubes for 10 clean bed pore-volumes (total 68 mL) in half pore-volume (34 mL) increments for a total of 20 samples. The concentration of food dye in the samples was measured using a spectrophotometer (details in analytical methods section). Digital photographs of the reactor were taken during this time to allow for a visual inspection of any preferential channels or macro pores.

Short Term vs. Long Term Capture

The immediate capture ability of the model reactor was determined for five pore-volumes of flow. This time was selected because breakthrough curves using a non-reactive tracer indicated that the majority of the tracer had passed through the reactor at this point in time. Sampling the reactors in this manner was effective for assessing initial capture of pathogens, but the reactors likely still contained reversely adsorbed bacteria that would detach and wash out if flow continued. Allowing the reactors to continue to operate for a longer duration and then stopping the flow would make it possible to determine what long-term capture was.

To investigate how pathogen capture was affected by a longer flow duration, the effluent was captured for 20 pore-volumes post-inoculation in 2 PV aliquots before stopping the flow. Operating the reactors for this additional time after inoculation allowed the tailing effect of the breakthrough to be observed until it reached a pseudo steady-state level. This also allowed reversibly attached bacterial cells additional time to detach and be transported further through the reactor. Increasing the effluent breakthrough monitoring from five pore-volumes to 20 pore-volumes increased the sampling duration approximately from 15 minutes to 60 minutes which was still a short enough duration that any growth or decay effects of *S. typhimurium* in the reactor did not need to be considered.

Analytical Methods

This section details the analytical methods used to verify the organic carbon substrate concentrations used for reactor feed water. It also details the methods used to enumerate the breakthrough and capture of *S. typhimurium* and the breakthrough of the non-reactive tracer.

Total Organic Carbon Determination

Total organic carbon (TOC) concentrations were verified with a Dohrmann DC-80 Carbon Analyzer. A 1,000 ppm stock standard solution was prepared by suspending 0.2375 grams of oven dried sucrose into 100 mL of deionized water in a volumetric flask. The 1,000 ppm standard was stored in a refrigerator and used to prepare 10 ppm standards on sample days by diluting 1:100 with nanopure water. After the baseline reading on the Dohrmann DC-80 stabilized, the carbon analyzer was calibrated by injecting three separate 1 mL aliquots of the 10 ppm standard. The average value of these three injections became the 10 ppm calibration point.

Samples were prepared for analysis by purging them of CO_2. This was accomplished by adding 2 drops of 20% H_3PO_4 and bubbling O_2 through the sample for six minutes. After purging the sample of CO_2, a 1 mL aliquot was injected into the Dorhmann DC-80 for analysis. The concentration of the organic carbon stock was diluted from its expected value to less than 10 ppm and verified. Carboy feed jugs for the reactor feed water were then adjusted to the desired concentration by adding carbon stock to sterilized RO water. The carbon loading rate supplied to the reactors was verified by collecting a sample of the reactor

influent water from the elevated reservoir and verifying that its TOC was 0.5 ppm higher than the TOC of the BAC water.

Salmonella typhimurium Enumeration

SS (Salmonella/Shigella) agar (Difco DF0074-17-2) was used to enumerate the concentrations of *S. typhimurium*. This selective medium was required to differentiate between *S. typhimurium* and native heterotrophs present in the Bozeman tap water and the BAC columns that were resistant to carbenicillin. SS agar contains bile salts, brilliant green, and citrates that inhibit the growth of gram-positive bacteria. The agar also contains lactose to differentiate enteric organisms. Lactose nonfermenters form colorless (opaque) colonies, while lactose fermenters produce acid. The acid in combination with a neutral red indicator results in the formation of red colonies. *Salmonella* is differentiated from other lactose nonfermenters by the inclusion of sodium thiosulfate and ferric citrate in the media which will result in a black centered colony due to the formation of hydrogen sulfide by *S. typhimurium*. The plates are incubated at 30°C for an initial 18 to 24 hours and incubated for an additional 24 hours if colony centers have not yet turned black.

Plates with SS agar media were prepared using the following procedure. A magnetic stir bar was placed in a 1 L media bottle and 48 grams of dehydrated SS agar were suspended in 800 mL of RO water. The media bottle was placed on a stirring hotplate and gently stirred to dissolve the powder until the media began to boil. After boiling for 2 to 3 minutes the media bottle was then transferred to a 65°C water bath. Once the media bottle had equilibrated with the water bath, it was placed on a non-heated stirplate. Carbenicillin stock (at 25 mg/mL) was added to the SS agar media to reach a final concentration of 250 μg/mL.

The media was gently stirred to evenly distribute carbenicillin without forming air bubbles on the media surface. Approximately 15 to 20 mL of SS agar was then poured into sterile Petri dishes and allowed to solidify. Plates were stored at 4°C until needed.

All of the collected samples that contained biofilm were homogenized (ESGE Bio-Homogenizer M133/1281-0) on the highest level for 30 seconds and then placed on ice. To prevent cross contamination between samples, the homogenizer tip was soaked in 95% ethanol, flame-sterilized, and rinsed twice with nanopure deionized water. Each sample was then serially diluted by pipetting 100 μL of the sample into a 1.5 mL microcentrifuge tube containing 900 μL of filter-sterilized BAC water for a 1-log reduction in concentration per dilution.

Serially diluted samples were plated on prepared SS agar medium using a drop plate method [*Herigstad,* 2001]. Each plate was separated into four quadrants to allow plating four different dilutions. A schematic of this is shown in Figure 14. A digital pipette (Rainin edp2) was used to pull up 100 μL of the selected dilution and to dispense five 10 μL drops into the appropriately labeled quadrant. The remaining 50 μL in the pipette was discarded. This was repeated for appropriate dilutions in all four quadrants. The drops were allowed to soak into the media after which the plate was flipped over in preparation for incubation. Dilutions used for plating were selected such that the expected sample concentration was bracketed by at least a dilution above and below it. This allowed for at least a 1-log variation in expected sample concentrations without the need to process the sample again.

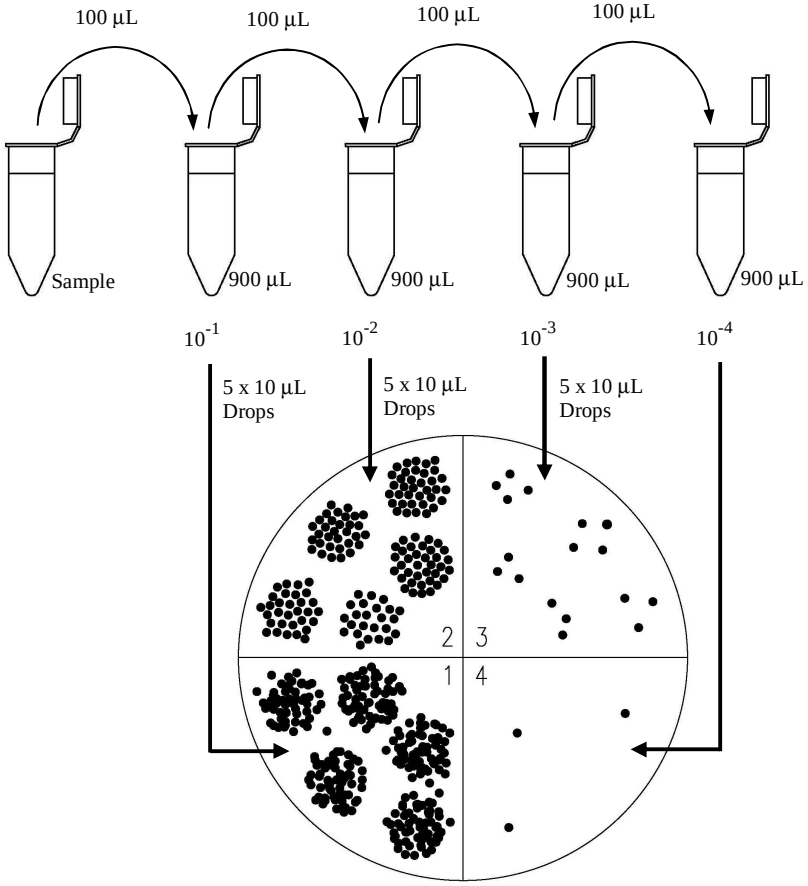

Figure 14. Serial dilution and drop plating technique schematic.

Herigstad, [2001] recommends counting colonies at the dilution for which a single drop produced 3 to 30 colonies. This was modified such that colonies were counted when a single drop produced 2 to 40 colonies. These adjusted values were selected to account for variability in individual drop sizes. The Rainin pipette accurately dispensed 10 µL at a time, but the drop size placed on the plate varied occasionally due to surface tension between the water and the pipette tip resulting in a smaller drop followed by a respectively larger drop. All plates were done in duplicate resulting in ten colony counts. The recorded concentration for a sample was the arithmetic mean from the ten drops multiplied by the dilution necessary

to count individual colonies. The total number of cells for each sample was calculated by multiplying the cell concentration in the sample fluid by the volume of the entire sample.

Mass Balance on *Salmonella typhimurium*

A mass balance was performed around the reactor on *S. typhimurium* using the total cell count results from the plate count data. This mass balance was done to compare the number of culturable cells injected into the reactor with the number of culturable cells recovered in the effluent water and within the reactor. The cells within the reactor include those in the bulk fluid within the pore spaces and the cells captured in the porous media and on the reactor surfaces. The mass balance results are reported in terms of percent recovery.

Non-Reactive Tracer Breakthrough Measurements

After collecting the 20 samples, the breakthrough of the tracer was enumerated with a spectrophotometer (Spectronic Instruments – Genesys 5) measuring sample absorbance at 520 nm. A 1.5 mL disposable cuvette was filled with 1 mL of BAC water that served as a baseline for zeroing the spectrophotometer. An additional cuvette was filled with 10 μL of the red food dye solution used to dose the reactor and 990 μL of BAC water to dilute the dye to a concentration close to the peak sample. This dilution kept the tracer concentration (C_0) within the same linear range as the effluent samples. 1 mL from each sample was then pipetted into separate cuvettes and measured in the spectrophotometer. Final breakthrough curve values were then graphed and reported as C/C_0.

Statistics

Minitab V14 was used to determine if the results from the short-term capture experiments (n=3 per each of 6 reactor conditions) were statistically significant using the log values of the total cell count. A two sample, one-sided t-test was used to compare the results of the colonized reactors to the uncolonized control reactors. A paired-sample t-test was used when comparing results from within one reactor condition. The null hypothesis for these tests was that the mean log values for the samples were equal. The null hypothesis was considered invalid when p-values were less than 0.05. Statistical analysis was not performed for the long-term capture experiments due to the smaller data set (n=2 per each of 6 reactor conditions).

Ancillary Studies

Additional experiments were performed to provide information about the mechanisms by which *S. typhimurium* cells were transported and captured in a porous media. These studies included experiments using a confocal microscope to directly observe the transport and capture of cells flowing through a porous media.

Confocal Microscope Experiments

The model reactor and sampling protocol used to study bacterial cell capture in porous media was able to quantify the extent of capture that occurred. However, it was not able to provide information on the nature of the capture mechanisms due to the destructive sampling protocol used. The confocal microscope was able to provide insight into these

capture mechanisms by allowing for the direct observation of microbial transport and capture in real time.

The confocal microscope operates by directing a filtered laser beam of a desired wavelength onto the sample. Fluorescent proteins contained within the bacterial cells would become excited by the laser beam and emit light that can be observed through the ocular lenses on the scope or via the microscope camera. The camera was attached to a computer to allow individual images to be saved for later analysis.

Flowcell Sample Preparation. Samples were prepared by packing a 0.9 mm x 0.9 mm square flowcell (inside dimensions, Friedrich and Dimmock, NJ) with 0.1 mm glass beads (Scientific Industries Inc. CAT # SI-BG01). Packing was accomplished by placing one end of the flowcell into a fluid suspension containing the beads and applying a vacuum to the other end of the flowcell with a syringe. The vacuum side of the flowcell was covered with a fine brass mesh to contain the beads within the flowcell and prevent them from washing out with the bulk fluid. The vacuum drew up the fluid and beads into the flowcell with beads becoming lodged against the brass mesh. The vacuum was applied until the entire 6-inch length of the flowcell was packed.

It was necessary to perform the experiments on both clean and colonized porous media to determine how the biofilm influenced the transport and capture of bacterial cells. Clean porous media was prepared by autoclaving the beads and nanopure water for packing the flowcell. Colonized porous media was prepared by adding sterilized 100 μm beads to a culture in a 50 mL Falcon tube containing 10 mL of LB media supplemented with 250 μg/mL of carbenicillin. The organism used for biofilm growth in the colonized flowcells was

a DsRed strain of *E. coli* K-12 (obtained from Albert Jacbos, Lyon, France) that would emit red light (558 nm excitation peak/582 nm emission peak) under the confocal microscope. The Falcon tube was placed on a shaking incubator table at 30°C and 200 rpm. The culture was allowed to grow for 6 hours before packing the flowcell. This culture suspension with beads was then used to pack the colonized flowcells. These flowcells were allowed to sit for 2 hours to allow for additional bacterial cells in the bulk fluid to attach to the surface of the beads.

Flowcell Operation. The flowcells were then fed water from sterile carboys with a peristaltic pump. The clean flowcell was fed with sterilized water such that microbial growth would not occur on the porous media. The colonized flowcells were fed with sterilized Bacto™ Tryptic Soy Broth (TSB) at 1 percent concentration. The flowrate through the reactor was set such that the Reynolds number in a clean flowcell matched the Reynolds number (Re = 1.14) in a clean model reactor. The calculation for Reynolds number (Re) is shown in equation 1 where v_s is the mean fluid velocity, L is the characteristic length (bead diameter), and ν is the kinematic fluid viscosity.

$$\mathrm{Re} = \frac{v_s * L}{\nu} \tag{1}$$

The clean and colonized flowcells were operated for 4 days prior to being placed under the confocal microscope. This allowed biofilm growth to occur on the surfaces of the beads in the colonized flowcells. After finding a suitable imaging location within the flowcell, the source water was switched from the sterilized TSB to a culture of GFP *S. typhimurium* (489 nm excitation peak/509 nm emission peak) with a cell density around 10^9

cells/mL that was prepared in the same manner as for the biofilm trap inoculations. These *S. typhimurium* cells would emit green light that allowed for the visualization of the GFP cells being inoculated into the clean flowcell. It also allowed for the GFP cells being inoculated into the colonized flowcell to be differentiated from the DsRed cells comprising the biofilm on the cell disruption beads.

While the flowcell was being supplied with sterilized feed water the computer attached to the microscope (40x objective) camera began saving images every 1.66 seconds for ten minutes. The source water was then switched to the *S. typhimurium* culture and the GFP cells were transported through the flowcell. The transport and capture of the GFP cells was observed and the source water was then returned back to the original sterilized feed water after approximately five minutes. As a result of only being able to take one image every 1.66 seconds it was not possible to track an individual cell through the field of view but collected images showed the location of cells in the bulk fluid and attached to the biofilm or bead surface. All images were taken on a Leica SPS2 AOBS single photon confocal microscope equipped with 488 laser set to 15% power for GFP excitation and a 561 nm laser set to 75% power for DsRed excitation to help minimize cross-over effects [*Klayman*, 2007].

Switching back to the sterilized feed water allowed the GFP cells in the bulk fluid to wash out of the flowcell and only the captured cells would remain. This made it possible to verify that suspected captured cells were indeed captured and also enabled watching any detachment events that occurred within the field of view. Some GFP cells were still visualized flowing through the reactor during this time. These cells were the result of detachment events that occurred upstream from the field of view that re-entered the bulk

fluid and could be seen flowing past the porous media. Some of these detached cells in the bulk fluid would be transported to the surface of the 100 μm beads or biofilm and be re-captured.

CHAPTER 4

RESULTS

Using *S. typhimurium* as a test organism, the model reactors were inoculated and sampled in a previously uncolonized state for the control experiments, and colonized with a mixed-species heterotrophic biofilm prior to inoculation during the test experiments. Constant flow (CF) and constant head (CH) reactors were operated for both the colonized test experiments and the uncolonized control experiments. CH reactors were operated under 0.5 ft or 1.0 ft of total operating head. A CF reactor (25 mL/min constant flowrate) was operated in parallel with each CH reactor and both were sampled after operating for the same time duration at a point where both had the same flowrate. In separate experiments, smaller porous media beads in a flowcell reactor were used to microscopically observe attachment patterns of the test organism. This chapter presents observations obtained during the biofilm growth phase for the reactors, experimental data for the transport and capture of a slug dose of *Salmonella typhimurium* into the reactors, and descriptions of attachment behavior in the flowcells.

Observations

Measurements of flowrate and reactor headloss were taken on almost daily basis during the reactor operation period. Although these measurements contained enough variability between replicates that they were not reproducible, several trends became apparent. A sample from one experiment is presented in Figure 15.

The flowrate for the CF reactors remained relatively stable at around 25 mL/min as expected. The pore space available for fluid flow decreased as biofilm accumulated in this reactor. The constant flowrate provided by the pump would cause an increase in the velocity within the available pore space, producing an increased frictional resistance and increased headloss.

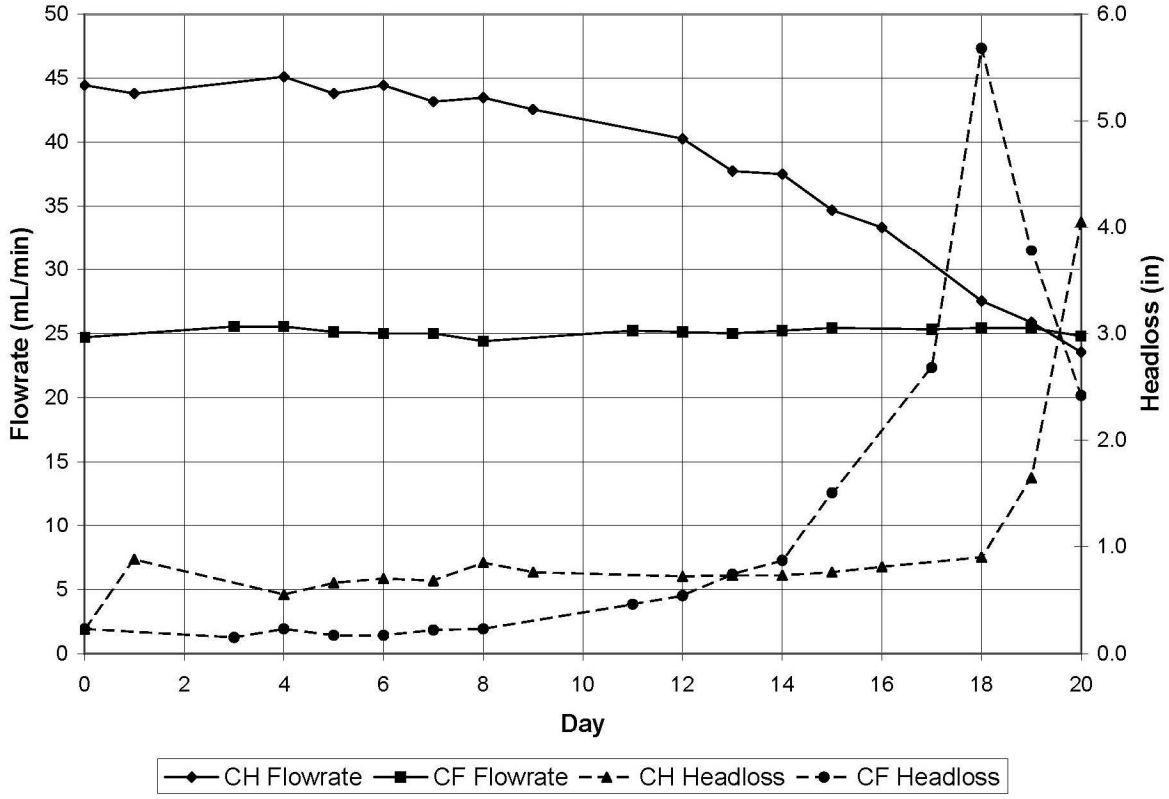

Figure 15. Sample constant head (CH) and constant flow (CF) reactor flowrates and headloss. The overall operating head for the CH reactor was 6 inches and the CF reactor operated at 25 mL/min.

The flowrates for the CH reactors start well above 25 mL/min. Biofilm accumulation in the CH reactors decreased the pore space available for fluid flow during the reactor

operations resulting in a decrease in flowrate. This continued for 20 ± 4 days until the flowrate approached the target rate of 25 mL/min at which point it was inoculated and sampled.

While the operating head for a CH reactor is constant throughout the experiment, the headloss across the reactor is not constant. Biofilm accumulated inside the CH reactors, yet the headloss across the reactor remained relatively constant for most of the reactor operation. An increase in headloss was observed on some reactors towards the end of the operational time as shown in Figure 15. The summation of the headloss through the entire flowpath (reactor and tubing) is equal to the operating head. During the course of an experiment, biofilm growth also occurs on the inside of the tubing, decreasing the effective diameter and altering the frictional properties of the tubing, thus changing the headloss. The combined headloss in the tubing and reactor is responsible for the observed variations in headloss across the reactor. Generally, one would expect that a small increase in biofilm thickness would have a much more profound effect on the small pore channels/throats in the porous media than in the circular tubing; the decrease in flow experienced by both would then translate to less friction in the tubing, while the porous media gains resistance faster than it loses velocity.

The CF reactors behaved in a markedly different manner. As the CF reactors accumulated biofilm, the peristaltic pump continued to force water through at the constant flowrate of 25 mL/min. Forcing this amount of water through a reduced pore space resulted in an increase in headloss across the reactor as shown in Figure 15. The headloss continued to increase until it peaked and subsequently diminished. The headloss for some reactors

peaked only once before being sampled (Figure 15) while others would peak multiple times (Figure 16).

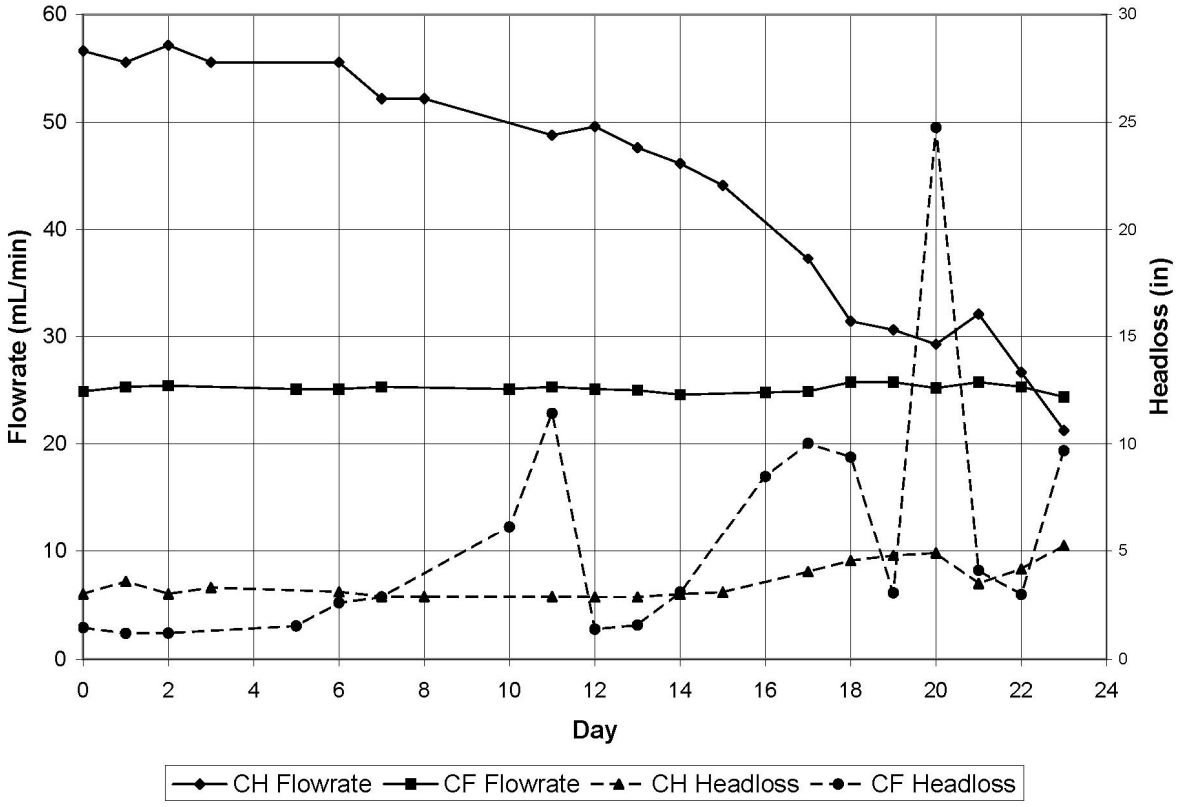

Figure 16. Sample constant head (CH) and constant flow (CF) reactor flowrates and headloss. The overall operating head for the CH reactor was 12 inches and the CF reactor operated at 25 mL/min.

The accumulation of biofilm within the reactor was not visible deep within the porous media, but was visible at the interface of the porous media and the reactor wall. At this interface, a gradient in biofilm accumulation was observed that decreased in the flow direction with little to no biofilm growth being visible near the reactor lid. It was not possible to visually determine how water flowed through the reactor. However, when the

non-reactive tracer studies were performed, the red food dye was visible at the outer edges moving through the reactor. Images from the tracer studies are shown in Figure 17 for the colonized CH and CF reactors. The CH reactor appears to utilize the majority of the pore space within the reactor whereas the CF reactor appears to have preferential flow channels and pore exclusion which does not fully utilize the pore space.

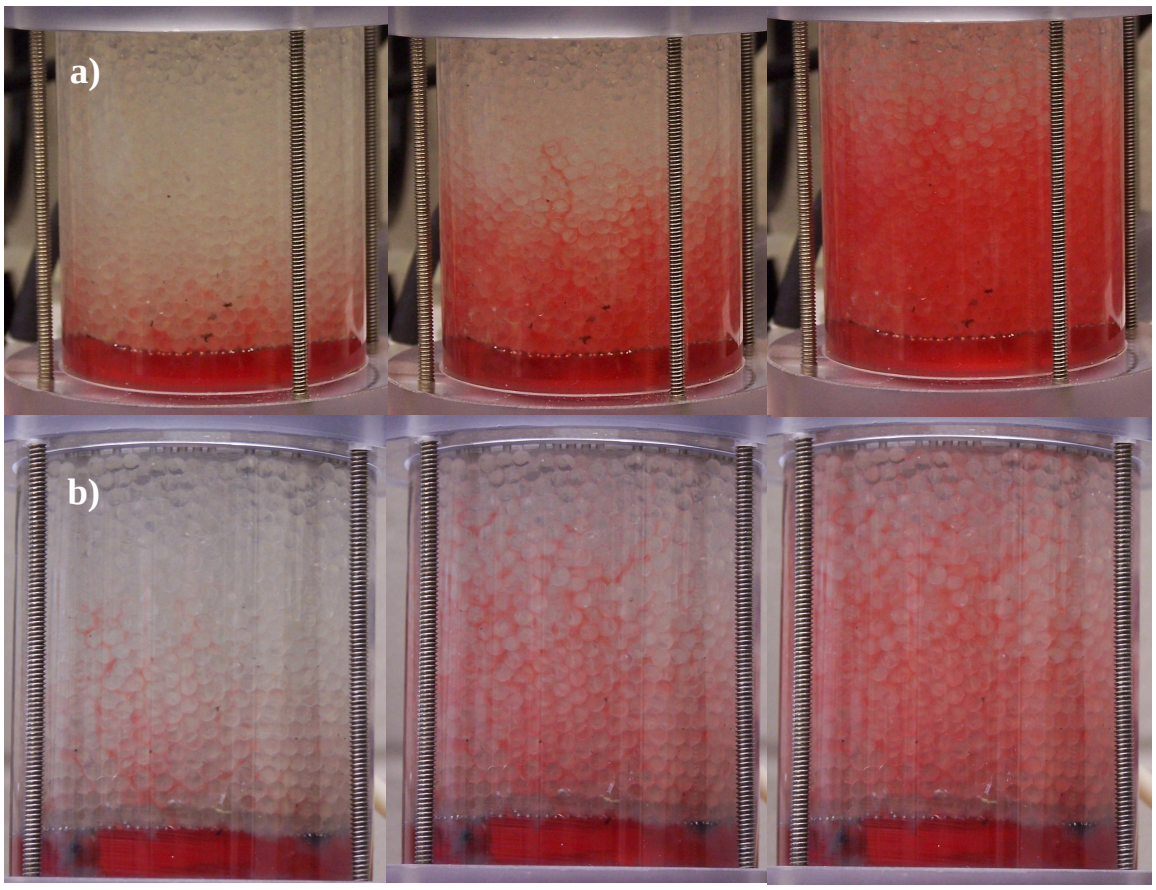

Figure 17. Tracer Study in a) constant head reactor displaying relatively uniform advective flow and b) constant flow reactor displaying preferential flow channels.

Experimental Data

Enumeration of *S. typhimurium* that was transported through the reactor and recovered in the effluent samples is reported graphically with breakthrough curves in two ways: on a logarithmic-scale of actual counts (CFU) and on a scale of fractional recovery (C/C_0, dimensionless). The results of the non-reactive tracer studies are also included on the fractional-scale breakthrough curves. Counts of *S. typhimurium* recovered from within the reactor are also reported on log-scale graphs. The results for the short-term (S.T.) capture experiments (5 pore-volume) are reported first followed by the results from the long-term (L.T.) capture experiments (20 pore-volume).

Short-Term Experiments

This section gives the results for the short-term experiments. After inoculating the reactor with a slug-dose of 1 mL of *S. typhimurium*, the reactor effluent was captured for 5 clean-reactor pore-volumes (68 mL) in half pore-volume increments (34 mL). At this point in time, the flow to the reactor was stopped and the reactor was destructively sampled. The last column of Table 4 lists the pore-volumes drained by gravity from each of the reactors. All of the values are less than the clean-reactor pore-volume of 68 mL. The clean reactors values (61-63 mL) are the closest to the true pore volume. The discrepancy for these reactors is due to some water wetting the interior surfaces of the reactor and not draining out. The colonized reactors have decreased pore-volumes (34-54 mL) due to biofilm growth in the reactor decreasing the available pore space for advective flow. Within a test experiment, the

CH and CF reactors operated in parallel display relatively similar available pore-volumes even though the flow-regime and organic mass-loading rates are not the same.

Short-Term Mass Balance Results

The mass balance on *S. typhimurium* performed around the reactor shows the relationship between the number of injected culturable cells with the number recovered in all of the collected samples. A recovery of 100% would demonstrate that the same number of cells injected into the reactor were recovered and suggests that the results were not greatly influenced by the growth or decay of cells, or the detection method (plate counts). The actual values for percent recovery are shown in Table 4. The majority of the percent recoveries are close to 100% indicating that plate counts are a viable detection method for the *S. typhimurium* inoculated into the reactor. The extreme range of recoveries is from 90.4% to 128.4%.

Table 5 presents a summary of Table 4 with average percent recoveries for each reactor condition sampled. All of the averaged percent recoveries are 100% or slightly greater. The values from Table 4 were compared for statistical significance ($p < 0.05$) using a two-sample, two-sided t-test. Percent recoveries were compared between the different flow regimes (CH or CF) within a reactor condition (clean control, 0.5 ft test, and 1.0 ft test) and between reactor conditions within a flow regime. Of these nine comparisons, the only difference in percent recoveries of statistical significance is between the CF control reactors and the "1.0 ft" CF test reactor ($p = 0.034$).

Table 4. Short-Term Mass Balance Percent Recoveries of *S. typhimurium*

Exp. #	Type	Colonized?	Flow Regime	Inoculum (CFU)	Recovered (CFU)	Percent Recovered	$V_{P.F.}$ (mL)
9	Control	No	CH	2.60E+09	2.58E+09	99.3%	61
9	Control	No	CF	2.93E+09	2.89E+09	98.4%	62
12	Control	No	CH	3.30E+09	3.38E+09	102.3%	62
12	Control	No	CF	3.95E+09	3.94E+09	99.7%	63
15	Control	No	CH	1.78E+09	2.08E+09	116.9%	62
15	Control	No	CF	1.86E+09	1.92E+09	103.6%	61
7	Test	Yes	CH	4.01E+09	3.95E+09	98.5%	48
7	Test	Yes	CF	3.26E+09	3.50E+09	107.3%	49
10	Test	Yes	CH	3.76E+09	3.99E+09	106.4%	49
10	Test	Yes	CF	3.45E+09	4.09E+09	118.7%	54
13	Test	Yes	CH	4.10E+09	3.71E+09	90.4%	48
13	Test	Yes	CF	2.70E+09	2.51E+09	92.8%	46
8	Test	Yes	CH	3.69E+09	3.86E+09	104.7%	46
8	Test	Yes	CF	3.96E+09	4.38E+09	110.7%	45
11	Test	Yes	CH	4.50E+09	5.00E+09	111.2%	54
11	Test	Yes	CF	4.35E+09	5.58E+09	128.4%	51
14	Test	Yes	CH	2.66E+09	2.50E+09	94.1%	34
14	Test	Yes	CF	3.29E+09	3.46E+09	105.2%	39

Values of CFU are the total number of colony forming units present in an entire sample, including effluent, pore fluid, and reactor and media surfaces.
The volume of the pore fluid ($V_{P.F.}$) is the volume which freely drained from the reactor.

Table 5. Short-Term Percent Recoveries Summary

Reactor Type	Colonized?	Avg. Percent Recovered
CF Control	No	100.0%
CH Control	No	106.7%
"0.5 ft" CF Test	Yes	104.1%
0.5 ft CH Test	Yes	100.6%
"1.0 ft" CF Test	Yes	108.8%
1.0 ft CH Test	Yes	109.2%

Short-Term *S. typhimurium* Breakthrough

The log-scale breakthrough curve (Figure 18) shows the total cell counts for each effluent sample collected. Also shown on this graph is the total cell count in the inoculum and in the pore-fluid drained from the reactor during the destructive sampling. Each bar on the graph represents the arithmetic average of the total cell count from the three replicates with the error bars showing the standard deviation between replicates. Some variation is seen in the inoculum values for the different reactor conditions. This variation will influence the values for the observed breakthrough. However, the general trend is consistent between all reactor conditions. Some early breakthrough is observed in the first sample (PV 0.5) with peak breakthrough occurring in the second sample (PV 1.0). The remainder of the pore-volume samples display a tailing effect with decreasing number of cells in the effluent.

Table 6 shows the concentration (CFU/mL) of cells present in the last pore-volume and the pore-fluid drained from the reactor during destructive sampling. Allowing gravity to drain the pore-fluid from the reactor reduces the count of cells present in the reactor. Table 6 also makes it possible to more accurately compare the amount of *S. typhimurium* present in the pore-fluid versus the last pore-volume. This distinction is important because the sample size of the drained pore-fluid is greater than the collected effluent samples. A cell concentration (CFU/mL) in the pore-fluid higher than the concentration in the last pore volume would indicate that a significant number of reversibly attached cells are detaching when the pore-fluid is drained. The concentration of cells in the drained pore-fluid is less than the concentration in the last effluent sample (PV 5.0) for all six reactor-conditions

suggesting that reversibly attached cells are not detaching in significant enough numbers to influence the concentration in the pore-fluid.

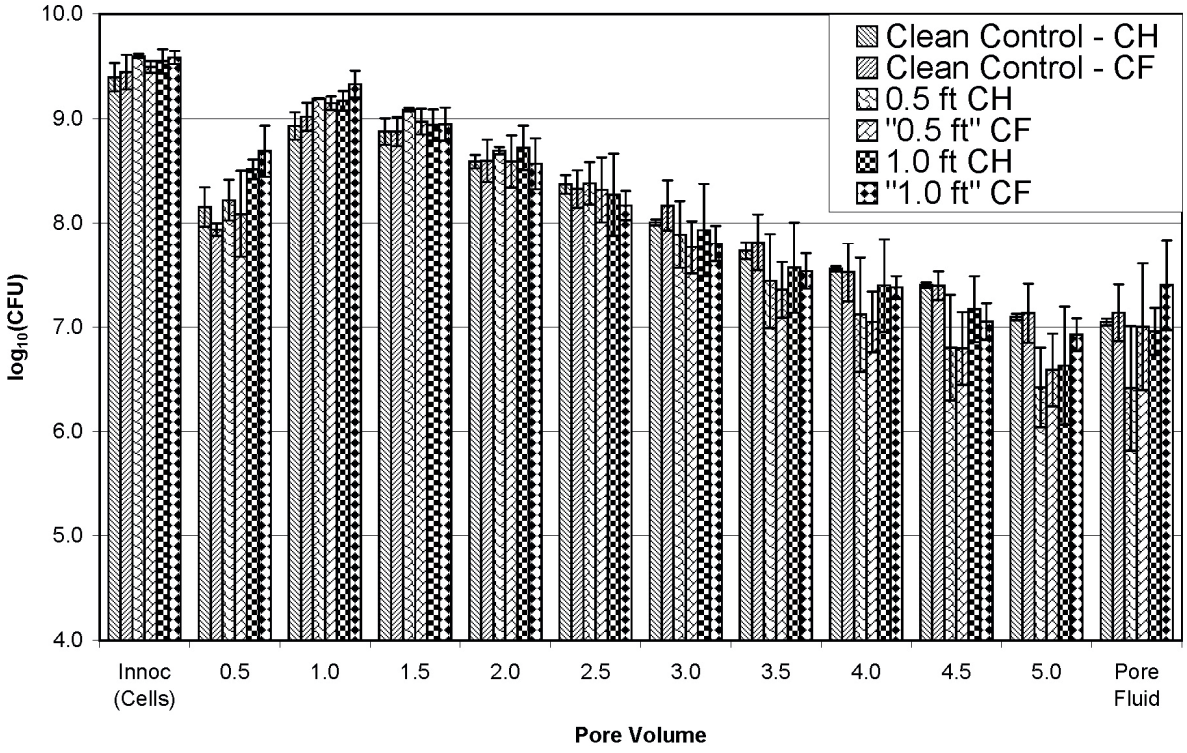

Figure 18. Log-scale breakthrough curve of *S. typhimurium* effluent samples from replicate, short-term (5 pore-volume) capture experiments (n = 3). Also included is the log values present in the inoculum and the pore-fluid drained from the reactor.

Table 6. Short-Term *S. typhimurium* Concentration in Drained Pore-fluid

Reactor Condition	Colonized?	PV 5.0 Conc. (CFU/mL)	Drained PF Conc. (CFU/mL)
CH Control	No	3.67E+05	1.37E+05
CF Control	No	4.51E+05	1.88E+05
CH 0.5 ft	Yes	3.07E+05	6.03E+04
CF "0.5 ft"	Yes	5.20E+05	2.33E+05
CH 1.0 ft	Yes	5.61E+05	1.53E+05
CF "1.0 ft"	Yes	1.44E+06	5.12E+05

The fractional-scale breakthrough curves show each replicate experiment individually on separate graphs for each reactor condition. The clean control, 0.5 ft, and 1.0 ft reactors are shown respectively in Figure 19Figure 20, and Figure 21. The ordinate in each of these graphs is the concentration in each sample (C) divided by the inoculation concentration (C_0). When biofilm growth occurs in the reactor, the actual pore-volume available for fluid flow is reduced from the 68 mL available in a clean reactor. As such, collecting 34 mL samples represents more than a true half pore-volume for reactors with biofilm growth. The abscissa of these graphs compensate for this fact by adjusting for the actual pore-volume (PV_{act}) collected using the volume of pore-fluid ($V_{Pore\text{-}fluid}$) collected during destructive sampling that would freely drain from the reactor (Equation 2). This can also be represented by t/θ by dividing through by the flowrate (Q) where *t* is the time at which a sample was collected and θ is the hydraulic residence time of the open pore-space in the reactor.

$$PV_{act} = \frac{V_{Sampled}}{V_{Pore\ Fluid}} = \frac{V_{Sampled} / Q}{V_{Pore\ Fluid} / Q} = \frac{t}{\theta} \qquad (2)$$

The actual pore-volumes for each reactor have a significant effect on these graphs and are listed in the last column of Table 4. The general effect of applying this equation to the data increases the value of t/θ for the collected sample points proportional to the decrease in reactor pore-fluid, thus shifting the data to the right. Non-reactive tracer breakthroughs that were performed on these reactors are also shown in their respective figures. The breakthrough of cells and the tracer are similar for the control reactors in Figure 19 suggesting that interactions with porous media surfaces does not significantly impact the transport of bacterial cells through uncolonized reactors. However, the breakthrough of cells in the colonized reactors (Figure 20 and Figure 21) is greater than the non-reactive tracer with less pronounced tailing suggesting that presence of biofilm in the reactor influences the transport of bacterial cells as compared to a non-reactive tracer.

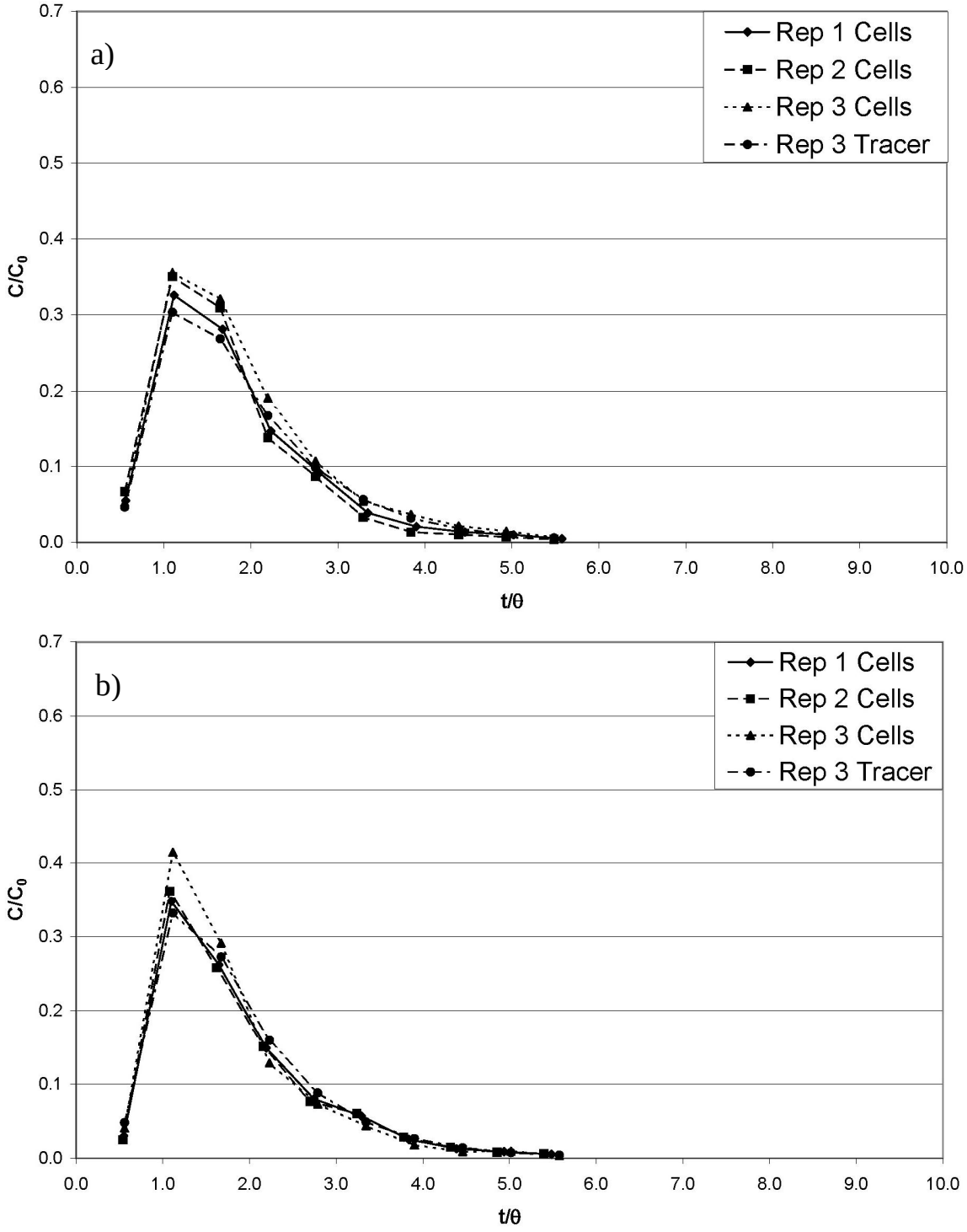

Figure 19. Fractional breakthrough curves of *S. typhimurium* and non-reactive tracer effluent samples from replicate short-term (5 pore-volume) capture experiments for clean control a) constant head reactors and b) constant flow reactors operated in parallel.

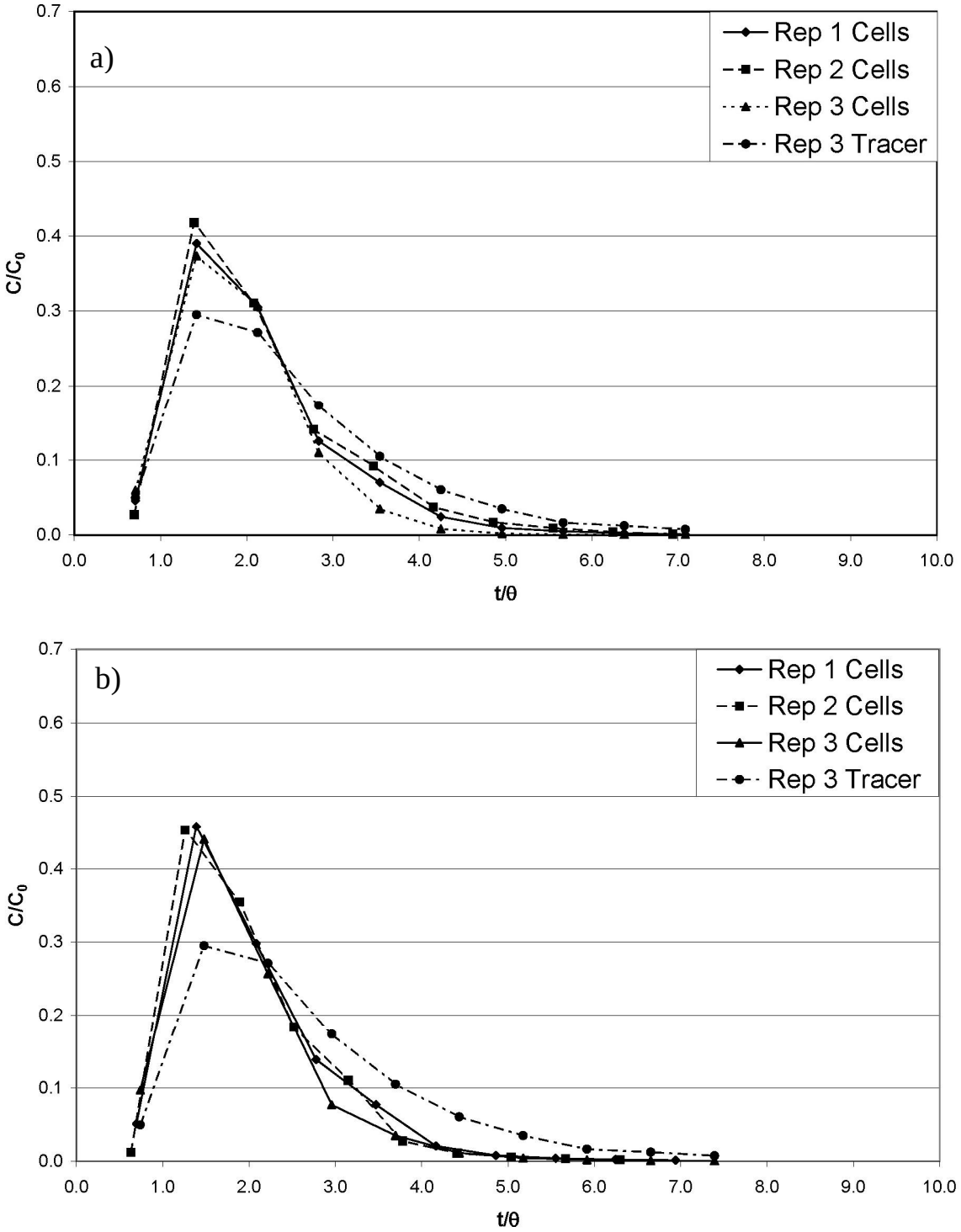

Figure 20. Fractional breakthrough curves of *S. typhimurium* and non-reactive tracer effluent samples from replicate short-term (5 pore-volume) capture experiments for colonized test (0.5 ft head) a) constant head reactors and b) constant flow reactors operated in parallel.

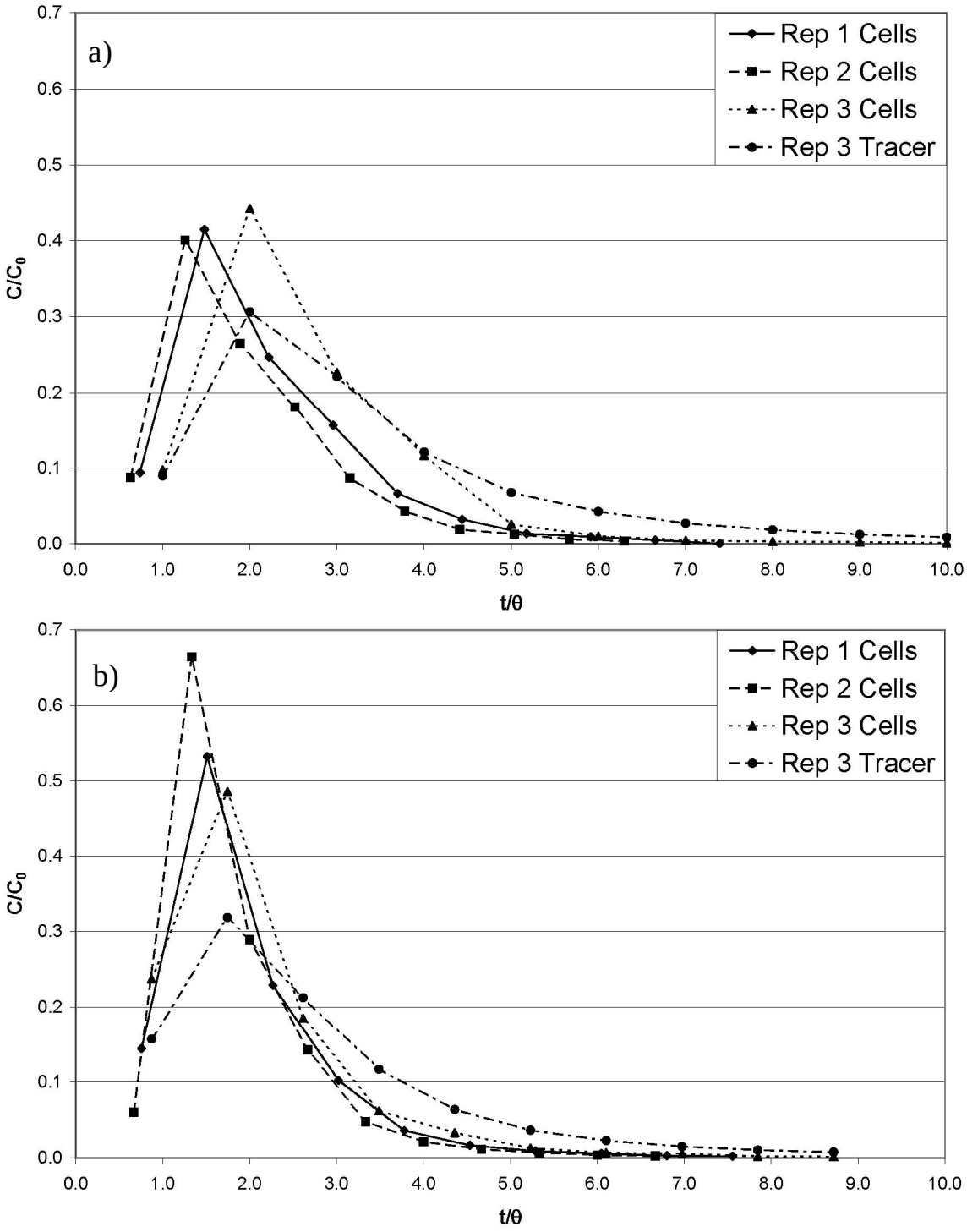

Figure 21. Fractional breakthrough curves of *S. typhimurium* and non-reactive tracer effluent samples from replicate short-term (5 pore-volume) capture experiments for colonized test (1.0 ft head) a) constant head reactors and b) constant flow reactors operated in parallel.

Short-Term Accelerated *S. typhimurium* Breakthrough

Retardation occurs when cell interactions with porous media surfaces attenuate the transport of the cells compared to the bulk fluid. A retardation factor (R_f) was calculated (Table 7) as the ratio of the t/θ value required for the arrival of center of mass for the *S. typhimurium* cells (CM_{cells}) to the t/θ value required for the arrival of center of mass for the non-reactive tracer (CM_{tracer}) using Equation 3. The center of mass for the cells (CM_{cells}) and the non-reactive tracer (CM_{tracer}) was calculated using Equation 4 where C/C_0 represents the fraction of inoculated cells present in the sample collected at t/θ.

$$R_f = \frac{CM_{cells}}{CM_{tracer}} \tag{3}$$

$$CM = \frac{\sum_{i=1}^{n} (C/C_0)(t/\theta)}{\sum_{i=1`}^{n} (C/C_0)} \tag{4}$$

Table 7. Short-Term *S. typhimurium* Retardation and Acceleration Factors

Reactor Condition	Colonized?	CM_{Tracer} (t/θ)	CM_{cells} (t/θ)	Retardation Factor (R_f)	Acceleration Factor (A_f)
CH Control	No	1.92	1.80	0.94	1.07
CF Control	No	1.80	1.79	1.00	1.00
CH 0.5 ft	Yes	2.49	2.05	0.83	1.21
CF "0.5 ft"	Yes	2.59	1.95	0.75	1.33
CH 1.0 ft	Yes	3.26	2.23	0.69	1.46
CF "1.0 ft"	Yes	2.62	1.91	0.73	1.37

The retardation and acceleration factors are the ratios of the centroid (CM) of the breakthrough curves for the cells and the non-reactive tracer.

The calculated retardation factors for the S.T. colonized experiments were less than 1.0, which means that the transport of the cells was not retarded but was accelerated as compared to the tracer. An acceleration factor (A_f) was calculated as being the inverse of the R_f values. The control experiments had acceleration factors equal to, or slightly greater, than the expected value of 1.0. The colonized reactors all had acceleration factors in excess of 1.0. The CH 1.0 ft and CF "1.0" ft reactors ran in parallel had acceleration factors greater than the CH 0.5 ft and the CF "0.5" ft reactors as expected due to the lower available pore-volume in the former reactors.

Short-Term *S. typhimurium* Capture

Each reactor was destructively sampled after the effluent samples were collected and the flow through the reactor was stopped. The total cell count of *S. typhimurium* captured was determined and is shown for each reactor condition in Figure 22 on a log-scale. The capture shown is what occurred on both the beads and the reactor surfaces, with any associated biofilm. Also shown is the *S. typhimurium* inoculum for each reactor condition. Each bar on the graph represents the arithmetic average of the total cell count from the three replicates with the error bars showing the standard deviation between replicates. On average, the colonized reactors display a 0.8 log increase in capture over the uncolonized control reactors. The CF ("1.0 ft") reactor also had an additional 0.5 log increase in capture over the other colonized reactors.

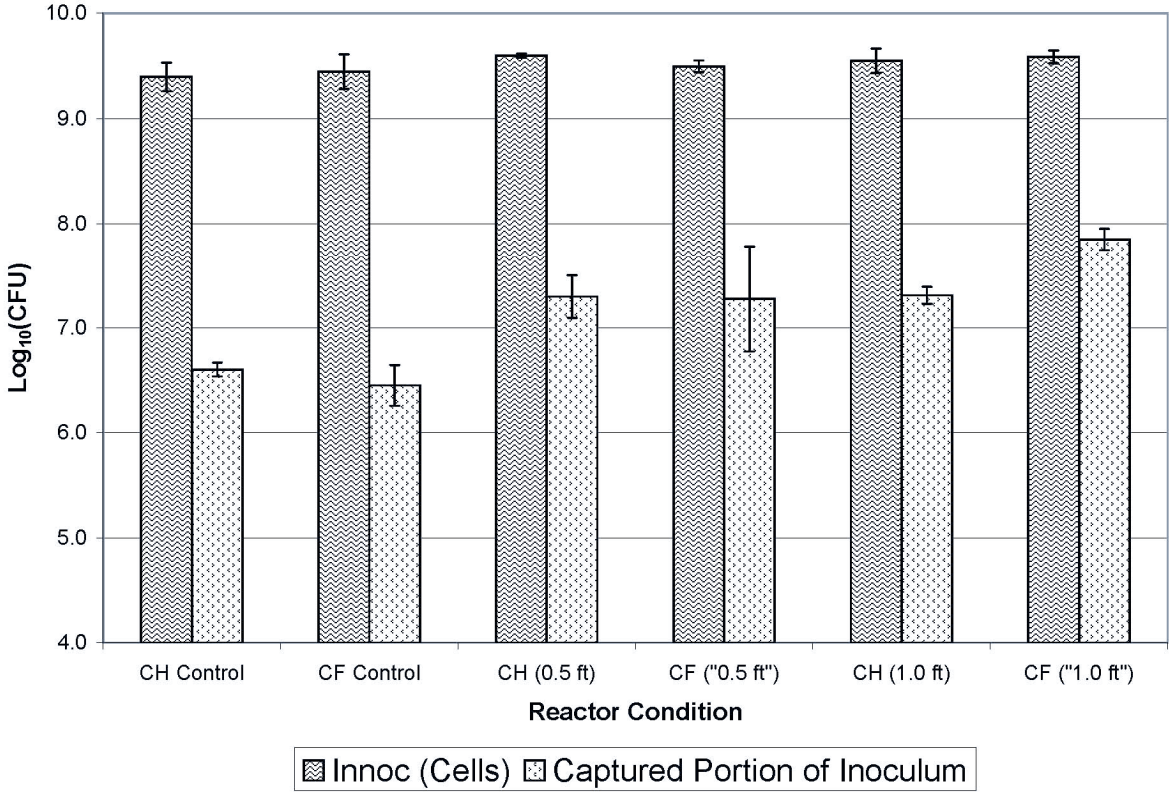

Figure 22. Total captured portion of *S. typhimurium* inoculum on reactor surfaces and porous media beads (combined) from replicate short-term (5 pore-volume) capture experiments (n = 3).

The average captured portion of the inoculum is shown in Table 8 in terms of total cells captured and as the percentage of the respective inoculum. The number and fraction captured in all of the colonized reactors was greater than the capture in the control reactors and statistically significant (p-value < 0.05) for every reactor. The larger p-value for the CF ("0.5 ft") is due to the larger standard deviation between the three replicate experiments as compared to the other colonized reactors.

Table 8. Short-Term Captured Portion of the Inoculum

Reactor Condition	Colonized ?	Inoculum (CFU)	Captured Cells (CFU)	Capture Percentage	P-value
CH Control	No	2.56E+09	4.04E+06	0.16%	n/a
CF Control	No	2.91E+09	3.02E+06	0.10%	n/a
CH 0.5 ft	Yes	3.96E+09	2.14E+07	0.54%	0.002
CF "0.5 ft"	Yes	3.14E+09	2.69E+07	0.86%	0.028
CH 1.0 ft	Yes	3.62E+09	2.07E+07	0.57%	<0.001
CF "1.0 ft"	Yes	3.87E+09	7.21E+07	1.87%	<0.001

The total cell count of *S. typhimurium* captured within the reactor can be split into respective amounts captured on the reactor surfaces and by the glass beads. This is done in Figure 23 on a log-scale graph. Also shown in this figure is the total cell count of *S. typhimurium* present in the pore-fluid drained from the reactor during destructive sampling. Each bar on the graph represents the arithmetic average of the total cell count from the three replicates, with the error bars showing the standard deviation between replicates.

All six reactor conditions display a greater capture of cells by the glass beads than by the reactor surfaces with this difference being greater for the control reactors than the colonized reactors. The colonized reactors display cell counts in the drained pore-fluid at a magnitude slightly lower than what was captured on the beads. The control reactors had a greater cell count in the drained pore-fluid than what was captured on the beads.

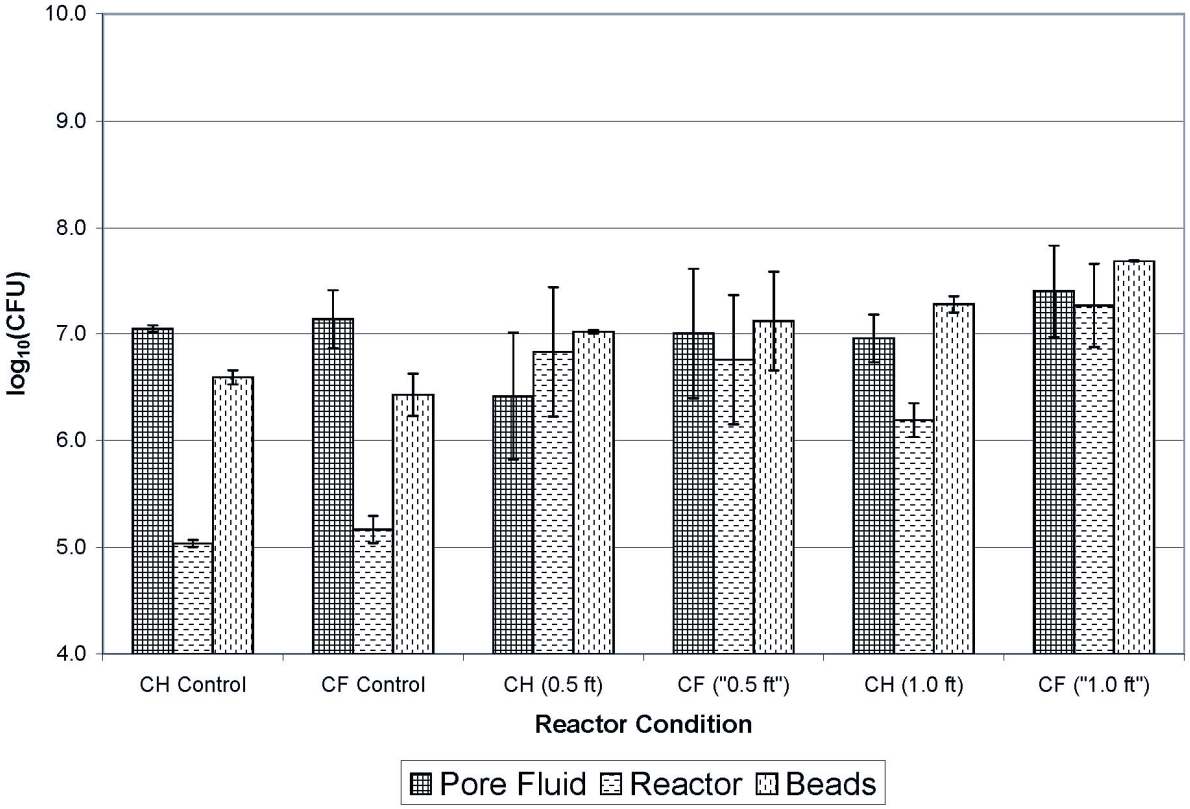

Figure 23. Log values of *S. typhimurium* present in drained pore-fluid and captured on reactor surfaces and porous media beads from replicate short-term (5 pore-volume) capture experiments (n = 3).

Table 9 shows the average amount of *S. typhimurium* captured on the reactor surfaces and the porous media beads with any associated biofilm, if present. The capture which occurred on the beads in the colonized reactor was statistically greater (p-value < 0.05) than on the beads in the control reactors for all the reactor conditions except the CF "0.5 ft" condition. This again is likely due to the greater standard deviation between replicate experiments for the CF ("0.5 ft") reactor condition.

Table 9. Short-Term *S. typhimurium* capture on reactor surfaces and porous media beads

Reactor Condition	Colonized?	Inoculum (CFU)	Captured Cells (CFU)		Captured Percentage		Bead Capture P-value
			Reactor	Beads	Reactor	Beads	
CH Control	No	2.56E+09	1.09E+05	3.94E+06	0.00%	0.15%	n/a
CF Control	No	2.91E+09	1.50E+05	2.86E+06	0.01%	0.10%	n/a
CH 0.5 ft	Yes	3.96E+09	1.09E+07	1.04E+07	0.28%	0.26%	0.004
CF "0.5 ft"	Yes	3.14E+09	9.18E+06	1.77E+07	0.29%	0.56%	0.070
CH 1.0 ft	Yes	3.62E+09	1.62E+06	1.91E+07	0.04%	0.53%	0.001
CF "1.0 ft"	Yes	3.87E+09	2.33E+07	4.22E+07	0.60%	1.09%	0.004

The cell capture that occurs on the glass beads and any associated biofilm is not uniformly distributed through the reactor. Figure 24 is log-scale graph which shows the total capture of *S. typhimurium* on the beads from Figure 23 and then breaks that total capture down into capture which occurred in the bottom-half and top-half of the glass beads. All six reactor conditions display a similar trend of increased capture in the bottom-half (influent side) over the top-half of the porous media. This trend is more pronounced in the colonized reactors and likely can be attributed to the visually observed decreasing gradient in biofilm from the influent side of the porous media towards the effluent. The CF (“1.0 ft”) reactor is again displaying an approximately 0.5 log increase in total capture over the other three colonized reactors.

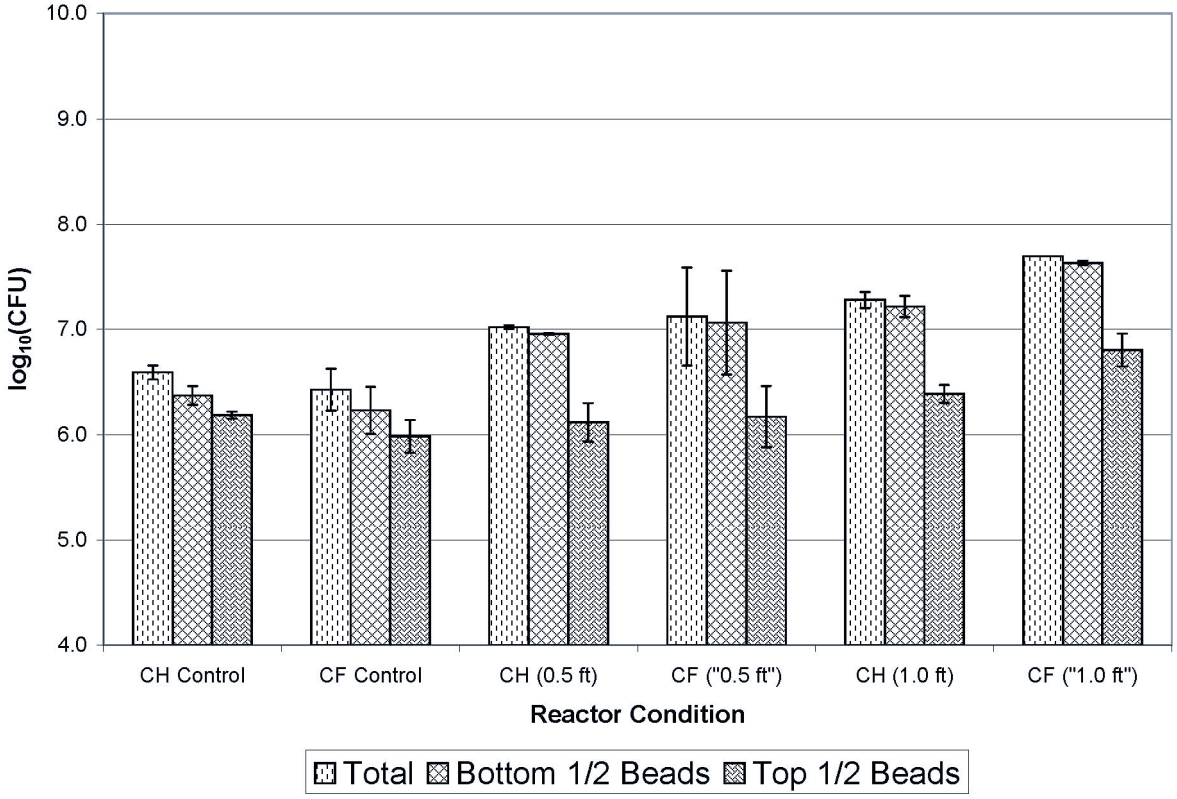

Figure 24. Log values of *S. typhimurium* captured in top and bottom halves of porous media beads from replicate short-term (5 pore-volume) capture experiments (n = 3).

The average capture that occurred in the bottom and top halves of the beads is shown in Table 10 in terms of total cells and their respective percentages of the inoculum. The capture that occurred in the bottom-half of the beads (influent-end of reactor) was statistically greater (paired t-test, p-value < 0.05) than the capture which occurred in the top-half of the beads for all the reactor conditions. The statistical significance is slightly greater (lower p-value) for the colonized reactors than for the control reactors which is expected after seeing the more pronounced trend in Figure 24 of greater capture near the influent.

Table 10. Short-Term *S. typhimurium* capture in top and bottom halves of beads

Reactor Condition	Colonized?	Inoculum (CFU)	Captured Cells (CFU)		Captured Percentage		P-value
			Bottom	Top	Bottom	Top	
CH Control	No	2.56E+09	2.39E+06	1.54E+06	0.09%	0.06%	0.024
CF Control	No	2.91E+09	1.86E+06	1.01E+06	0.06%	0.03%	0.022
CH 0.5 ft	Yes	3.96E+09	9.05E+06	1.39E+06	0.23%	0.04%	0.016
CF "0.5 ft"	Yes	3.14E+09	1.60E+07	1.71E+06	0.51%	0.05%	0.017
CH 1.0 ft	Yes	3.62E+09	1.66E+07	2.48E+06	0.46%	0.07%	0.014
CF "1.0 ft"	Yes	3.87E+09	4.22E+07	6.62E+06	1.09%	0.17%	0.015

Long-Term Experiments

This section gives the results for the long-term experiments conducted. After inoculating the reactor with a slug-dose of 1 mL of *S. typhimurium*, the reactor effluent was captured for 20 clean-reactor pore-volumes (68 mL) in two pore-volume increments (136 mL). At this point in time the flow to the reactor was stopped and the reactor was destructively sampled. The last column of Table 11 lists the pore-volumes drained by gravity from each of the reactors. As was seen in the short-term experiments, all of the values are less than the clean-reactor pore-volume of 68 mL. The drained pore-volumes for the uncolonized control reactors are again close to, but slightly less than, the true pore-volume of 68 mL due to some water wetting the interior reactor surfaces and not draining out. The colonized reactors have decreased pore-volumes (40-54 mL) due to biofilm growth in the reactor decreasing the available pore space for advective flow.

Long-Term Mass Balance Results

The mass balance on *S. typhimurium* performed around the reactor shows the relationship between the number of the culturable cells injected into the reactor with the number recovered. A recovery of 100% would demonstrate that the same number of cells injected into the reactor were recovered in the collected samples and suggests that the results were not greatly influenced by the growth or decay of cells or the detection-method (plate counts). The actual values for percent recovery are shown in Table 11 and vary from 83.4% to 107.9%. These values are less than what was recovered in the short-term experiments (90.4% to 128.4%) possibly suggesting than some of the cells had died or entered a viable but not culturable (VBNC) state during the extending sampling period.

Table 11. Long-Term Mass Balance Percent Recoveries of *S. typhimurium*

Exp. #	Type	Colonized?	Flow Regime	Inoculum (CFU)	Recovered (CFU)	Percent Recovered	$V_{P.F.}$ (mL)
18	Control	No	CH	3.60E+09	3.55E+09	98.6%	64
18	Control	No	CF	3.25E+09	3.48E+09	107.3%	63
21	Control	No	CH	2.24E+09	2.29E+09	102.3%	62
21	Control	No	CF	3.25E+09	3.50E+09	107.9%	60
16	Test	Yes	CH	3.55E+09	3.27E+09	92.2%	51
16	Test	Yes	CF	1.15E+09	1.18E+09	103.2%	51
19	Test	Yes	CH	1.77E+09	1.84E+09	104.2%	48
19	Test	Yes	CF	2.30E+09	1.97E+09	85.9%	47
17	Test	Yes	CH	2.76E+09	2.54E+09	92.1%	48
17	Test	Yes	CF	3.25E+09	3.16E+09	97.2%	54
20	Test	Yes	CH	2.71E+09	2.26E+09	83.4%	40
20	Test	Yes	CF	3.30E+09	3.41E+09	103.3%	53

Values of CFU are the total number of colony forming units present in an entire sample. The volume of the pore-fluid ($V_{P.F.}$) is the volume which freely drained from the reactor.

Table 12 presents a summary of Table 11 with average percent recoveries for each reactor condition sampled. These results were not compared for statistical significance due to the limited data set (n = 2 per reactor condition). However, it is interesting to note that control reactors had average percent recoveries slightly greater than 100% while all the colonized reactors with biofilm were below 100%.

Table 12. Long-Term Percent Recoveries Summary

Type	Colonized?	Percent Recovered
CF Control	No	103.0%
CH Control	No	105.1%
"0.5 ft" CF Test	Yes	97.7%
0.5 ft CH Test	Yes	89.0%
"1.0 ft" CF Test	Yes	94.7%
1.0 ft CH Test	Yes	93.4%

Long-Term *S. typhimurium* Breakthrough

The log-scale breakthrough curve (Figure 25) shows the total cell counts for each effluent sample collected. Also shown on this graph are the total cell counts in the inoculum and in the pore-fluid drained from the reactor during the destructive sampling. Each bar on the graph represents the arithmetic average of the total cell count from the two replicates with the error bars showing the standard deviation between replicates. The final effluent cell count is approximately a log lower in the colonized long-term experiments (PV 20) than in the colonized short-term experiments (PV 5) shown previously in Figure 18. Figure 25 also displays a different tailing behavior between the control reactors and the colonized reactors.

The tailing in the colonized reactors is leveling off around near PV 20 while the cell count in the control reactors is approximately a log lower and continuing to drop. This could suggest that some of the *S. typhimurium* cells are being detached from the biofilm in colonized reactors at a relatively constant rate. It could also suggest that a small amount of growth of *S. typhimurium* cells is occurring which releases a relatively constant number of cells.

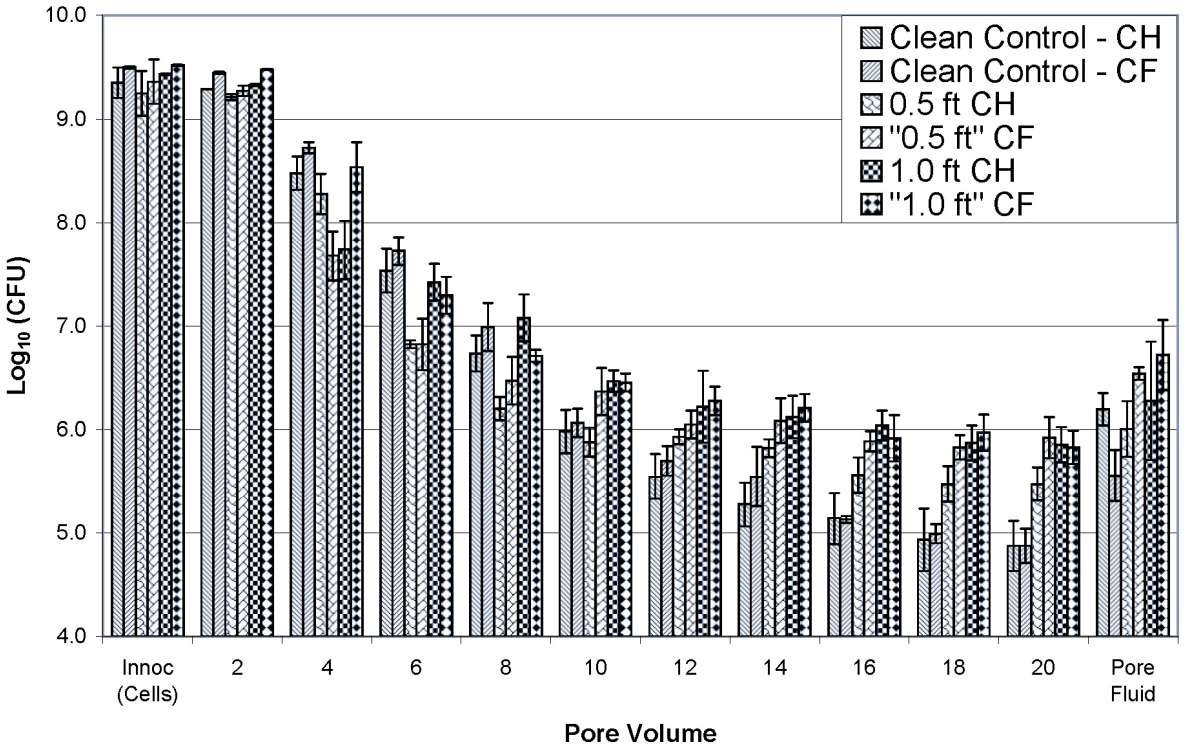

Figure 25. Log-scale breakthrough curve of *S. typhimurium* effluent samples from replicate, long-term (20 pore-volume) capture experiments (n = 2). Also included is the log values present in the inoculum and the pore-fluid drained from the reactor.

Table 13 shows the concentration (CFU/mL) of cells present in the last pore-volume (PV 20) and the pore-fluid drained from the reactor during destructive sampling. Unlike in the short-term experiments, all of long-term experiments display a concentration in the

drained pore-fluid higher (0.76 ± 0.25 logs) than what was present in the final effluent sample collected. This greater concentration in the drained pore-fluid suggests that the reversed fluid-direction during draining is detaching some *S. typhimurium* cells from the clean and the colonized reactors.

Table 13. Long-Term *S. typhimurium* Concentration in Drained Pore-fluid

Reactor Condition	Colonized?	PV 20 Conc. (CFU/mL)	Drained PF Conc. (CFU/mL)
CH Control	No	4.98E+03	1.89E+04
CF Control	No	3.04E+03	3.19E+03
CH 0.5 ft	Yes	1.94E+04	4.26E+04
CF "0.5 ft"	Yes	1.56E+04	4.05E+04
CH 1.0 ft	Yes	2.94E+04	1.12E+05
CF "1.0 ft"	Yes	2.66E+04	1.41E+05

The fractional-scale breakthrough curves show each replicate experiment individually on separate graphs for each reactor condition. The clean control, 0.5 ft, and 1.0 ft reactors are shown respectively in Figure 26, Figure 27, and Figure 28. These graphs compensate for the actual pore-volumes collected as was done for the short-term experiments (Equation 2). The actual pore-volumes for each reactor have a significant effect on these graphs and are listed in Table 11. Non-reactive tracer breakthroughs that were performed on these reactors are also shown in their respective figures.

The appearance of these long-term graphs is significantly different than the short-term graphs. While the effluent concentration in both the short-term and long-term experiments started low, peaked, and then tailed for the remainder of the effluent, this detail is not observed in the long-term graphs due to the increased sample size. The first four

samples in the short-term experiments are combined into one sample in the long-term experiments that contains upwards of 90% of the effluent cells or tracer. The percentage of cells in the remaining effluent samples drops significantly and by PV 10 the collected samples contain 0.10% or less. It should be noted that the maximum x-axis value shown is tripled and the step size is four times larger to account for the increased sample size and sampling duration in the long-term experiments.

The shape and values of the breakthrough curves for cells and the non-reactive tracer are similar for the control reactors (Figure 26). In the colonized reactors (Figure 27 and Figure 28) the shape of the breakthrough curves are similar between the cells and the non-reactive tracer. However, these reactors do display a slightly increased fraction of tracer over cells in the second effluent sample collected. This is similar to the increased tracer tailing observed in the short-term experiments, but the loss of detail due to larger sampling sizes makes it difficult to be certain.

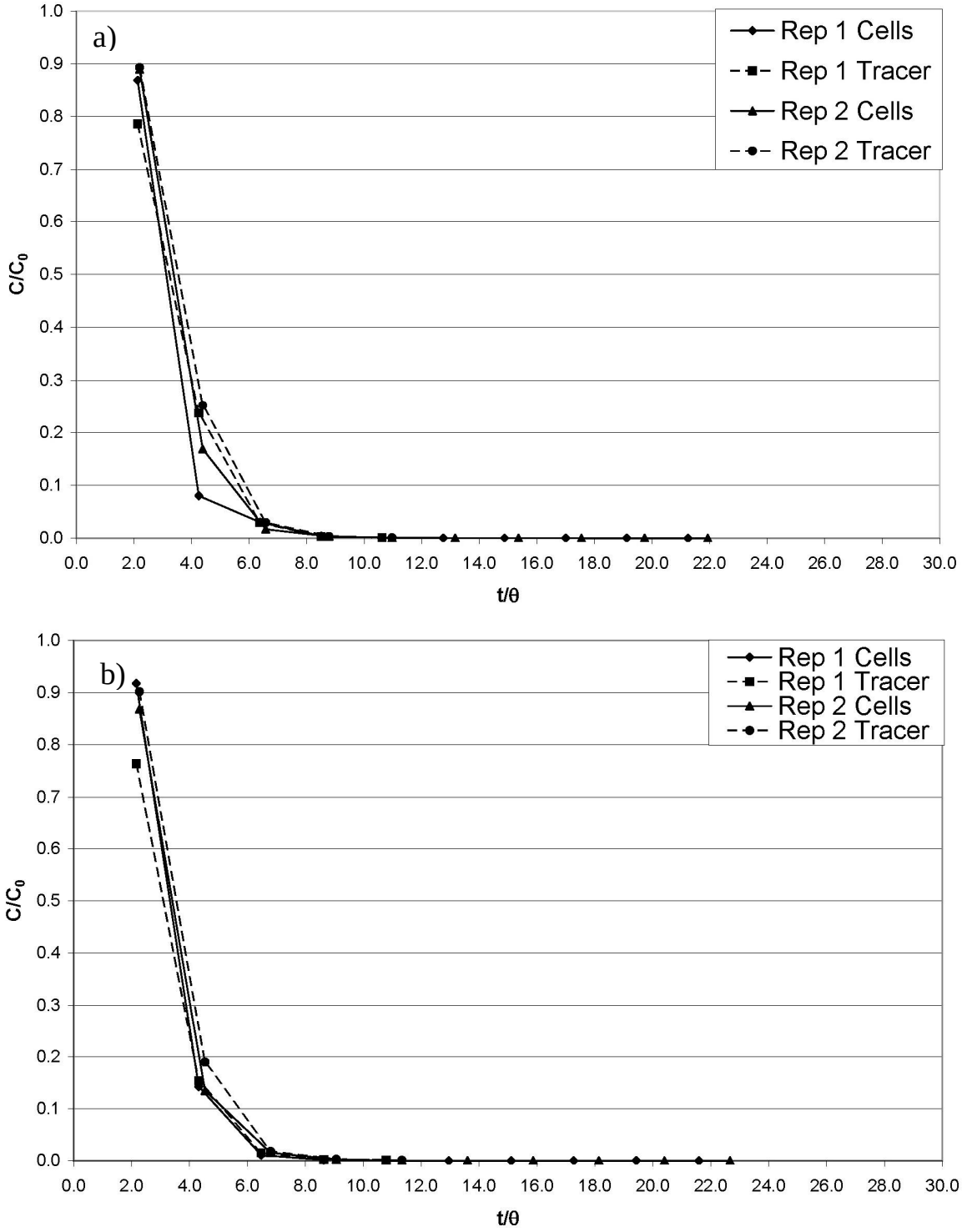

Figure 26. Fractional breakthrough curves of *S. typhimurium* and non-reactive tracer effluent samples from replicate long-term (20 pore-volume) capture experiments for clean control a) constant head reactors and b) constant flow reactors operated in parallel.

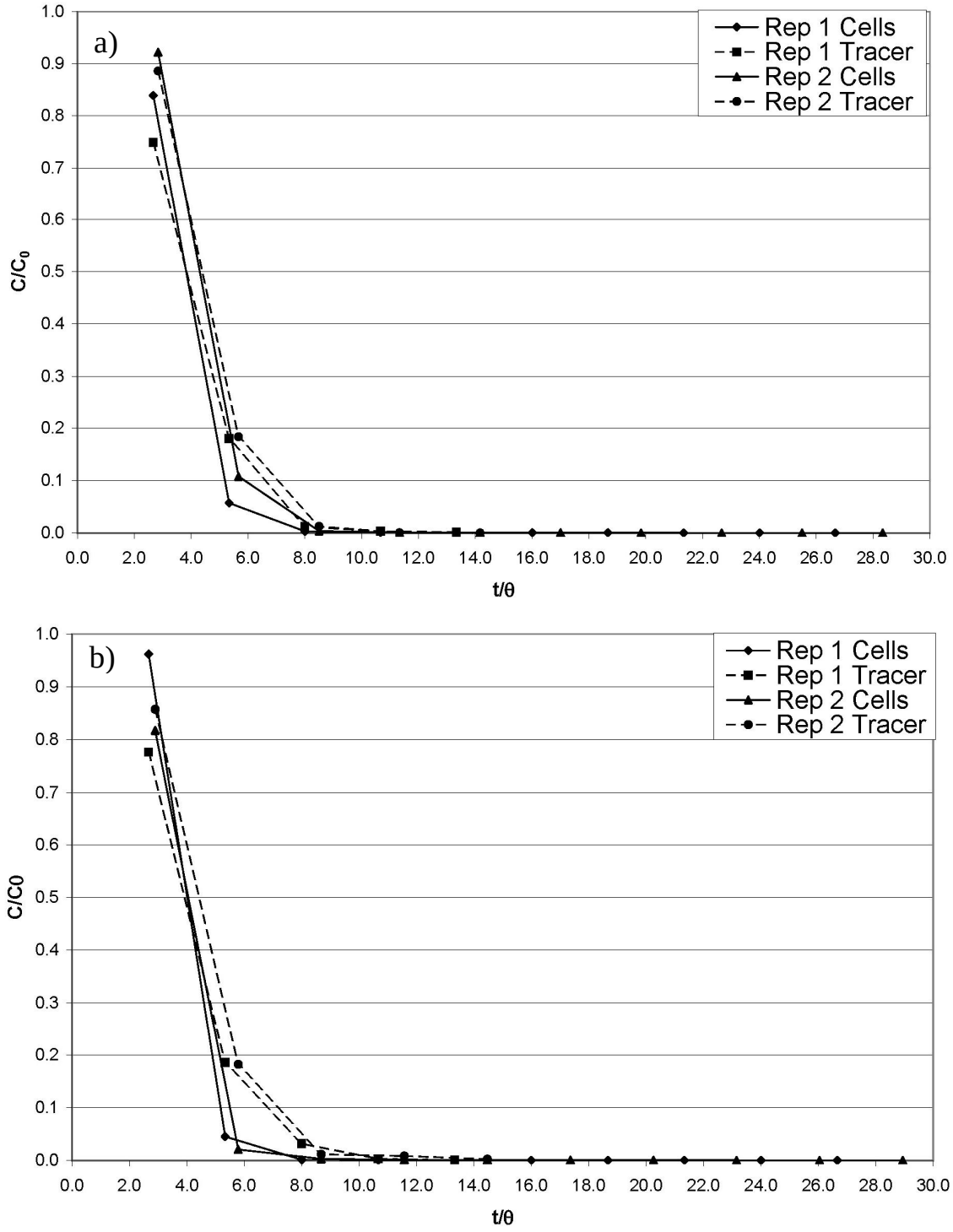

Figure 27. Fractional breakthrough curves of *S. typhimurium* and non-reactive tracer effluent samples from replicate long-term (20 pore-volume) capture experiments for colonized test (0.5 ft head) a) constant head reactors and b) constant flow reactors operated in parallel.

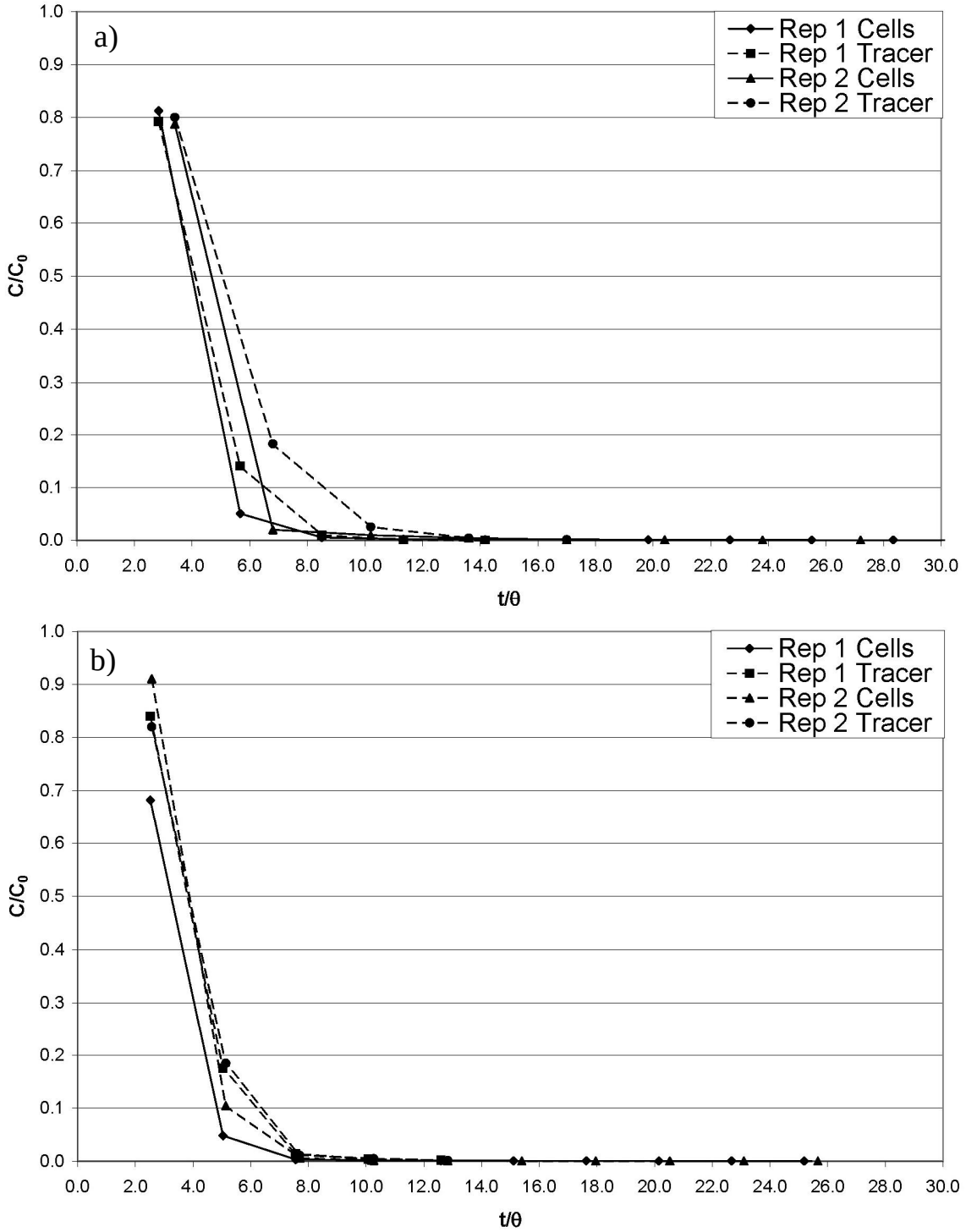

Figure 28. Fractional breakthrough curves of *S. typhimurium* and non-reactive tracer effluent samples from replicate long-term (20 pore-volume) capture experiments for colonized test (1.0 ft head) a) constant head reactors and b) constant flow reactors operated in parallel.

Long-Term Accelerated *S. typhimurium* Breakthrough

The breakthrough of *S. typhimurium* cells is expected to be accelerated over a non-reactive in these long-term experiments as was observed in the short-term experiments. The increased sample size in the long-term experiments results in an averaging effect and a loss of detail. As such, acceleration factors for L.T. experiments were not calculated.

Long-Term *S. typhimurium* Capture

Each reactor was destructively sampled after the effluent samples were collected and the flow through the reactor was stopped. The total cell count of *S. typhimurium* captured was determined and is shown for each reactor condition in Figure 29 on a log-scale. The capture shown is what occurred in both the beads and the reactor surfaces, with any associated biofilm. Also shown on the graph is the inoculum concentration. Each bar on the graph represents the arithmetic average of the total cell count from the two replicates with the error bars showing the standard deviation between replicates. The capture in the control reactors is similar between the CF and CH flow regimes. The capture in all four of the colonized reactors is around the same magnitude and is approximately 1.5 logs higher than the capture in the control reactors.

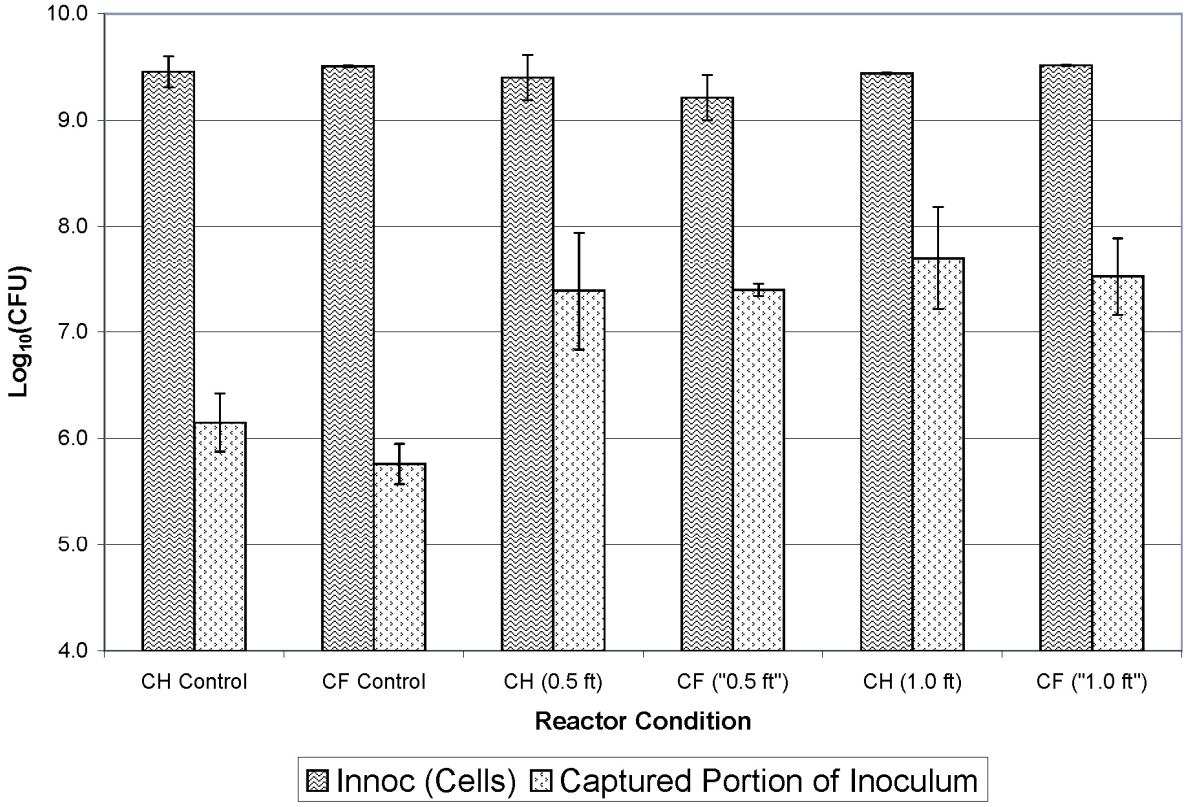

Figure 29. Total captured portion of *S. typhimurium* inoculum on reactor surfaces and porous media beads (combined) from replicate long-term (20 pore-volume) capture experiments (n = 2).

The average captured portion of the inoculum is shown in Table 14 in terms of total cells captured and the percentage of the respective inoculum. The capture in all of the colonized reactors was approximately 1.5 orders of magnitude greater than the capture in the control reactors. The capture which occurred in the CH 1.0 ft reactors is approximately 1% greater than the capture which occurred in the remainder of the colonized reactors.

Table 14. Long-Term Captured Portion of the Inoculum

Reactor Condition	Colonized?	Inoculum (CFU)	Captured Cells (CFU)	Capture Percentage
CH Control	No	2.92E+09	1.55E+06	0.05%
CF Control	No	3.20E+09	6.03E+05	0.02%
CH 0.5 ft	Yes	2.66E+09	3.48E+07	1.31%
CF "0.5 ft"	Yes	1.72E+09	2.49E+07	1.45%
CH 1.0 ft	Yes	2.74E+09	6.61E+07	2.42%
CF "1.0 ft"	Yes	3.28E+09	3.93E+07	1.20%

The total cell count of *S. typhimurium* captured within the reactor can be split into respective amounts captured on the reactor surfaces and by the glass beads. This is done in Figure 30 on a log-scale graph. Also shown in this figure is the total cell count of *S. typhimurium* present in the pore-fluid drained from the reactor during destructive sampling. Each bar on the graph represents the arithmetic average of the total cell count from the two replicates with the error bars showing the standard deviation between replicates.

The capture results for the long-term experiments are similar to the short-term results. All six reactor conditions display a greater capture of cells by the glass beads than by the reactor surfaces, with the exception of the CF (“0.5 ft”) reactors. The colonized reactors all display greater capture on the reactor surfaces and the beads than the clean-control reactors. All of the reactor conditions have cells counts in the pore-fluid at the same magnitude, or lower, than what was captured on the beads.

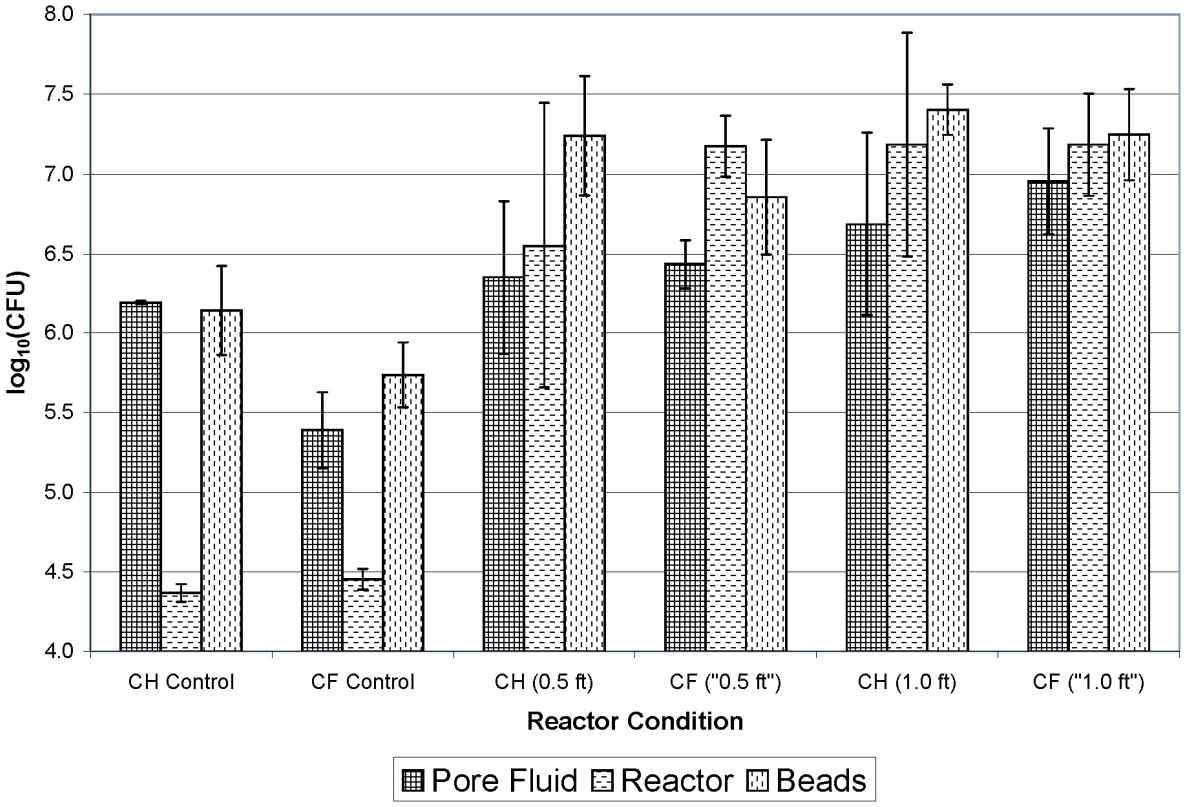

Figure 30. Log values of *S. typhimurium* present in drained pore-fluid and captured on reactor surfaces and porous media beads from replicate long-term (20 pore-volume) capture experiments (n = 2).

Table 15 shows the average amount of *S. typhimurium* captured on the reactor surfaces and the porous media beads with any associated biofilm, if present. The capture which occurred on the beads and reactor surfaces in the colonized reactor was greater than the capture which occurred in the control reactors for all reactor conditions. This would likely be of statistical significance if a third replicate experiment was performed.

Table 15. Long-Term Reactor and Beads Capture

Reactor Condition	Colonized?	Inoculum (CFU)	Captured Cells (CFU)		Captured Percentage	
			Reactor	Beads	Reactor	Beads
CH Control	No	2.92E+09	2.34E+04	1.53E+06	0.00%	0.05%
CF Control	No	3.20E+09	2.87E+04	5.74E+05	0.00%	0.02%
CH 0.5 ft	Yes	2.66E+09	1.42E+07	2.07E+07	0.53%	0.78%
CF "0.5 ft"	Yes	1.72E+09	1.64E+07	8.44E+06	0.96%	0.49%
CH 1.0 ft	Yes	2.74E+09	3.99E+07	2.62E+07	1.46%	0.96%
CF "1.0 ft"	Yes	3.28E+09	1.97E+07	1.96E+07	0.60%	0.60%

The cell capture that occurs on the glass beads and any associated biofilm is not uniformly distributed across the reactor. Figure 31 is log-scale graph which shows the total capture of *S. typhimurium* on the beads from Figure 30, and then breaks that total capture down into capture which occurred in the bottom-half and top-half of the glass beads. All four of the colonized reactor conditions display an approximately one log greater capture in the bottom-half (influent side) over the top-half of the porous media similar to the short-term experiments. The capture in the control reactors is different from what occurred in the short-term experiments as the bottom-half of the beads captured the same number or less than the top half.

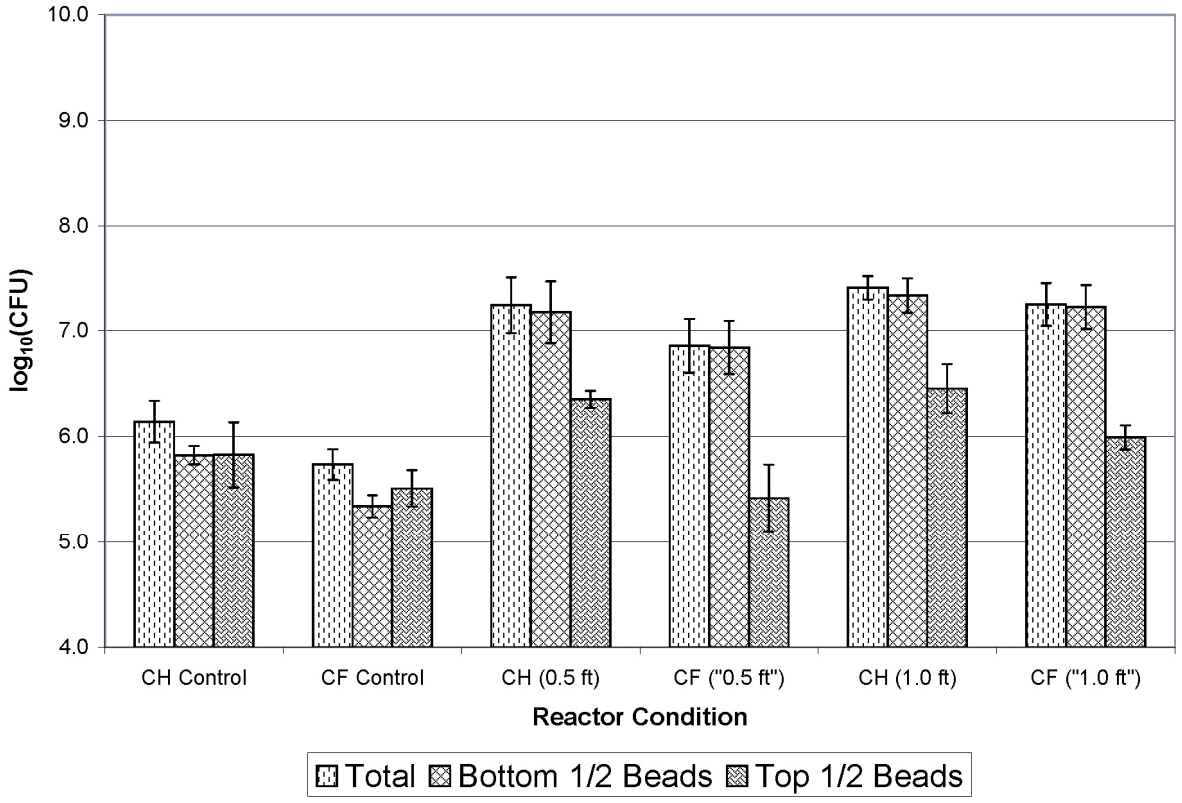

Figure 31. Log values of *S. typhimurium* captured in top and bottom halves of porous media beads from replicate long-term (20 pore-volume) capture experiments (n = 2).

The average capture that occurred in the bottom and top halves of the beads is shown in Table 16 in terms of total cell counts and their respective percentages of the inoculum. The capture that occurred in the bottom-half (influent-end of reactor) of the beads was significantly greater than the capture which occurred in the top-half of the beads for all the colonized reactors. However, the uncolonized control reactors capture which occurred in the top-half was the same or more than the bottom-half.

Table 16. Long-Term capture in top and bottom halves of porous media beads

Reactor Condition	Colonized?	Inoculum (CFU)	Captured Cells (CFU)		Captured Percentage	
			Bottom	Top	Bottom	Top
CH Control	No	2.92E+09	6.79E+05	8.47E+05	0.02%	0.03%
CF Control	No	3.20E+09	2.25E+05	3.49E+05	0.01%	0.01%
CH 0.5 ft	Yes	2.66E+09	1.84E+07	2.28E+06	0.69%	0.09%
CF "0.5 ft"	Yes	1.72E+09	8.11E+06	3.35E+05	0.47%	0.02%
CH 1.0 ft	Yes	2.74E+09	2.29E+07	3.25E+06	0.84%	0.12%
CF "1.0 ft"	Yes	3.28E+09	1.86E+07	1.01E+06	0.57%	0.03%

Short Term vs. Long Term Capture

Table 17 contains logarithmic values for the capture of S. typhimurium in the reactor porous media previously shown graphically in Figure 18 & Figure 25. Table 18 displays similar results for the capture which occurred on the reactor surfaces and contains the mean inoculum for each reactor condition. Table 19 compares the capture between the long-term reactors and the short-term reactors. The values displayed are the difference of the mean logs between L.T. and S.T. experiments with a combined standard deviation.

Table 17. Comparison of *S. typhimurium* capture on short and long-term reactor porous media beads. Counts are $\log_{10}$(CFU) presented as mean ± standard deviation.

Reactor Condition	Colonized?	Beads - Bottom		Beads - Top	
		S.T.	L.T.	S.T.	L.T.
CH Control	No	6.37 ± 0.09	5.82 ± 0.09	6.19 ± 0.03	5.83 ± 0.31
CF Control	No	6.23 ± 0.22	5.34 ± 0.10	5.99 ± 0.16	5.51 ± 0.17
CH 0.5 ft	Yes	6.96 ± 0.01	7.17 ± 0.29	6.12 ± 0.18	6.35 ± 0.08
CF "0.5 ft"	Yes	7.06 ± 0.49	6.84 ± 0.25	6.17 ± 0.29	5.42 ± 0.32
CH 1.0 ft	Yes	7.21 ± 0.10	7.33 ± 0.16	6.39 ± 0.08	6.45 ± 0.23
CF "1.0 ft"	Yes	7.62 ± 0.02	7.22 ± 0.21	6.80 ± 0.16	5.99 ± 0.11

Table 18. Comparison of *S. typhimurium* inoculation and capture on short and long term reactor surfaces. Counts are $\log_{10}$(CFU) presented as mean ± standard deviation.

Reactor Condition	Colonized?	Inoculation		Reactor Surfaces	
		S.T.	L.T.	S.T.	L.T.
CH Control	No	9.39 ± 0.14	9.45 ± 0.15	5.03 ± 0.03	4.37 ± 0.06
CF Control	No	9.44 ± 0.17	9.50 ± 0.01	5.17 ± 0.13	4.45 ± 0.07
CH 0.5 ft	Yes	9.60 ± 0.02	9.40 ± 0.21	6.83 ± 0.61	6.55 ± 0.89
CF "0.5 ft"	Yes	9.49 ± 0.06	9.36 ± 0.21	6.76 ± 0.60	7.18 ± 0.19
CH 1.0 ft	Yes	9.55 ± 0.12	9.44 ± 0.01	6.19 ± 0.16	7.19 ± 0.70
CF "1.0 ft"	Yes	9.58 ± 0.06	9.52 ± 0.00	7.27 ± 0.39	7.19 ± 0.32

Table 19. Difference of long and short-term mean log capture values

Reactor Condition	Colonized?	Log_{10}(L.T) - Log_{10}(S.T.) ± (L.T. + S.T. st. dev)		
		Beads - Bottom	Beads - Top	Reactor Surfaces
CH Control	No	-0.55 ± 0.18	-0.36 ± 0.34	-0.67 ± 0.09
CF Control	No	-0.89 ± 0.33	-0.48 ± 0.33	-0.71 ± 0.19
CH 0.5 ft	Yes	0.22 ± 0.30	0.23 ± 0.26	-0.28 ± 1.50
CF "0.5 ft"	Yes	-0.22 ± 0.74	-0.76 ± 0.61	0.42 ± 0.80
CH 1.0 ft	Yes	0.12 ± 0.26	0.06 ± 0.32	0.99 ± 0.86
CF "1.0 ft"	Yes	-0.40 ± 0.23	-0.81 ± 0.27	-0.08 ± 0.71

Negative values in Table 19 are the result of decreased captures for the long-term experiments compared to the short-term experiments. Negative values would be expected as the additional effluent sampling time for the L.T. experiments allows more reversibly attached cells to detach from the porous media. This occurs for the uncolonized control reactors and the colonized CF test reactors. The colonized CH test reactors show an increased capture for the L.T. experiments over the S.T. experiments. The CF “0.5 ft” and CH 1.0 ft colonized test reactors also show increased capture on the reactor surfaces. It is important to note that the standard deviation for many of these conditions exceed the

difference of logs which means that the variance for those results overlap and they are not considered to be significant.

Constant Head vs Constant Flow Capture

The total capture of *S. typhimurium* cells on the porous media beads for all six reactor condition, and for short-term and long-term experiments, is listed in Table 20. Values for capture that include reactor surfaces are not included as the capture difference due to constant flow and constant head flow regimes is related to the spatial orientation of biofilm within the porous media. A two-sample, two-sided t-test was used to evaluate whether the difference between CH and CF was of statistical significance for the short-term experiments ($n = 3$). The CH (1.0 ft) and the CF ("1.0 ft") reactor conditions were the only ones of statistical significance ($p = 0.011$) indicating that the increased capture in the CF reactors over the CH reactors was statistically different. Using a two-sample, one-sided t-test the capture in the CF ("1.0 ft") reactors was statistically greater ($p = 0.006$) than the capture in the CH (1.0 ft) reactors. While the long-term results were not analyzed for statistical significance ($n = 2$) it is worth noting that the CH reactors had greater capture in the uncolonized control reactors and the two colonized test reactors. This greater capture in the CH reactors during long-term experiments contradicts the greater capture in the CF reactors during the short-term experiments.

Table 20. Total Capture on Porous Media Beads

Reactor Condition	Colonized?	Beads - Total (Short-Term)			Beads - Total (Long-Term)			Short-Term p-value
CH Control	No	6.59	±	0.07	6.14	±	0.20	0.309
CF Control	No	6.43	±	0.20	5.74	±	0.14	
CH 0.5 ft	Yes	7.02	±	0.02	7.24	±	0.26	0.736
CF "0.5 ft"	Yes	7.12	±	0.46	6.86	±	0.25	
CH 1.0 ft	Yes	7.28	±	0.08	7.40	±	0.11	0.011
CF "1.0 ft"	Yes	7.69	±	0.01	7.25	±	0.20	

Confocal Microscope Capture

Pathogen capture on a global scale can be determined using the model reactors, but with the destructive sampling nature of these reactors it is not feasible to extract information on pathogen capture at a localized scale. The confocal microscope fills this gap with its non-destructive observation capabilities that makes it possible to observe pathogen capture in real-time and at a scale that individual cells can be seen attaching to single collectors, in the grain-to-grain crevices of two collectors, or to biofilm attached to the a collector.

Images were collected of GFP-labeled *S. typhimurium* passing through and being captured in porous media packed into a 0.9 mm square flowcell. These experiments were performed in both clean and colonized flowcells to differentiate between capture on the glass beads themselves and capture due to biofilm growth. Image collection was performed with a 10x objective that allowed observation across the entire width of the flowcell and with a 40x objective that zoomed in to observe capture on only a few of the 100 μm glass beads.

Figure 32 shows two images (40x) from a sterile flowcell inoculated with approximately $3*10^9$ CFU/mL of *S. typhimurium*. The first panel is an overlay of the transmitted light image showing the beads and the fluorescent signal from GFP *S. typhimurium* cells traveling through the flowcell. The second panel is an overlay of the transmitted light image and the fluorescent signal from captured GFP *S. typhimurium* cells after the spike had passed through the reactor and the feed water had been switched back to a sterile flow. A few cells were captured by intercepting the surface of a collector while others were strained in the upstream grain-to-grain contact point between two adjacent collectors. Some cells were still observed in the bulk fluid after the feed water had been returned to the sterile source. These cells are believed to reversibly attached cells from upstream that detached and re-entered the bulk fluid. The slightly different arrangement of 100 μm beads in these pictures is the result of the beads shifting during imaging.

Figure 33 shows four images (40x) from a flowcell previously colonized with an *E. coli* K-12/DsRed that produced a biofilm that was challenged with approximately $3*10^9$ CFU/mL of *S. typhimurium* containing GFP. The first panel is an overlay of the transmitted light image with the background K-12/DsRed biofilm colonizing the pore space prior to inoculation with *S. typhimurium*. The second panel is an overlay of the transmitted light image with the background K-12/DsRed biofilm and the spike of GFP *S. typhimurium* cells traveling through the flowcell. The third panel is an overlay of the transmitted light image and the captured GFP *S. typhimurium* cells within the K-12/DsRed biofilm after the spike had passed through the reactor and the feed water had been switched back to a sterile flow. The fourth panel is from a different field of view within the flowcell that was also taken after

the feed water had been switched back to a sterile flow. Cells were observed being captured within the K-12/DsRed biofilm. Based on the images in panel c of GFP cells retained in open pore spaces not directly in contact with a red biofilm cell, it is believed that the K-12 biofilm was not uniformly expressing the DsRed protein. Some *S. typhimurium* cells were still observed in the bulk fluid after the feed water had been returned to the sterile source. These cells are believed to have detached upstream and re-entered the bulk fluid, similar to what was observed in the sterile flowcell.

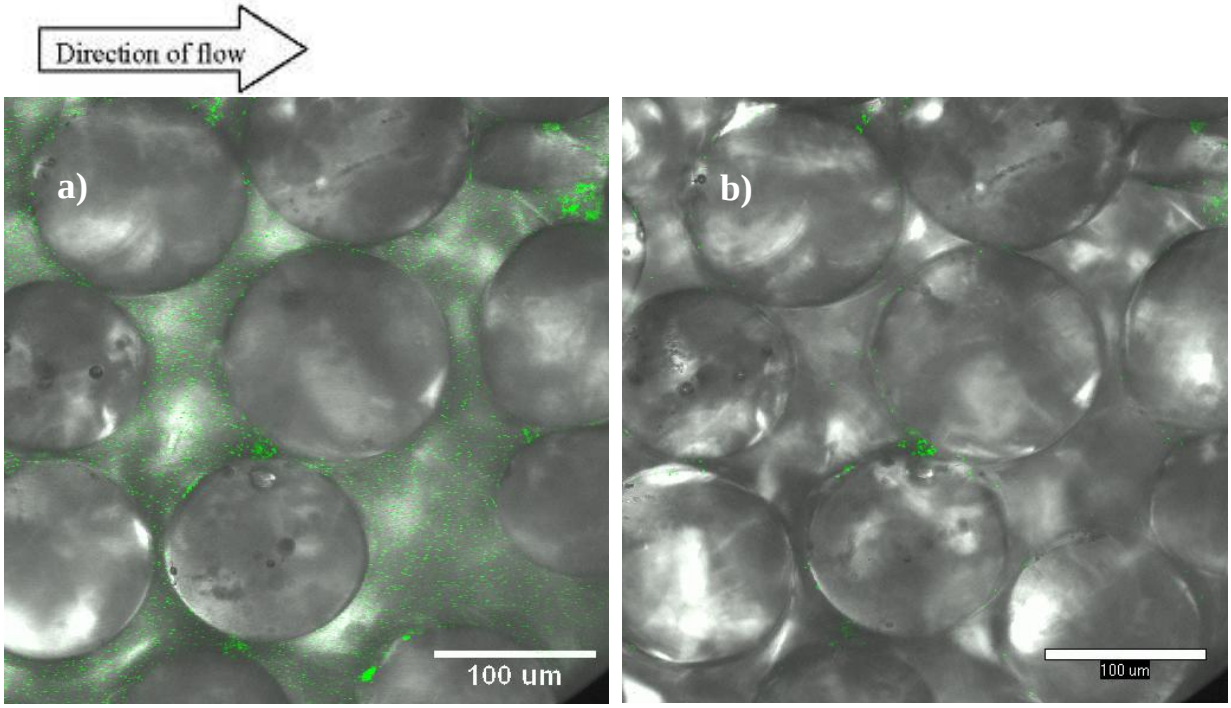

Figure 32. Confocal images of GFP *S. typhimurium* (green) transport and capture in a sterile 0.9 mm square flowcell packed with 100 μm glass beads taken a) during spike innoculation and b) after spike innoculation.

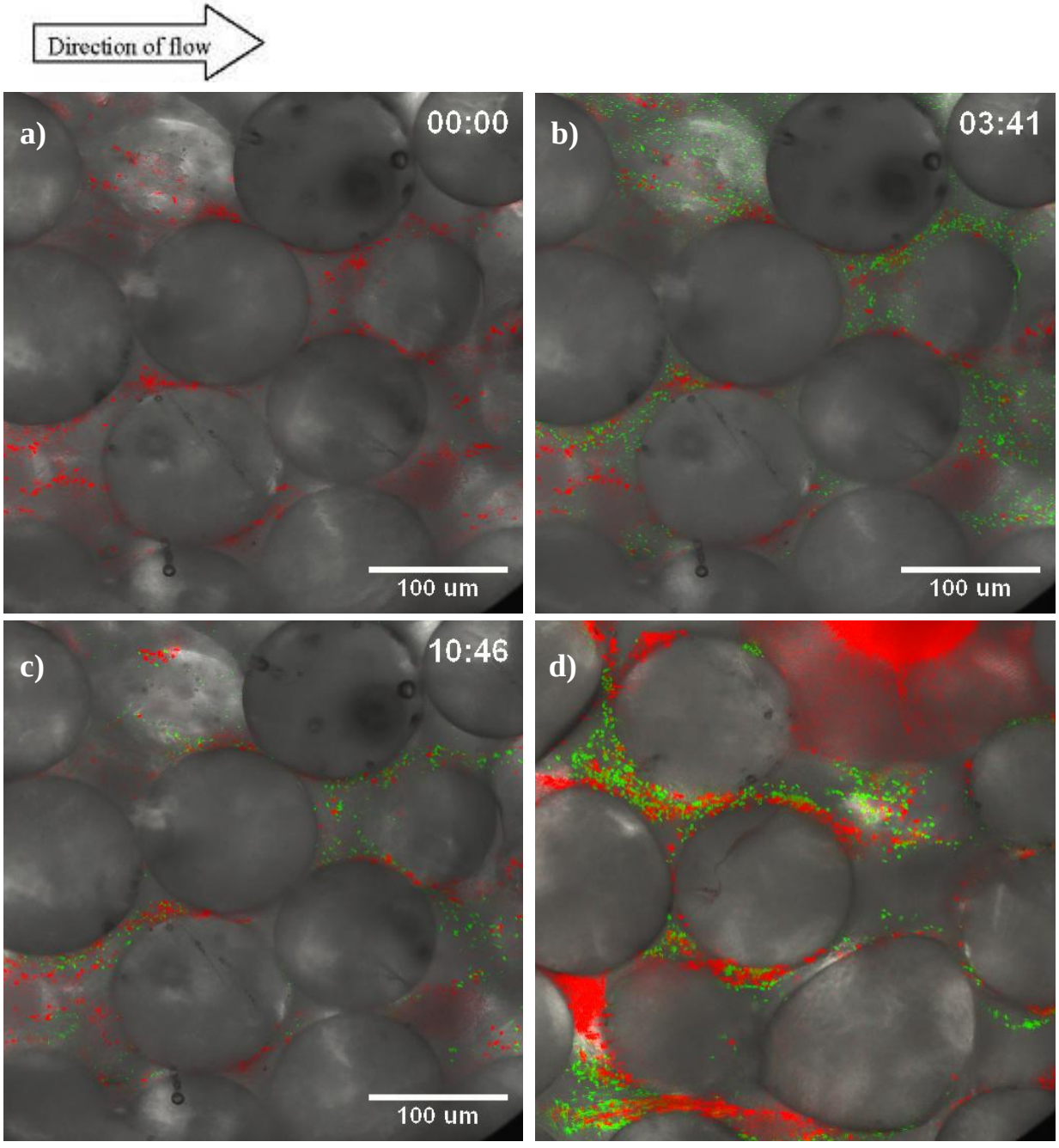

Figure 33. Confocal images of GFP *S. typhimurium* (green) transport and capture in a DsRed K-12 colonized 0.9 mm square flowcell packed with 100 μm glass beads taken a) prior to inoculation b) during spike inoculation c) after spike inoculation and d) after spike inoculation in a different field of view.

CHAPTER 5

DISCUSSION

Observations

Figure 15 and Figure 16 show two samples of flowrate through and headloss across simultaneously operated constant head (CH) and constant flow (CF) reactors. The flowrate in the CF reactors would remain at 25 mL/min as long as the pump remained on. However, the flowrate in the CH reactor, and resulting pore velocity, would continue to drop as the reactor fouled until flow through the reactor stopped. Theoretically, if the CH reactor was allowed to foul so thoroughly that the flow through the reactor stopped, the headloss across the reactor would peak at the operating head (0.5 or 1.0 feet for respective reactor conditions).

This differs from the CF reactor where spikes in the headloss occurred due to water being pumped through at a constant rate regardless of the reduced permeability from the biofilm growth. Some CF reactors had headloss values that peaked in excess of two feet before returning to normal values. This increase in headloss across the reactor is believed to continue until the fluid shear-force is great enough to detach some biofilm from within the porous media to open up pore space for flow. These detachment events are believed to change existing, or form new, preferential flow paths consistent with observations by *Sharp et al.* [2005]. The repetitive spikes in headloss observed in the CF reactors that are believed to be the result of new channel formations is supported by modeling work by *Stewart and Kim* [2004] examining the interactions of biomass-plug formations and the breakthrough of

new channels in a two-dimension network. Their work demonstrated that oscillations occur in pressure drop (headloss) and permeability due to biomass plug propagation in reactors with constant flow rates.

The existence of preferential flow paths in the CF reactors is supported by images collected during the tracer studies as shown in Figure 17. The CF reactors displayed these preferential flow paths through the glass beads while other flow paths were partially blocked. This phenomenon is consistent with research by *Seymour* [2004] that used magnetic resonance microscopy to image the flowrate variations between blocked and open pore channels within a single sample. Under the operating conditions used, the CF reactors displayed multiple preferential flowpaths at one time, in contrast with research by *Sharp et al.* [1999] with flatplate reactors containing a single preferential flowpath. The CH reactors did not appear to have these preferential flow paths and fully utilize the available porous media.

It is important to note that the tracer path observations occurred at the interface of the porous media and the reactor wall on a single side of the reactor. Images were not taken at other angles, and furthermore it is not possible to visually observe the flow of a tracer through the interior of the porous media. It is, however, possible to draw some conclusions about the tracer flow through this region based upon the calculated breakthrough centroids presented in Table 7. The control reactors displayed similar centroids (t/θ) for the CH reactors (1.92) and the CF reactors (1.80). The slightly lower values for the CF reactors may be the result of increased longitudinal mixing as a result of the small pulses in flow imparted by the peristaltic pump. The 0.5 ft colonized reactors also displayed similar centroids for the

CH reactors (2.49) and the CF reactors (2.59) indicating that the overall transport of tracer through the reactors with biofilm was not likely influenced by the difference in flow-regimes. The 1.0 ft colonized reactors had different tracer centroids for the CH reactors (3.26) as opposed to the CF reactors (2.62). Because a longer time was required for CH reactor flow to drop to 25 mL/min these reactors developed more biofilm, possibly to the point of developing more preferential flowpaths through the interior of the porous media. This earlier tracer breakthrough in a CF reactor is consistent with research by *Sharp et al.* [2005] with flatplate reactors.

Mechanisms of Capture

All three of the mechanisms discussed in the literature review contribute to the capture of *S. typhimurium* in the model reactors under different conditions. In clean reactors the mechanisms are attachment and straining as the pore spaces are too large for mechanical filtration to occur. While some straining was observed in the confocal experiments, attachment may be the dominant mechanism as little straining would be expected due to a $d_p/d_m = 0.0003$ which is an order magnitude lower than the suggested extreme minimum value of $d_p/d_m = 0.0017$ by *Bradford et al.* [2005]. This low value of d_p/d_m is the result of using 3 mm glass beads to comprise the porous media as compared to column studies done by *Bradford et al.* [2004] using sands with diameters of 710, 360, 240, and 150 μm. The colloids used by *Bradford et al.* [2005] were inert microspheres rather than bacterial cells which may also influence straining. The *S. typhimurium* used in the confocal experiments displayed a ripening behavior where cells from the bulk fluid would attach to previously

strained cells. This combination of straining and ripening could greatly increase the capture of bacterial cells in straining locations if it occurs in the model reactor. The 100 μm glass beads used as porous media in the flowcell increases the value of d_p/d_m to 0.01 suggesting an increase in straining behavior in the flowcell over the model reactor ($d_p/d_m = 0.0003$).

Straining could also play a greater role in the model reactor due to the uniform porous media rather than natural heterogeneous porous media such as sand or soil. A three dimensional trajectory analysis done by *Cushing and Lawler* [1998] indicated that the hydrodynamics through uniform porous media in a cubic packing arrangement funneled colloids to straining contact points. While the arrangement of the 3 mm glass beads within the model reactor used for this research was random, portions of the beads were likely arranged in a cubic packing arrangement. This could result in greater straining within the model reactors and flowcells used in this research compared with natural heterogeneous porous media.

Additional capture mechanisms and capture locations exist in the colonized model reactors that were not present in the clean control reactors. In addition to straining that occurs at the grain-to-grain boundary of two porous media collectors, cells in the bulk fluid can be strained by the biofilm attached to the porous media as was observed with the confocal experiments. Cells can also be mechanically filtered if sufficient biofilm growth nearly closes off the pore-throat between collectors. This is supported by confocal images of captured *S. typhimurium* cells in the middle of a pore throat colonized by the Ds-RED K-12 biofilm.

Mechanisms of Transport

Two of the three mechanisms of transport to colloid surfaces are likely to be mainly responsible for transport leading to attachment within the reactor. These two mechanisms are interception and diffusion as the cell size is around the 1 μm minimum where both processes contribute to transport [*Yao et al*., 1971]. Sedimentation is not likely to occur to any great extent with the experiments performed. This is due to the bacterial cells having a density (1.05 g/cm^3) which is close to that of water (0.998 g/cm^3) [*Murphy and Ginn*, 2000] and the reactor being operated in an up-flow mode opposing gravity.

Fate & Recovery of *S. typhimurium*

The calculated percent recoveries of close to 100% demonstrate that the inoculated cells could be adequately recovered, and this made it possible to determine the ultimate fate of the *S. typhimurium* cells. Recovery values close to 100% also indicate that the detection method selected (plate counts) was reliable. Recovery values greater than 100% could indicate that growth was occurring in the samples before being plated, or inside the column while collecting effluent samples. However, this is not believed to be occurring to a great extent due to the short sampling duration (15 min for short-term, 1 hr for long-term experiments) and the short time duration (1 hr) between collecting the samples and processing them, during which time the samples were kept on ice. Recovery values less than 100% could indicate that some cells were recovered but were not culturable, or that some cells were not recovered. Some cells were likely attached to the interior of the effluent tubing. Slight discrepancies in volumes pipetted during serial dilutions, or multiple cells

growing into one colony on SS agar plates could also account for recovery values not equaling 100%.

Breakthrough

The short-term (S.T.) and the long-term (L.T.) breakthrough showed considerable tailing. The concentration in the tailing of the S.T. colonized reactors was still dropping at the final effluent sample (PV 5.0) but appeared to level off in the L.T. colonized reactors at approximately 10^4 CFU/mL after PV 10. While the effluent cell concentration in the L.T. colonized reactors levels off, the concentration in the final effluent sample in the L.T. uncolonized reactors continued to drop. The increased concentration in the effluent of the colonized reactors is consistent with reversibly attached cells detaching and re-entering the bulk flow. This behavior was also observed with the confocal microscope where reduced numbers of *S. typhimurium* cells were observed in the bulk fluid after the flow had been returned to a sterile source.

The cell concentration in the drained pore-fluid is approximately half the concentration in the final effluent sample (PV 5.0) for all of the S.T. reactors. This result is expected as the concentration of cells in the reactor pores attenuates with time as seen in the breakthrough curves. However, for all of the long-term (L.T.) reactors, the cell concentration in the drained pore-fluid is greater than the concentration in the final effluent sample (PV 20). This increased concentration suggests that reversibly attached bacteria are detaching when the flow direction reverses while the pore-fluid is drained from the reactor. This is

likely occurring in the S.T. reactors as well, but not to a great enough extent that it is evident over the higher background levels present at PV 5.0 compared to PV 20.

The fractional-scale breakthrough curves are shown for individual experiments. In the control reactors (Figure 19), the general shape of the breakthrough for each experiment is the same suggesting that no large variations in hydrodynamics exist. The results of the tracer study are very similar to the cell breakthrough for the control experiments. This suggests that cell interactions with the porous media do not greatly impede the breakthrough of cells as compared to the non-reactive tracer. Differences in peak concentrations on these graphs may be due to percent recoveries varying as was shown previously in Table 4 and Table 11. Experiments with recoveries greater than 100% will have greater values of C/C_0 than experiments with recoveries less than 100%.

The peak breakthrough values are greater in the colonized reactors (Figure 20 and Figure 21) than in the control reactors for the S.T. experiments. This is consistent with the idea of accelerated breakthrough due to reduced pore space available for advective flow. Unlike the control reactors, these colonized reactors show a discrepancy between cell breakthrough and tracer breakthrough. The peak breakthrough values are less for the tracer than for the cells. The tracer also displays increased tailing when compared with the cells. This probably is due to the cells mainly being transported advectively through the open pore space while the tracer dye is transported advectively and also diffuses into the biofilm. This diffusion of tracer into the biofilm accounts for the reduced peak values. It also accounts for the increased tailing as the tracer diffuses back out of the biofilm as the tracer concentration diminishes from its peak. This behavior is consistent with tracer study results in flat plate

reactors by *Sharp et al* [1999] who found that the growth of biofilm in a porous media created primary porosity (advective) flow channels and secondary porosity due to diffusion-like dye transport through the biofilm.

This also occurred in the L.T. experiments but is not as evident due to the larger sample sizes collected. The tracer studies do exhibit a slightly lower breakthrough in the first sample (PV 2) than the *S. typhimurium* cells and higher breakthrough in the second sample (PV 4), which is consistent with the S.T. results. The larger sample sizes produce an average value that would contain four separate sample points in the S.T. experiments. This averaging effect results in the loss of detail that shows the difference between cell breakthrough and tracer breakthrough.

The nature of the reactor design is responsible for some of the observed tailing effect in the reactors. The mixing chamber at the influent of the reactor is effectively a constantly stirred-tank reactor (CSTR) which contains a peak concentration of cells, or tracer dye, immediately after being inoculated. As water flows from the mixing chamber into the porous media, the concentration in the mixing chamber is diluted as it is mixed with the influent BAC water. This accounts for some of the initial tailing that is observed in the effluent samples. The diffusion of the tracer dye into, and back out of, the biofilm also accounts for some of the initial tailing that is observed in those studies. Tracer study data was not collected after PV 10 as the spectrophotometer used was not sensitive enough to detect the low concentrations of red food dye. Cell interactions with the porous media surface (i.e. reversible attachment followed by detachment events) are responsible for tailing effects observed in the long-term colonized experiments.

S. typhimurium Capture

The colonized reactors show a significant increase in the capture of *S. typhimurium* over the control reactors due to the presence of biofilm. The biofilm presents more favorable attachment conditions than the clean beads, increasing the amount of capture that occurs [*Donlan*, 2002]. Additionally, cells can either attach to the outer surface of the biofilm or they can integrate into the biofilm formation as it contains a network of channels through which flow can carry sessile cells [*Donlan and Costerton*, 2002; *Klayman* 2007]. The presence of biofilm in porous media increases the surface roughness as compared to the clean beads. This lowers the exposure a cell has to shear forces which could detach the cell, and the biofilm also increases the surface area available for capture compared to the clean beads [*Donlan*, 2002].

This increased capture is observed on the reactor surfaces and on the porous media beads when the biofilm is present. The capture on the beads is greater than that on reactor surfaces for the S.T. experiments, but the reactor surfaces do contribute a substantial amount to the total capture. This occurs because the majority of the biofilm in the reactor samples observed during destructive sampling was on the underside of the lower screen, extending downward into the mixing chamber. This biofilm likely captures the majority of the retained *S. typhimurium* cells. It is exposed to peak concentrations of cells for long time durations. The nature of the mixing chamber results in a more turbulent flow pattern than the laminar flow in the pore channels. This turbulent flow would increase the number of cell collisions with the biofilm, resulting in more chances for capture to occur [*Donlan and Costerton*, 2002]. The amount of biofilm present on the lower screen was not consistent between

experiments (date not shown) and is believed to accumulate when biofilm sloughs off the influent tubing and cannot pass through the lower screen.

Greater capture is observed in the bottom-half of the beads than in the top-half of the beads for all of the S.T. experiments. This may be because straining has been demonstrated to be a depth-dependent phenomenon with the greatest amount of straining occurring near the inlet side of a porous media [*Bradford et al*., 2005]. Additionally, in the colonized reactors, the observed gradient in biofilm growth across the reactor means there is more biofilm present to capture *S. typhimurium* in the bottom-half of the beads than in the top-half of the porous media.

The L.T. colonized experiments displayed the same trend as the S.T. experiments where increased capture was observed in the bottom-half of the beads. However, the control reactors displayed a shift in trends such that the top-half of the beads capture as much, or more than, the bottom-half of the beads. This suggests that the capture observed in the S.T. control experiments is mostly reversible. By allowing the reactor to operate longer in the L.T. experiments, many of the reversibly attached cells detach and reenter the bulk flow. These detached cells can continue to reversibly attach and detach while being transported through the reactor, or they can become irreversibly attached.

Constant Head vs. Constant Flow Capture

Bacterial capture was expected to occur to a greater extent in the CH reactors as compared to the CF reactors due to the CH reactors utilizing more of the available pore space for advective flow. The results do not support this hypothesis as the capture in the CF

reactors is equal to, or greater than, the capture in the CH reactors. It is possible that this result occurs because the reduced pore space available in the CF reactor will transport a proportionally increased concentration of *S. typhimurium*. This increased concentration causes an increased number of colloid collisions to occur with the porous media surface presenting more opportunities for capture to occur [*Stevik et al.,* 2004]. This increased collision frequency may offset the fact that the bacterial cells are exposed to less surface area for capture.

Transport and Capture Comparison

The transport comparison based upon breakthrough centroids indicates that the breakthrough of *S. typhimurium* cells is accelerated in comparison with a non-reactive tracer. This conclusion contradicts earlier work [*Bauman,* 2007] done with the same model reactor using *E. coli 0157:H7* as the model pathogen which indicated that the transport of cells was accelerated when compared to a non-reactive tracer (fluorescein). The reactors were operated under constant flow conditions at 25 mL/min with 0.5ppm of the same supplemental organic carbon for two weeks (thin biofilm condition) and three weeks (thick biofilm condition), at which point in time the reactor was inoculated with a spike does of *E. coli 0157:H7*.

Breakthrough centroids were calculated for the cells in terms of mean cell residence times (sec). The mean hydraulic residence time (sec) for a clean control reactor was calculated as the ratio of the reactor pore volume to the flowrate. Mean hydraulic residence times for the colonized reactors were calculated as the ratio of the available reactor pore

volume (based on draining the pore fluid) to the flowrate. Retardation factors were then calculated as the ratio of the mean cell residence time to the mean hydraulic residence time. The resulting retardation factors for the reactor conditions were 1.11 (control), 1.62 (thin biofilm), and 1.74 (thick biofilm). These retardation factors could be represented as acceleration factors of 0.90, 0.62, and 0.57 respectively. These values contradict the average acceleration factors determined by this research of 1.33 and 1.37 for constant flow reactors. The reason for this discrepancy is believed to be due to the method that *Bauman* [2007] used to determine hydraulic residence times for the reactors. They were mathematically calculated values based on available pore volumes rather than using the centroid of a non-reactive tracer. Calculating residence times based on pore volumes and flowrates does not account for the diffusion of the tracer through the biofilm that accumulates within the porous media.

Bauman [2007] also determined the capture of *E. coli 0157:H7* that occurred in these same model reactors. The captured percentages of the inoculum for the three reactor conditions used were 0.22% (control), 0.75% (thin biofilm) and 9.37% (thick biofilm). The control reactor capture with *E. coli 0157:H7* compares with the control capture of *S. typhimurium* values of 0.10% (CF) and 0.16% (CH). The thin biofilm capture of *E. coli 0157:H7* is also comparable to the average capture of *S. typhimurium* in all the colonized short-term reactors of 0.96%. However, the thick biofilm capture of *E. coli 0157:H7* exceeds the observed capture of *S. typhimurium* in any of the reactor conditions that were operated.

The available pore space in these thick biofilm reactors was approximately 26 mL. Comparing this to the pore volumes determined in this research (34 – 54 mL), greater

amounts of biofilm were present in the reactors operated by *Bauman* [2007] which may account for the greater capture. However, percent recoveries can be misleading with respect to the actual captured cell count. The average inoculum of *E. coli 0157:H7* (n = 14) was $1.19*10^9$ CFU while the average inoculum of *S. typhimurium* (n = 30) was $3.11*10^9$ CFU. If the total cell count captured in a reactor for the two different pathogens was the same, this difference in inoculum would result in capture percentages of *S. typhimurium* that were a factor of 2.6 lower than the *E. coli 0157:H7*.

The capture percentage observed in these model reactors is considerably different than other published research that examines bacterial capture in column studies using sand or soil as the porous media. *Gerlach* [2001] packed a column 30 cm long and 1.5 cm in diameter with 40 mesh quartz sand (d_m < 420 μm) and examined the transport and capture of *Shewanella algae* BrY through the column. The average capture of vegetative cells in the column was 72%. When the column size was increased to 300 cm long and 2.54 cm in diameter the capture increased to 99.3%. These values are significantly greater than the observed capture of *S. typhimurium* in the model reactor. This difference is partially attributed to the increased surface area and roughness of the quartz sand and the smaller collector size (d_m < 420 μm compared to d_m = 3 mm) that results in an increased straining parameter (d_p/d_m). The other factor that becomes apparent is the size of the column. *Gerlach* [2001] demonstrated an increase in capture from 72% to 99.3% by increasing the column length and diameter. The model reactors used for the capture of *S. typhimurium* were 7 cm long and 5.7 cm in diameter. Due to the number of variables which can affect capture, Table 21 compares the values of several parameters between the research mentioned.

The columns operated by *Gerlach* [2001] were larger than the model reactor used and contained smaller diameter porous media resulting in significantly greater surface areas for capture. However, the porosity and interstitial velocity are similar between all four columns listed. While the inoculation concentration was lower for *Gerlach* [2001], it occurred for two pore-volumes rather than as a spike dose as was done with the model reactors. The total CFU inoculated into the columns operated by *Gerlach* [2001] are one to two orders of magnitude larger than in the model reactors.

Table 21. Capture Comparison for variable column setups.

Researcher	Model Reactor	Bauman	Gerlach (0.3 m)	Gerlach (3m)
Biofilm Present?	No	No	No	No
Column Length (cm)	7	7	30	300
Column Diameter (cm)	5.7	5.7	1.5	2.54
Media Diameter -d_m (μm)	3000	3000	< 420	< 420
Media Surface Area (m^2)	0.182	0.182	15.1	434
Porosity (θ)	0.43	0.43	0.49	0.49
Interstital Velocity - v_s (cm/min)	2.28	2.28	2.33	3.82
Hydraulic Residence Time (min)	3.1	3.1	12.9	78.5
Inoc. Conc. (CFU/mL)	3.1E+09	1.2E+09	1.2E+08	8.3E+07
Inoc. Volume (mL)	1.0	1.0	150	1500
Total Inoc. (CFU)	3.11E+09	1.19E+09	1.85E+10	1.24E+11
Capture Percentage	0.13%	0.22%	72.0%	99.3%

Army Research Office - Biofilm Trap Feasibility

The difference between short-term and long-term experiments conducted in this study demonstrates how capture is affected by increasing the flow duration from approximately 15

minutes to 60 minutes. Both of these are still relatively short time durations and it is of interest to know what occurs at longer time durations (e.g. a week) . In the clean model reactors it becomes apparent that the reversibly attached cells are slowly moving through the porous media with a shift in capture locations from the influent end (short-term) to the effluent end (long-term). If the flow was allowed to continue for upwards of a week it is possible that the majority of the cells that were initially retained would likely detach and washout from the clean reactor. Some cells may remain captured in the reactor in straining locations or in surface irregularities on the glass beads.

Contrary to the clean reactors, the colonized reactors with biofilm present within the porous media captured significantly more *S. typhimurium* cells and displayed better retention during the long-term experiments (1 hour). This is due to the ability for a pathogen to integrate into a drinking water biofilm. Extrapolating from the breakthrough curves makes it possible to speculate on the extent of capture cells remaining in the reactor after a week. The apparent leveling off of *S. typhimurium* cells in the collected effluent is suspected of being the result of a quasi steady-state release of captured cells back into the bulk fluid, the growth of *S. typhimurium* cells within the biofilm and subsequent release of those cells, or a combination of the two.

It is difficult to accurately predict how the total cell counts in the reactor and cell concentrations in effluent samples would behave over the course of a week without knowing the extent of growth occurring in the reactor. If growth did not occur, the effluent concentrations could continue to drop as biofilm containing captured *S. typhimurium* cells sloughed off the porous media beads until no detectable cells remained in the reactor. If the

cell growth-rate equaled the combined rate that cells died and re-entered the bulk fluid, a steady-state concentration would be found in the reactor effluent and in the porous media.

Camper et al. [1998] modeled distribution system biofilms and were able to detect *S. typhimurium* cells for over a week using plate counts and selective media (XLD). After 10 to 15 days the culturability of cells with this method had declined to the level of detection (10^{-1} CFU/cm^2 biofilm). Cells were detectable for over 50 days using fluorescent antibodies. This work indicates that *S. typhimurium* is capable of persisting in distribution system biofilms for extended periods of time. However, these cells are not always detectable using standard culture methods. While pathogens captured within a biofilm are capable of persisting, most do not appear capable of extensive growth; this may be due to an inability to compete with indigenous organisms in the biofilm [*Donlan*, 2002]

Even with the low percent capture of cells in the model reactor used, sufficient capture occurred (10^5 to 10^7 CFU diluted in 100 mL of water) to allow for the detection of *S. typhimurium* cells in the reactor. *Camper et al* [1998] demonstrated detection of *S. typhimurium* cells at concentrations below 10^{-1} CFU/mL. Based on this information, it is believed that the biofilm trap could feasibly be used as a monitoring device attached to distribution mains in a centralized water system (CWS). However, the feed water for the model reactors was highly controlled while the quality of treated water will vary between every CWS based on the nature of the source water used and the treatment methods. This variability (e.q. pH, alkalinity, secondary disinfection, total organic carbon, corrosion products, particulates, temperature) between treated water will affect the operation of the biofilm trap. As such, it would be recommended that all centralized water systems conduct

pilot tests with a biofilm trap and their treated water prior to installing devices around their distribution system.

CHAPTER 6

CONCLUSIONS

- The capture of *Salmonella typhimurium* is significantly increased in porous media reactors containing biofilm grown under drinking water conditions than in a clean reactor.
- The main mechanisms of colloid transport to collector surfaces in these reactors are interception and diffusion.
- The main mechanisms of colloid capture in these reactors are attachment and straining with the potential for mechanical filtration if sufficient biofilm growth nearly closes off the pore throat between porous media beads.
- The breakthrough of colloids in a porous media biofilm system is accelerated as compared to a non-reactive tracer that can diffuse into the biofilm.
- Constant flow reactors display preferential flow channeling that occurs as a result of spatial variations in biofilm accumulation under this flow regime.
- Constant head reactors do not display preferential channeling and utilize more of the available pore space.
- The capture of *S. typhimurium* in constant flow reactors is equal to, or greater than, the capture that occurs in constant head reactors under the experimental conditions used.

REFERENCES

Abedon, S. (2007, March). *Bacteria Cell Shapes and Arrangements*. Retrieved March 21, 2007, from http://www.mansfield.ohio-state.edu/~sabedon/biol2010.htm

Auset, M. & Keller, A. A. (2006). Pore-scale visualization of colloid straining and filtration in saturated porous media using micromodels. *Water Resources Research, 42*.

Bauman, W. (2007). Retention of a model pathogen in a porous media biofilm. Master's Thesis, Montana State University, College of Engineering.

Bradford, S. A., Yates, S. R., Bettahar, M., & Simunek, J. (2002). Physical factors affecting the transport and fate of colloids in saturated porous media. *Water Resources Research, 38*.

Bradford, S. A., Simunek, J., Bettahar, M., Tadassa, Y. F., van Genuchten, M. T., & Yates, S. R. (2005). Straining of colloids at textural interfaces. *Water Resources Research, 41*.

Bradford, S. A., Simunek, J., Bettahar, M., van Genuchten, M. T., & Yates, S. R. (2006). Significance of straining in colloid deposition: Evidence and implications. *Water Resources Research, 42*.

Bradford, S. A. & Bettahar, M. (2006). Concentration dependent transport of colloids in saturated porous media. *Journal of Contaminant Hydrology, 82,* 99-117.

Camper AK, Wamecke M, Jones WL, McFeters GA. (1998) Pathogens in model distribution system biofilms. *Denver: American Water Works Association Research Foundation*

Centers for Disease Control and Prevention. (2006). Surveillance for Waterborne Disease and Outbreaks Associated with Recreational Water — United States, 2003–2004, MMWR 2006;55(No. SS-12).

Cunningham, A.B. & Ross, R.J. (2006) Introduction to Biofilms: What are biofilms? *Biofilms: The Hypertextbook.* Retrieved March 22, 2007, from http://www.erc.montana.edu/biofilmbook/MODULE_01/Mod01_Blue/Mod01_S01_Blue.htm

Cushing, R. S. & Lawler, D. F. (1998). Depth filtration: Fundamental investigation through three dimensional trajectory analysis. *Environmental Science & Technology, 32,* 3793-3801.

Donlan, R. M. (2002). Biofilms: Microbial life on surfaces. *Emerging Infectious Diseases, 8,* 881-890.

Donlan, R. M. & Costerton, J. W. (2002). Biofilms: Survival mechanisms of clinically relevant microorganisms. *Clinical Microbiology Reviews, 15,* 167-+.

Duguid, J. P., Anderson, E. S., & Campbell, I. (1966). Fimbriae and Adhesive Properties in Salmonellae. *Journal of Pathology and Bacteriology, 92,* 107-&.

Ellis, B. D., Butterfield, P., Jones, W. L., McFeters, G. A., & Camper, A. K. (1999). Effects of carbon source, carbon concentration, and chlorination on growth related parameters of heterotrophic biofilm bacteria. *Microbial Ecology, 38,* 330-347.

Gerlach, R. (2001). Transport and activity of dissimilatory metal reducing bacteria in porous media for the remediation of heavy metals and chlorinated hydrocarbons. PhD Dissertation, Montana State University, College of Engineering.

Herigstad, B., Hamilton, M., & Heersink, J. (2001). How to optimize the drop plate method for enumerating bacteria. *Journal of Microbiological Methods, 44,* 121-129.

Herzig, J. P., Leclerc, D. M., & Legoff, P. (1970). Flow of Suspensions Through Porous Media - Application to Deep Filtration. *Industrial and Engineering Chemistry, 62,* 8-&.

Klayman, B.J. (2007). A quantitative description at multiple scales of observation of accumulation and displacement patterns in single and dual species biofilms. PhD Dissertation. Montana State University, College of Engineering.

Korber, D. R., Lawrence, J. R., & Caldwell, D. E. (1994). Effect of Motility on Surface Colonization and Reproductive Success of Pseudomonas-Fluorescens in Dual-Dilution Continuous-Culture and Batch Culture Systems. *Applied and Environmental Microbiology, 60,* 1421-1429.

Madigan, M.T., Martinko, J.M., & Parker, J. (2003) *Brock Biology of Microorganisms.* Pearson Education, Inc.

Mcdowellboyer, L. M., Hunt, J. R., & Sitar, N. (1986). Particle-Transport Through Porous-Media. *Water Resources Research, 22,* 1901-1921.

Murphy, E. M. & Ginn, T. R. (2000). Modeling microbial processes in porous media. *Hydrogeology Journal, 8,* 142-158.

Omoike, A. & Chorover, J. (2004). Spectroscopic study of extracellular polymeric substances from Bacillus subtilis: Aqueous chemistry and adsorption effects. *Biomacromolecules, 5,* 1219-1230.

Salerno, M. B., Flamm, M., Logan, B. E., & Velegol, D. (2006). Transport of rodlike colloids through packed beds. *Environmental Science & Technology, 40,* 6336-6340.

Seymour, J. D., Gage, J. P., Codd, S. L., & Gerlach, R. (2004). Anomalous fluid transport in porous media induced by biofilm growth. *Physical Review Letters, 93.*

Sharp et al., R. R., Cunningham, A. B., Komlos, J., & Billmayer, J. (1999). Observation of thick biofilm accumulation and structure in porous media and corresponding hydrodynamic and mass transfer effects. *Water Science and Technology, 39,* 195-201.

Sharp et al., R. R., Stoodley, P., Adgie, M., Gerlach, R., & Cunningham, A. (2005). Visualization and characterization of dynamic patterns of flow, growth and activity of biofilms growing in porous media. *Water Science and Technology, 52,* 85-90.

Sirivithayapakorn, S. & Keller, A. (2003). Transport of colloids in saturated porous media: A pore-scale observation of the size exclusion effect and colloid acceleration. *Water Resources Research, 39*.

Stevik, T. K., Aa, K., Ausland, G., & Hanssen, J. F. (2004). Retention and removal of pathogenic bacteria in wastewater percolating through porous media: a review. *Water Research, 38,* 1355-1367.

Stewart, T. L. & Kim, D. S. (2004). Modeling of biomass-plug development and propagation in porous media. *Biochemical Engineering Journal, 17,* 107-119.

Todar, K. (2004) *Todar's Online Textbook of Bacteriology: Structure and Function of Procaryotic Cells.* Retrieved March 25, 2007, from http://textbookofbacteriology.net/structure.html

Yao, K. M., Habibian, M. M., & Omelia, C. R. (1971). Water and Waste Water Filtration - Concepts and Applications. *Environmental Science & Technology, 5,* 1105-&.

Water Science and Technology Board (WSTB). (2006) Drinking water distribution systems: Assessing and reducing risks. Committee on Public Water Supply Distribution Systems. Retrieved June 12, 2007, from http://www.nap.edu/catalog/11728.html#toc